Åbo Akademi University

Lidia I. Godina

Aqueous-Phase Reforming of Renewable Polyols for Sustainable Hydrogen Production

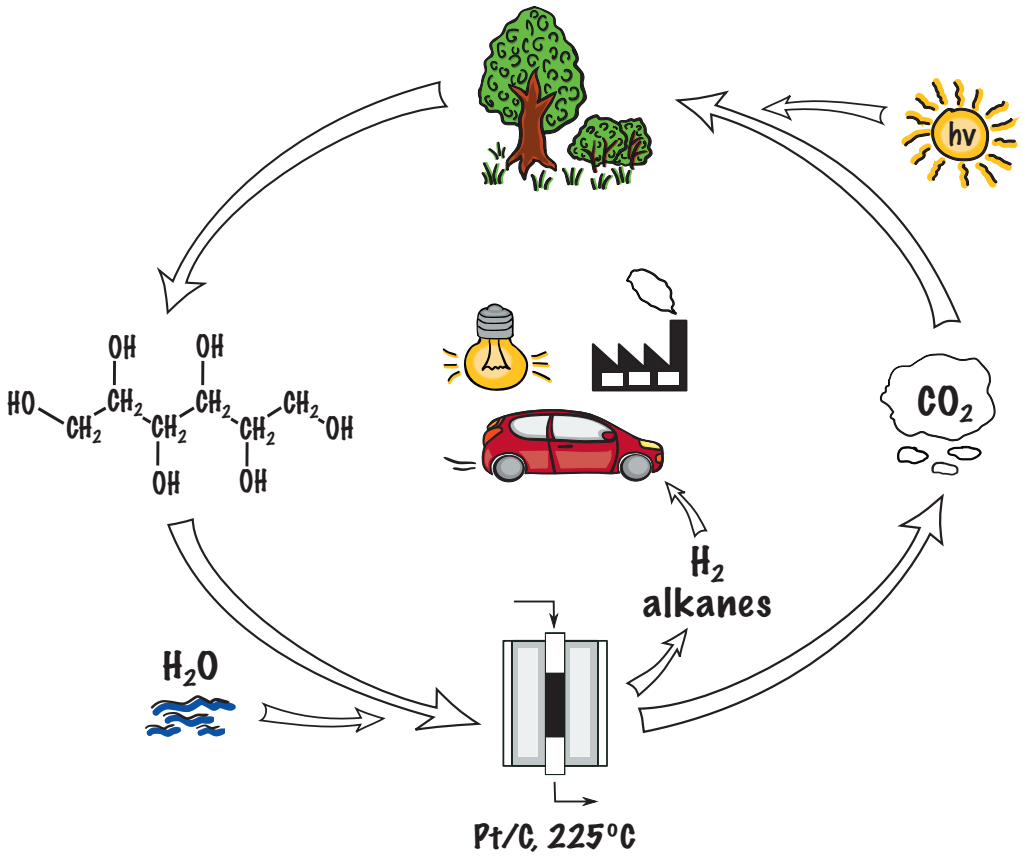

Lidia I. Godina

Born in Dolgoprudny, Russia

Engineer, M.Sc., Mendeleyev University of Chemical Technology of Russia (MUCTR), Faculty of Technology of Organic Substances and Chemical Pharmaceutical Compounds, Department of Chemistry and Organic Synthesis Technology, Russia, 2012

Aqueous-phase reforming of renewable polyols for sustainable hydrogen production

Doctoral thesis

Lidia I. Godina

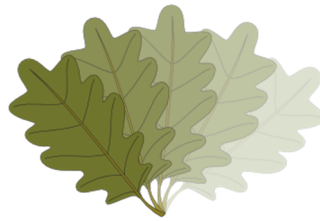

Johan Gadolin
Process Chemistry Centre

Laboratory of Industrial Chemistry and Reaction Engineering

Faculty of Science and Engineering /Chemical Engineering

Åbo Akademi University

Turku/Åbo 2019

Supervised by

Professor Dmitry Murzin

Laboratory of Industrial Chemistry and Reaction Engineering

Faculty of Science and Engineering /Chemical Engineering

Åbo Akademi University

Reviewers

Professor Leonid M. Kustov

N. D. Zelinsky Institute of Organic Chemistry, Russian Academy of Science

Moscow, Russia

Professor Sébastien Paul

Centrale Lille, Unité de Catalyse et Chimie du Solide

Lille, France

Opponent

Professor Sébastien Paul

École Centrale de Lille, Unité de Catalyse et Chimie du Solide

Lille, France

ISBN 978-952-12-3778-2 (printed) / ISBN 978-952-12-3779-9 (electronic)

Painosalama Oy – Turku, Finland 2019

In a hole in the ground there lived a hobbit.

J.R.R. Tolkien

PREFACE

This work was carried out between 2013 and 2018 at the Laboratory of Industrial Chemistry and Reaction Engineering, Faculty of Science and Engineering, Åbo Akademi University. Doctoral studies were a part of activity at Johan Gadolin Process Chemistry Center (PCC). Research was conducted within the frameworks of a SusFuelCat project, which received funding from the European Union's Seventh Framework Programme for research, technological development and demonstration under Grant Agreement No. 310490 (www.susfuelcat.eu). COST Action CM0903, Finnish Catalysis Society, and Åbo Akademi University are acknowledged for financial support.

I would like to acknowledge Professors Dmitry Yu. Murzin and Tapio Salmi for supervision of my doctoral studies and for deep scientific discussions. Prof. Dmitry Murzin is especially acknowledged for his "always open door" concept and scientific advices. Prof. Johan Wärnå is acknowledged for kinetic modelling. Docent Kari Eranen is acknowledged for his support with the instrumentation and analysis. Dr. Vincenzo Russo and Dr. Teuvo Kilpiö are acknowledged for dynamic model simulations. Dr. Dmitry A. Sladkovskiy is acknowledged for process design and techno-economical analysis. Docent Pasi Tolvanen, Professor Tapio Salmi and Dr. Jussi Rissanen are acknowledged for abstract translation to swedish and finnish languages.

I am very grateful to my colleagues from the SusFuelCat project, which was a fruitful and successful collaboration. Docent Irina Simakova, Dr. Yulia Demidova, Dr. Sonia García, Dr. Jesus Lemus, and Jan Gläsel are acknowledged for synthesis of most of catalysts and a part of characterisation. Dr. Roberto Schimmenti, Dr. Remedios Cortese, and Prof. Dario Duca are acknowledged for quantum-mechanical calculations. And, finally, Dr. Hans Heeres, Kaisa Vikla, and Prof. Leon Lefferts are acknowledged for valuable scientific discussions.

Anton Tokarev and Alexey Kirilin are especially acknowledged for mentoring and constant help in various spheres of life, both professional and personal. I would never become the person who I am today without those two. I would like to acknowledge my colleagues and friends, who made the deepest marks in my heart: Imane Hachemi, Karolina Maduna-Valkaj, Soudabeh Saeid, Ricardo Pezoa Conte, Ewelina Leino, Bartosz Rozmyslowicz, Ekaterina Korotkova, Zhanna Boeva, Yury Brusentsev,

Vladimir Shumilov, Denis Mavrinskiy, Alexandra Torozova, Yulia Demidova, Antonina Kupareva, Elena Privalova, Cesar Araujo, Jussi Rissanen, Atte Aho, Pasi Tolvanen, Farhan Saleem, Andrea Perez Nebreda, Nemanja Vucetic, Ikenna Anugwom. Thank you for being around and making life better.

I would like to acknowledge my family for support and freedom to choose my own way.

Thank you, Artem, for being with me for more than a decade, pushing me forward, and sharing all bright and dark sides of life. And thank you, my small Mira, for giving me strength and the meaning of life.

ABSTRACT

Aqueous-phase reforming of renewable polyols for sustainable hydrogen production

Lidia I. Godina

Doctoral Thesis, Laboratory of Industrial Chemistry and Reaction Engineering, Johan Gadolin Process Chemistry Centre, Faculty of Science and Engineering, Åbo Akademi University, 2019.

Keywords: aqueous-phase reforming, platinum, sorbitol, xylitol, kinetic model, techno-economical analysis

Renewable biomass can be utilized for sustainable hydrogen production via aqueous-phase reforming (APR), which implies catalytic conversion of aqueous solutions of alcohols and polyols over transition metals at comparably low temperatures with formation of hydrogen, CO_2, light alkanes, and a number of products in the liquid phase.

The current work is devoted to studies of APR of several alcohols and polyols and their technical mixtures over mono- and bimetallic catalysts [**I-IV, VII**]. A realistic APR reaction network [**I, VII**] and a kinetic model [**V**] were proposed, reactor modelling and process design were performed in [**V**, **VI**], and techno-economical analysis of APR was provided in [**VI**].

Propanol-1, propane-1,2-diol, glycerol, xylitol and sorbitol were studied in APR over different Pt/C catalysts. Influence of feed chirality was investigated for the first time in APR of sorbitol and galactitol over Pt/Al_2O_3 catalyst. Conversion of the technical mixture of sorbitol and mannitol was compared to commercial sorbitol in APR over Pt/C. Mono- and bimetallic carbon-supported catalysts were compared in terms of activity and selectivity in xylitol APR.

The reliability of the liquid-phase product analysis was considerably improved. Plausible reaction pathways were proposed according to the product distribution and discussed from a thermodynamic point of view. Different reaction paths of 1,2-propanediol APR were computationally screened on a Pt(111) model surface specifically addressing the competition between C–H, O–H, and C–C bond cleavages.

Experimental data obtained in the xylitol APR was utilized for reaction kinetics modeling, dynamic reactor simulation, and process design development. The process can be considered as a self-sufficient one, since the reactor heat demand is fully covered by the combustion of alkanes produced in APR.

Simulation of in-situ phase equilibrium was based on the results of the sorbitol APR. Process design of a hydrogen production plant with 500 kg/h capacity operating with sorbitol syrup was developed and optimized. A detailed techno-economical analysis was performed for the first time for estimation of hydrogen production price.

REFERAT

Vattenfasreformering av förnybara polyoler för hållbar väteproduktion

Lidia I. Godina

Doktorsavhandling, Laboratoriet för teknisk kemi och reaktionsteknik, Johan Gadolin Processkemiska centret, Fakulteten för naturvetenskaper och teknik, Åbo Akademi, 2019

Nyckelord: vattenfasreformering, platina, sorbitol, xylitol, kinetisk modell, teknoekonomisk analys

Förnybar biomassa kan utnyttjas för en hållbar vätgasproduktion genom vattenfasreformering (APR), vilket innebär katalytisk omvandling av alkoholer samt polyoler lösta i vatten till vätgas, koldioxid och flyktiga alkaner i närvaro av övergångsmetaller.

Detta arbete är ägnat för att utforska APR av flera alkoholer och polyoler samt deras tekniska blandningar genom att använda bimetalliska katalysatorer [**I-IV, VII**], att föreslå ett realistiskt nätverk för APR-reaktionsförloppet [**I, VII**], att utveckla en kinetisk modell [**V**], att utföra reaktormodellering och prosessdesign [**V**, **VI**] samt att utveckla en teknoekonomisk analys av APR [**VI**].

Propanol-1, propen1,2-diol, glycerol, xylitol och sorbitol studerades med APR i närvaro av olika Pt/C-katalysatorer. Inverkan av utgångslösningens kiralitet studerades för första gången med reformering av sorbitol och galaktitol med Pt/Al_2O_3 som katalysator. Omvandling av den tekniska blandingen innehållande sorbitol och mannitol jämfördes med kommersiell sorbitol med APR i närvaro av Pt/C-katalysator. Mono- samt bimetalliska katalysatorer på kolbärare jämfördes i avseende på aktivitet och selektivitet, då APR utfördes med xylitol.

Tillförlitligheten av produktanalysen av vätskefasen förbättrades signifikant i detta arbete. Möjliga reaktionsrutter föreslogs i avseende på produkt-fördelningen, samt deras termodynamiska aspekter diskuterades ingående. Olika reaktionsrutter för 1,2-propandiol söktes med hjälp av datorberäkningar då en Pt(111) modellyta användes, som specifikt fokuserade på klyvandet av C-H, O-H och C-C bindningar.

Experimentella data extraherad från APR av xylitol utnyttjades för modellering av reaktionskinetiken, dynamiska reaktorsimuleringar, samt för process-utveckling.

Processen kan anses vara självförsörjande, då reaktorns värmebehov går att helt upprätthållas genom förbränning av de alkaner som bildats i APR-steget.

En simulering av in-situ fasjämvikt baserades på de resultat som erhölls från APR av sorbitol. En processdesign av en vätgasfabrik med en kapacitet på 500 kg/h utvecklades och optimerades, utgående från sorbitolsirap som råvara. En detaljerad teknoekonomisk analys utfördes för första gången för att estimera den totala kostnaden för vätgasproduktionen.

РЕФЕРАТ

Производство водорода из возобновляемых сахарных спиртов путем водяного риформинга

Лидия И. Година

Ключевые слова: водяной риформинг, платина, сорбитол, ксилитол, кинетическая модель, техно-экономический анализ

Водяной риформинг – это процесс, позволяющий производить водород из возобновляемого сырья, например, из биомассы. Водные растворы спиртов и полиолов в присутствии переходных металлов при сравнительно невысоких температурах могут вступать в каталитическую реакцию водяного риформинга с образованием водорода, углекислого газа, алканов, а также целого ряда продуктов, находящихся в жидкой фазе. Данная работа посвящена изучению водяного риформинга спиртов и полиолов, а также их технических смесей, в присутствии моно- и биметаллических катализаторов [**I-VII**]. В данной работе представлена схема реакций, происходящих во время риформинга [**I, VII**]. В ходе исследований были разработаны кинетическая модель реакций [**V**] и модель реактора водяного риформинга [**VI**], а также был спроектирован процесс производства водорода из ксилитола и сорбитола [**V**, **VI**]. Для процесса получения водорода из сиропа сорбитола был проведен техно-экономический анализ с оценкой стоимости конечного продукта (водорода) [**VI**].

Различные платиновые катализаторы были протестированы в водяном риформинге пропанола-1, пропан-1,2-диола, глицерина, ксилитола и сорбитола. Влияние хиральности исходного сырья на распределение продуктов было изучено на примере водяного риформинга двух эпимеров, сорбитола и галактитола, в присутствии Pt/Al_2O_3. Было изучено влияние примесей на распределение продуктов на примере водяного риформинга сорбитола и технической смеси сорбитола и маннитола, полученной в результате гидрирования сахарозы. Был проведен скрининг моно- и биметаллических катализаторов на примере водяного риформинга ксилитола.

Повышение чувствительности и увеличение точности метода анализа жидкой фазы привело к уточнению схемы реакций водяного риформинга. Возможность существования некоторых наиболее вероятных реакций была обсуждена с

точки зрения термодинамики. Также с помощью квантово-химических расчетов были смоделированы превращения 1,2-пропандиола в ходе водяного риформинга на поверхности Pt(111), была изучена вероятность разрыва C–H, O–H и C–C связей.

На основе экспериментальных данных, полученных в результате водяного риформинга ксилитола на Pt/C катализаторе, была получена кинетическая модель, использованная в дальнейшем вместе с разработанной моделью реактора для проектирования процесса производства водорода мощностью 500 кг/час. Расчеты фазового равновесия позволили уточнить расчет теплового баланса для реактора водяного риформинга сорбитола. Детальный технико-экономический анализ процесса производства водорода мощностью 500 кг/час из коммерчески доступного сиропа сорбитола позволил оценить стоимость производимого водорода в зависимости от различных параметров.

TIIVISTELMÄ

Vedyn tuottaminen kestävästi uusiutuvista, moniarvoisista alkoholeista katalyyttisen vesifaasireformoinnin avulla.

Lidia I. Godina

Väitöskirja, teknillisen kemian ja reaktiotekniikan laboratorio, Johan Gadolin Prosessikemian keskus, Luonnontieteiden ja tekniikan tiedekunta, Åbo Akademi, 2019.

Hakusanat: vesifaasireformointi, platina, sorbitoli, ksylitoli, kineettinen mallinnus, teknillis-taloudellinen analyysi.

Uusiutuva biomassa tarjoaa tulevaisuudessa keinon kestävään vedyn tuotantoon vesifaasireformoinnin avulla, jossa sekä yksi- että moniarvoisten alkoholien vesiliuokset yhdessä siirtymämetallikatalyyttien kanssa tuottavat vetyä, hiilidioksidia ja kevyitä alkaaneja verrattain matalissa lämpötiloissa (180 – 250 °C).

Tässä työssä tutkittiin tiettyjen, niin yksi- kuin moniarvoisten- sekä sokerialkoholien ja niiden teollisten seosten vesifaasireformointia käyttäen mono- ja bimetallisia katalyyttejä [**I-IV**, **VII**]. Esitettyjen todennäköisten vesifaasireformoinnin reaktiomekanismien pohjalta [**I**, **VII**] kehitettiin kineettinen mallit [**V**], jotka puolestaan toimivat pohjana onnistuneelle reaktori- mallinnukselle ja prosessisuunnittelulle [**V**, **VI**], johtaen onnistuneeseen teknillis-taloudelliseen analyysiin [**VI**].

1-propanolia, 1,2-propaanidiolia, glyserolia, ksylitolia ja sorbitolia tutkittiin erityyppisillä platina-hiilikatalyyteillä käyttäen vesifaasireformointimenetelmää. Lähtöaineseoksen kiraalisuuden vaikutusta tutkittiin ensimmäistä kertaa epimeereillä, sorbitolilla ja galaktitolilla vesifaasireformoinnissa käyttäen Pt/Al_2O_3-katalyyttiä. Teollisesta lähteestä saadun sorbitoli-mannitoliseoksen ja kaupallisen sorbitolin konvertoitumista Pt/C katalysoidussa vesifaasi-reformoinnissa vertailtiin keskenään. Samoin mono- ja bimetallisia, hiilikantajan sisältäviä katalyyttejä, vertailtiin aktiivisuuden ja selektiivisyyden osalta ksylitolilla vesifaasi-reformoinnilla saatuihin tuloksiin.

Nestemäisen välituotteen osalta analyysin luotettavuutta onnistuttiin parantamaan huomattavasti ja realistisempien reaktiomekanismien esittäminen, termodynamiikka huomioon ottaen kävi mahdolliseksi. Erilaiset reaktioreitit mallinnettiin

Pt(111)-pinnalla käyttäen tiheysfunktionaaliteoriaa, jolloin osoitettiin C-H-, O-H-, ja C-C-sidoksien katkeamisten välillä vallitseva kilpailutilanne.

Kineettinen mallintaminen, dynaaminen reaktorisimulointi ja prosessisuunnittelu suoritettiin ksylitolin vesifaasireformoinnista saatuihin tietoihin perustuen. Tärkein tulos oli varmuus prosessin omavaraisuudesta, koska prosessin sivutuotteiden, eli alkaanien palaminen, tuottaa reaktorin toiminnan kannalta, riittävän lämpömäärän.

Faasitasapainon in-situ -simulointi ja prosessinsuunnittelu tehtiin ja optimoitiin sorbitolin vesifaasireformoinnista saatujen kokeellisten tulosten pohjalta. Samoin kehitettiin ja optimoitiin prosessisuunnitelma sorbitolisiirappia 500 kg/h hyödyntävää, vetyä tuottavaa tehdasta varten. Näin ensimmäistä kertaa vedyn teollisesta tuotannosta luotiin teknillis-taloudellinen analyysi, jonka perusteella voitiin arvioida vedyn tuotantohinta.

LIST OF PUBLICATIONS

I. Godina, L.I., Kirilin, A.V., Tokarev, A.V., Murzin, D.Yu. Aqueous phase reforming of industrially relevant sugar alcohols with different chirality. *ACS Catal.* **2015**, *5*, 2989.

II. Godina, L.I., Tokarev, A.V., Simakova, I.L., Mäki-Arvela P., Kortesmäki E., Gläsel J., Kronberg L., Etzold B., Murzin D.Yu. Aqueous-phase reforming of alcohols with three carbon atoms on carbon-supported Pt. *Catal. Today* **2018**, *301*, 78.

III. Godina L.I., Kirilin A.V., Tokarev A.V., Simakova I.L., Murzin D.Yu. Sibunit-supported mono- and bimetallic catalysts used in aqueous-phase reforming of xylitol. *Ind. Eng. Chem. Res.* **2018**, *57*, 2050.

IV. Godina L.I., Heers H., Garcia S., Bennett S., Poulston S., Murzin D.Yu. Hydrogen production from sucrose via aqueous-phase reforming (submitted)

V. Murzin D.Yu., Garcia S., Russo V., Kilpiö T.T., Godina L.I., Tokarev A.V., Kirilin A.V., Simakova I.L., Poulston S., Sladkovskiy D.A., Wärnä J. Kinetics, modelling and process design of hydrogen production by aqueous phase reforming of xylitol. *Ind. Eng. Chem. Res.* **2017**, *56*, 13240.

VI. Sladkovskiy D.A., Godina L.I., Semikina K.V., Sladkovskaya E.V., Smirnova D.A., Murzin D.Yu. Process design and techno-economical analysis of hydrogen production by aqueous phase reforming of sorbitol. *Chem. Eng. Res. Des.* **2018**, *134*, 104.

VII. Schimmenti R., Cortese R., Godina L.I., Prestianni A., Ferrante F., Duca D., Murzin D.Yu. A combined theoretical and experimental approach for platinum catalyzed 1,2-propanediol aqueous phase reforming. *J. Phys. Chem. C* **2017**, *121*, 14636.

This thesis is based on seven original publications. The author of the thesis is the main author of articles I-IV, where the contribution includes experimental catalyst evaluation, a part of catalysts synthesis and characterisation, development of analytical methods, thermodynamic calculations, mass-transfer calculations, and article writing and editing.

For the publications V-VII the author conducted the catalytical experiments, performed a part of catalysts characterization, and contributed to writing and editing the article.

LIST OF RELATED PUBLICATIONS

1. Godina L.I., Tokarev A.V., Gläsel J., Kirilin A.V., Etzold B.J.M., Murzin D.Yu.: "Aqueous-phase reforming of alcohols with three carbon atoms on carbon-supported Pt catalyst", 17th Nordic Symposium on Catalysis 2016, Lund, Sweden, June 14-16, 2016 – *poster presentation*

2. Godina L.I., Kirilin A.V., Tokarev A.V., Demidova Yu.S., Lemus J., Calvo L., Schubert T., Gilarranz M.A., Simakova I.L., Murzin D.Yu: "Aqueous-phase reforming of xylitol on carbon-supported catalysts", tcbiomass2015: Technology for the Bioeconomy, Chicago, IL, USA, 2-5 November, 2015 – *poster presentation*

3. Godina L.I., Kirilin A.V., Tokarev A.V., Murzin D.Yu: "Analysis of liquid-phase intermediates generated during aqueous-phase reforming of sorbitol on Pt/Al_2O_3", tcbiomass2015: Technology for the Bioeconomy, Chicago, IL, USA, 2-5 November, 2015 – *poster presentation*

4. Godina L.I., Kirilin A.V., Tokarev A.V., Demidova Yu.S., Lemus J., Calvo L., Schubert T., Gilarranz M.A., Simakova I.L., Murzin D.Yu: "Aqueous phase reforming of xylitol over mono- and bimetallic carbon-supported catalysts", the XII European Congress on Catalysis (Europacat 2015), Kazan, Russia, August 30 – September 4, 2015 – *oral and poster presentation*

5. Godina L.I., Simakova I.L., Calvo L., Demidova Yu.S., Tokarev A.V., Gilarranz M., Murzin D.Yu. : "Motor fuel components through xylitol aqueous phase reforming over VIII group metals catalysts", the 24th North American Meeting (24th NAM), Pittsburgh, PA, USA, June 14th- 19th, 2015 - *poster presentation*

6. Godina L.I., Kirilin A.V., Tokarev A.V., Murzin D.Yu.: "Aqueous phase reforming of sorbitol and galactitol: the influence of chirality", 3rd International symposium on Green Chemistry (ISGC 2015), La Rochelle, France, May 3-7, 2015, 771/OC – *poster presentation*

7. Godina L.I., Kirilin A.V., Tokarev A.V., Murzin D.Yu.: "Aqueous phase reforming of industrially relevant sugar alcohols with different chirality", the 4th International Workshpop of COST Action CM0903 (UBIOCHEM IV), Valencia, Spain, October 14-16, 2013, O-10 – *oral presentation*

CONTENTS

1. Introduction

1. Introduction

Biomass, and especially carbohydrates obtained from starch-rich and cellulosic materials, can be a dominant feedstock for the sustainable production of fuels, chemicals and materials, according to Lynd et al. [1]. The existing sustainable technologies of first generation biofuel production are established for utilization of fermentable sugars obtained mainly from sugarcane and starchy crops, e.g. biomass-to-ethanol process. Lignocellulosic biomass, such as agricultural residues, wood, etc., is a second generation feedstock containing cellulose and hemicelluloses as a source of carbohydrates. Due to its complexity, liberating sugars from lignocellulosic biomass requires a multiple pretreatment approach, thus being more demanding compared to processing of starch rich feeds [2].

Carbohydrates can be utilized in various processes to produce fuels and chemicals. One of them is aqueous-phase reforming (APR) process, allowing production of hydrogen and alkanes at relatively low temperatures and pressures. Conversion of an aqueous solution of a certain substrate is performed over a heterogeneous catalyst typically at 453-523 K and low pressures (25-60 bar) [3] to maintain the liquid phase. Various transition metals in combination with various supports can be applied as catalysts in APR. However, this reaction requires a catalyst with high hydrothermal stability and resistance to impurities potentially present in the feedstock.

APR is as a promising technology, which possess certain advantages. First, the net effect to green-house emissions is zero, since all CO_2 produced was captured from the atmosphere during formation of carbohydrates in the plant. Second, APR is economically beneficial in terms of hydrogen production compared to one of the most wide spread processes, such as methane steam reforming [4,5]. Steam reforming requires 800-900 K operation temperature, while APR occurs already at 453-523 K, allowing hydrogen production from sorbitol with the same yield of 50-60% [6]. The third advantage is that water acts simultaneously as a solvent and as a reactant, being converted into additional hydrogen via the water-gas shift reaction (WGS). APR can be potentially applied for hydrogen production, if the installation of a small-scale methane steam reforming unit is not economically attractive, for example at a stand-alone green diesel production plant located close to a pulp mill [**VI**].

APR is a highly adjustable process, which can result in a selective production of hydrogen or alkanes. Activity and selectivity in APR can be modified by different

parameters, such as the active metal, support type, or reaction conditions (pressure, temperature, acidic or basic additives, presence of the carrier gas, reactor type). The influence of those parameters is discussed below.

1.1. Metal variation

Various transition and especially noble metals are active in APR. Moreover, metalloids, e.g. boron [7], or specific materials like graphene [8] were shown to be active in glycerol reforming. An extensive review of catalysts used for APR was published by Coronado et al. [9]. A short summary is provided in the current work.

A broad metal screening was performed for catalysts, supported on alumina [10], titania [11], silica [12], carbon multi-walled nanotubes [13,14], carbon nano-fibers [15], carbon black [16], activated carbon [17–19]. Pt was shown to be highly active and selective to hydrogen in most cases. Both activity and selectivity could be improved by addition of a second transition metal, like Ni or Co.

A certain number of attempts were made to find a replacement of the expensive noble metal by a cheaper alternative, e.g. nickel, cobalt or iron. The results were controversial due to stability issues. The successful trials of nickel catalysts demanded utilization of basic additives [20], mixed-oxides [21–23] or hydrotalcites as supports [24].

The current state of the art in metal screening performed for carbon-supported catalysts is summarized in Figure 1. More details can be found in the Appendix, Tables A1 and A2. Some transition metals were tested in as a monometallic catalyst. The major bimetallic group is presented by Pt catalysts modified with a second metal. Another considerably smaller group is formed by Ni-based catalysts. Some other bimetallic catalysts were also tested. The discussion below is devoted mainly to carbon-supported catalysts directly related to this work, such as Pt, Ni, Co, Re, Ru, Pt-Ni, Pt-Co, Pt-Re and Pt-Ru.

Monometallic Ni/C and Co/C catalysts are not stable at APR conditions due to the metal leaching [15,20]. Several studies were devoted to investigate Ni (or Pt-Ni) catalysts in APR with mostly metal oxides used as supports [9]. The results vary significantly depending on the support and the reactor type.

Deactivation of mono- and bimetallic Ni catalysts occurred due to coking, oxidation or leaching of the active metal [25–29]. An interesting approach was suggested

combining a hydrogenation ability of Ni with highly acidic zeolite supports to obtain high selectivity towards alkanes with a high molar mass, e.g. pentane from xylitol [30,31].

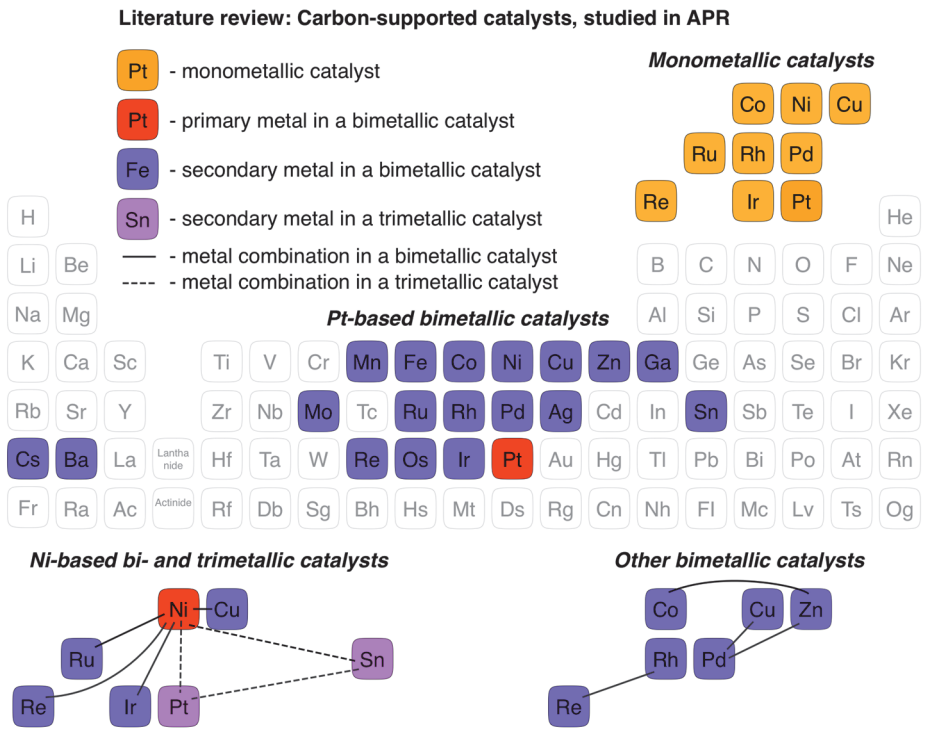

Figure 1. Mono-, bi- and trimetallic carbon-supported catalysts studied in APR.

Ni/C, Co/C and Pt/C supported on carbon nanofibers were tested in the ethylene glycol APR performed in a batch reactor [15]. Activity of the Ni catalyst (14.5% conversion) was slightly lower compared to Pt (17%). At the same time, Pt/C showed an approximately 2.5 times higher selectivity to hydrogen (53%) compared to Co/C (21%) and Ni/C (15%), due to high methane formation rates for the latter two metals. Significant leaching of cobalt occurred due to high concentrations of acids in the liquid phase – 8.9% of the metal was lost after 24 hours. The leaching rate of Ni was slower compared to Co (1.9% of metal leached after 24 h). No leaching of Pt was

detected (< 0.1 ppmw). Deactivation of Pt and Ni catalysts was mainly explained by metal particle sintering, however, one need to take into account the contribution of coke deposition for Ni/C catalyst [32].

Bimetallic Pt-Ni/C and Pt-Co/C catalysts were shown to have better activity compared to monometallic Pt [13,32]. However, stability of Pt-Co/C is an issue due to high formation rates of acids and, hence, corresponding low pH, that facilitates the leaching of cobalt [33,34]. Stability of Pt-Ni/C catalyst was discussed for the sorption-enhanced APR of glycerol [13]. Addition of Co to Pt (molar ratio 1:1) increased the reaction site-time yields by a factor of 2 for the glycerol APR performed over the catalyst supported on carbon nanotubes [33]. The conversion level of glycerol was chosen in the range of 2-4% for operation in a differential reactor mode, which makes it challenging to compare the results with the majority of other literature data and the current work. Pt-Co/C supported on single-wall nanotubes (SWNT) showed higher hydrogen yields [32] and higher conversion levels [35] compared to the monometallic Pt/C under the same reaction conditions for the ethylene glycol APR.

Monometallic Re/C was reported to have a low activity in APR of ethylene glycol [36] and glycerol [37]. Ru/C catalyst was active in the sorbitol APR performed in a washcoated microreactor [38,39]. Nevertheless, very low hydrogen production rates were observed over Ru/C.

Carbon-supported bimetallic Pt-Re catalysts showed an outstanding activity accompanied by the shift of reaction pathways towards alkane formation [18,37,40–43]. Addition of Ru to Pt also increased catalyst activity in the sorbitol APR [38].

1.2. Support variation

APR reaction pathways depend strongly on the support [36,44,45]. Lewis or Brønsted acid sites present on the support can catalyze a number of reactions, for instance, dehydration. Surface groups, polarity, and hydrophobicity are playing a crucial role in the product distribution [45]. Different support types were tested for the same active metal, mainly for Pt and Ni [29,44,46–52]. Such supports as Al_2O_3, TiO_2 and carbon exhibited the highest activity for the hydrogen production in the ethylene glycol APR [44]. The effect of support basicity was studied in the glycerol APR performed in a fixed-bed reactor [29,50]. The catalysts can be ranked in the following order based on their activity:

$Pt/MgO > Pt/Al_2O_3 > Pt/CeO_2 > Pt/TiO_2 > Pt/SiO_2 > Pt/HUSY\ (SiO_2{:}Al_2O_3{=}4.8) >$ Pt/activated carbon > Pt/SAPO-11 ($Si_{0.129}Al_{0.499}P_{0.397}O_2$)

However, the most active and selective to hydrogen Pt/MgO catalyst deactivated after 25 hours of time-on-stream with formation of magnesium hydroxide and carbonate. Support basicity was found to be beneficial for conversion of the feed to the gas phase products and formation of hydrogen. At the same time, low hydrothermal stability prevents selection of many solid bases as catalyst supports.

Carbon materials are generally very attractive as catalyst supports due to their tunable chemical and textural surface properties. They were shown to have a high hydrothermal stability at APR conditions [48,53]. Different carbon support type were compared for Pt [54–57] and Pd-Zn catalysts [58]. A summary of carbon-supported catalysts utilized in APR is shown in Table A2 and discussed below.

Application of mesoporous carbon supports could significantly enhance the catalyst performance in APR compared to catalysts supported on activated carbon [48,54]. Platinum supported on the ordered mesoporous carbon CMK-3 showed a more than twofold increase in hydrogen production in the ethylene glycol APR, compared to catalysts supported on activated carbon and alumina [48]. A 3D bimodal mesoporous carbon (3D-BMC) was developed as an alternative to a high-cost ordered mesoporous carbons from the CMK family; the corresponding Pt/3D-BMC catalyst was more effective for hydrogen production in the sorbitol APR compared to Pt/CMK-3 [54]. Bimetallic Pd-Zn catalyst supported on CNT appeared to be more active than Pd-Zn supported on carbon black in the ethanol APR due to pore confinement effects [58]. Other mesoporous materials were applied in APR as supports, such as single- and multi-wall carbon nanotubes (SWCNT and MWCNT), Sibunit [55], [**II**], polymer based spherical activated carbons (PBSAC) [**II**, **VII**] or carbide-derived carbon (CDC) [55]. In addition, graphene appeared to be an exception, being active even without any metal [8].

One of the most serious drawbacks of a classical activated carbon-based catalyst is the nature of fine powders or granules of poor mechanical strength always encompassed by fines. This leads to a high pressure drop in continuous reactors or a tedious filtration in a batch operation. Contrary to natural precursors with large variability, which are widely employed for synthesis of activated carbon, polymers are well-defined precursors with a constantly high quality. As the polymer can be provided in

a different shape like fibers, foams or spheres, corresponding structured and shaped porous carbons can be synthesized. Especially spherical shaped carbons have received a growing attention due to excellent fluid dynamic properties and a high abrasion resistance, leading to a practically dust-free handling [59–62]. This is of particular interest in a continuous operation requiring a low pressure drop, such as aqueous phase reforming. The spherical shape and the particulate character improve the handling properties during the reactor (un-)loading and catalyst preparation. Polymer based spherical activated carbon (PBSAC) is already widely employed in gas- and liquid-phase sorption processes due to the high surface area and the large pore volume [59–61,63–66]. Very recently PBSAC was introduced as a support for noble metals and was employed in hydrogenation reactions [67]. PBSAC-supported Pt catalyst was utilized for propanol-1, propane-1,2-diol and glycerol APR in the publications [**II**, **VII**].

Mesoporous carbonaceous material Sibunit is considered as an attractive one due to a high mechanical crushing and abrasion strength (up to 200–300 kg/cm^2) and a high surface area (up to 700 m^2/g) [68]. It combines the properties of graphite and activated carbon. Sibunit catalysts can in principle be produced in a large scale in a number of shape units, such as whole and hollow cylinders, rings, etc., allowing their application in fixed bed reactors. The carbon material is synthesized via deposition of pyrolytic carbon from C_1-C_3 hydrocarbons over granulated carbon blacks followed by chemical vapour deposition and steam activation. A subsequent activation stage with steam at 973–1123 K is needed to remove a part of carbon by gasification, leading to a sponge-like system with meso- and macropores. A detailed preparation procedure is described by Fenelonov et al. [69]. Sibunit-supported Pt catalyst was tested in xylitol APR [55], [**III**] and exhibited moderate results in terms of hydrogen production compared to Pt supported on birch activated carbon (BAC) or TiC-derived carbon (TiC-CDC), being more active than the above-mentioned catalysts. Those results were explained by an outstanding hydrothermal stability and open mesoporous structure, porosity and acidity of the support [48,55].

1.3. Feed variation

Most of studies reported in the literature are devoted to investigation of APR of model compounds, such as neat alcohols and polyols ranging from C_1 to C_6. Methanol, ethylene glycol, glycerol, xylitol and sorbitol are often applied as a feed [4,70–72]. A

summary of the feed investigated up to the current moment is presented in the Appendix, Table A3. The Table is separated into three columns, depending on the measured or calculated pH: basic, acidic and neutral. Various additives were utilized, such as acids or bases and organic and inorganic salts, in order to improve the catalyst stability or to emulate the real feed, e.g. crude glycerol.

Acidity/basicity of the reaction media could possibly alter the distribution of the reaction products. Addition of KOH significantly promoted hydrogen formation along with a drastic increase of methane yield in another study of ethylene glycol APR over a non-pyrophoric Ni catalyst [73]. Studies of glycerol APR over Ni–La/Al_2O_3 catalyst at a wide range of pH (2.46-13.4) revealed no influence of pH on the reaction mechanism, but showed that the catalyst deactivation caused by basic or acidic additives (KOH or acetic acid) led to significant changes in hydrogen production and the liquid-phase product distribution [74,75].

The difference between polyols with the different carbon chain length was demonstrated in [36,76]. An increase in the carbon chain length promotes higher alkane selectivity and leads to a decrease in hydrogen selectivity.

Sugar solutions (fructose, glucose, sucrose) were tested over transition metal catalysts, such as Ni/Al_2O_3, Ni/Ce_2O-Al_2O_3, Ni/ZrO_2, Pd/Al_2O_3, Pt-Ni/Al_2O_3, Pt/Al_2O_3, Pt/Ce_2O-Al_2O_3, Pt/ZrO_2 [77]. Coke formation was identified as the main reason for catalyst deactivation. Glucose APR was studied over doped graphene [7], Pt/C [17,78], Pt/Al_2O_3 [76,79,80]. Severe degradation of glucose through side reactions was also detected over Ni/Al_2O_3 [81]. Comparably low selectivity to hydrogen was obtained during the glucose APR over carbon-supported transition metals (Pt, Pt-Ni, Pt-Ru, Pt-Sn, Pt-Ni-Sn) [14]. Lactose APR was investigated over Ni-La/Al_2O_3, Ni-Co/Al_2O_3-MgO, and Ni-La/Al_2O_3 catalysts [82,83] and an overlayer of Pt on Ni or Co on Pt [84].

The overall conclusion from studies on sugar APR is that sugars appeared to be a problematic feed due to high coke formation rates and subsequently fast catalyst deactivation. An additional step – hydrogenation of sugars – should be applied to reduce coke formation and to increase the total hydrogen production by increasing the degree of feed utilization [85].

Several attempts were made for direct biomass gasification and utilization of various biomass with minimal pretreatments. Such feedstock, as wood, cellulose, lignin and its monomers, hydrolysate of lignocellulosic biomass, are discussed below.

Direct wood gasification was performed batch-wise via combination of acid hydrolysis and APR over Pt/Al_2O_3 [80]. Pine sawdust and waste paper were found to be similar to glucose and ethylene glycol in terms of hydrogen production per mass of feed. More acidic conditions promoted hydrogen production due to more effective hydrolysis of polysaccharides.

Screening of carbon support was performed for the APR of wheat straw hydrolysate over Pt/C catalysts [57]. Various carbon supports were tested, such as activated carbon (AC), graphene oxide (GO), multi-walled carbon nanotubes (MWCNT), super-Darco carbon (SDC), and single-walled carbon nanotubes (SWCNT). The best performance was obtained with activated carbon and SWCNT, this mainly due to the large size of the polysaccharide molecules not being able to reach Pt sites located inside graphene layers. Bimetallic and trimetallic catalysts were compared in terms of activity and selectivity to hydrogen in the glucose and wheat straw hydrolysate APR [14]. The following metals and metal combinations were supported on AC and MWCNT: Pt, Pt-Ni, Pt-Ru, Pt-Sn, Pt-Ni-Sn. Wheat straw hydrolysate was more selective to hydrogen compared to glucose. Pt-Ru/AC, Pt-Ni/AC and Pt-Ru/MWCNT appeared to be the best candidates for hydrogen production among all tested catalysts. APR of kenaf hydrolysate was performed over Pt/C [86], Pt/Al_2O_3 and Ru/C [85]. Higher hydrogen production was obtained in the experiment with the hydrogenated kenaf hydrolysate compared to glucose and the non-hydrogenated hydrolysate. Optimum conditions were determined for the APR of sorghum hydrolyzate over Raney-Ni [87].

Direct conversion of cellulose arouse interest of many researchers. The degree of crystallinity was found to be crucial for hydrogen production via APR of various sources of cellulose (filter paper, degreased cotton, microcrystalline cellulose) over Pt/C [17]. At the same time, hydrogen selectivity and yield were significantly lower in the case of glucose APR. According to the same study, platinum appeared to be the best metal for cellulose conversion among the studied metals (Pt, Pd, Ni, Co and Ir). Cellulose conversion to hydrogen appeared to be slightly more efficient over Pt/Al_2O_3 than over Pt and Pt-Ru catalysts supported on carbon textile [88]. Cellulose conversion to polyols and directly to hydrogen via APR was studied over Pt/Na(H)ZSM-5 [89]. Pt/C catalyst was compared to a powdered tungsten and tungsten coated oxidized Si wafers prepared by magnetron sputtering of tungsten coating in the cellulose APR [90]. Sputtered tungsten catalyst was stable in the presence of sulphur- and nitrogen-containing compounds, being 10-fold more active

compared to Pt/C. Nickel catalysts supported on layered double oxides were found to be efficient and stable for the cellulose conversion to hydrogen [91].

Biomass hydrolysate usually contains relatively large polysaccharides, therefore certain mass-transfer limitations can take place during degradation of this feed [14]. Thus, certain unsolved problems are associated with the direct reforming of biomass.

APR of lignin and several monomers (catechol, guaiacol, methanol, phenol, syringol) was performed over Pt/ZrO_2, Pt/Al_2O_3, Pt/C, Pt/TiO_2, and Ni/C in order to propose the corresponding reaction network [52]. Phenol was tested over Ni/ZSM-5 [92,93].

Besides lignocellulosic biomass, alginate APR was performed over Pt/C focusing on the influence of operation parameters [94].

Byproducts of pyrolitic bio-oil production, such as aqueous phase and low boiling fractions of pyrolysis oil, were tested in APR. This type of feed has a large potential, since the produced hydrogen can be utilized on-site for bio-oil upgrading. An aqueous fraction of pyrolytic bio-oil was applied in APR over Pt/Al_2O_3 [95]. APR was performed with hydrogenated and not treated feed. Hydrogen selectivity obtained utilizing the hydrogenated feed was similar to the values observed during the sorbitol APR. The distillate of crude bio-oil was converted over Pt/Al_2O_3 [96,97] and Pt/CeO_2-TiO_2 and Pt/CeO_2-ZrO_2 catalysts [97]. Mixed zirconia-ceria and ceria-titania oxides were as selective to hydrogen as alumina, and showed a higher hydrothermal stability. The influence of temperature and concentration on the APR of low-boiling fraction of rice husk pyrolyzed bio-oil was investigated over Pt/Al_2O_3 [98].

APR of crude glycerol was studied over Ni/SiO_2-Al_2O_3 focusing on the feed concentration, temperature and the role of impurities [99]. A pronounced inhibition effect on hydrogen production was shown in the crude glycerol APR over Pt supported on alumina, carbon and magnesium aluminate due to formation of long chain olefins and aliphatics from sodium salts of fatty acids [51]. The role of operating conditions was thoroughly studied in the crude glycerol APR over Ni-La/Al_2O_3 catalyst [100].

The APR of waste lipids with formation of linear hydrocarbons was performed over Pt-Re/C [101].

Slightly more exotic examples are APR of cheese whey [82,83], fermentation broth [102], and tuna-cooking waste water [103]. Optimum parameters were proposed for

cheese whey valorization via APR over Ni-La/Al_2O_3, Ni-Co/Al_2O_3-MgO, and Ni-La/Al_2O_3 [82,83].

Various feed utilized for APR over carbon-supported catalysts is presented in Figure 2. Most of short-chain alcohols and polyols were tested, as well as some sugars, phenolics and complex feed, such as cellulose, plants hydrolyzates and crude glycerol. In some cases basic additives were utilized to enhance hydrogen production.

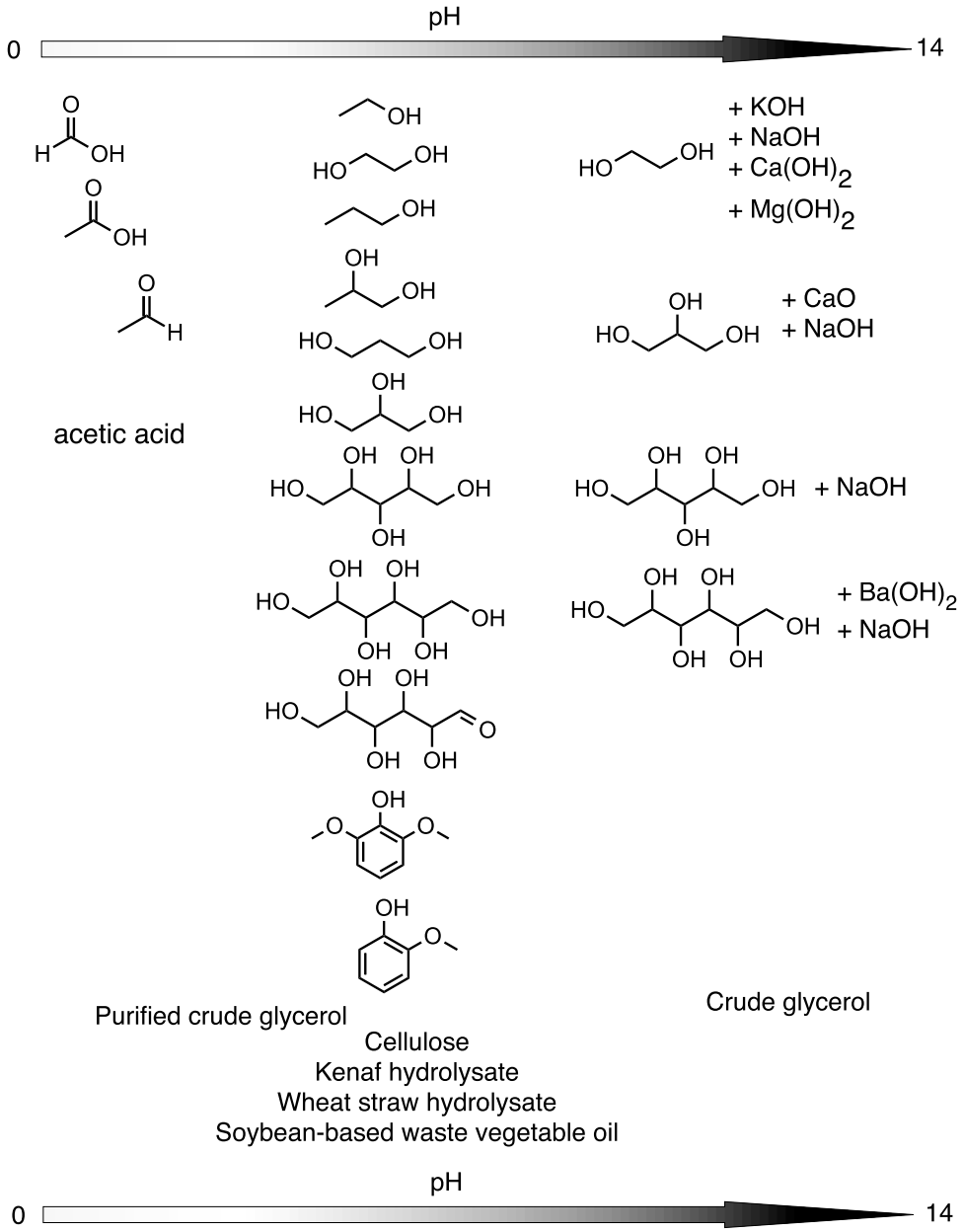

Figure 2. Feed utilized in APR over carbon-supported catalysts.

1.4. Influence of other parameters

Hydrogen mass-transfer has a large impact on product selectivity [104]. Even if this was shown for the sorbitol APR in a microchannel reactor, it should be taken as a general rule rather than an exception. An extensive description of influence of tunable parameters was provided for a three-phase reactor model [105]. The most important parameter was hydrogen pressure, which exhibited a pronounced negative effect on the reforming rate. Hydrogen produced during APR is consumed again in hydrogenation/hydrogenolysis reactions, e.g. for alkane production. Thus, the reactor type, and especially the degree of back-mixing, determines the hydrogen to alkane ratio [39,104,105]. Hydrogen can be removed from the reaction zone using a reactive-separation approach in membrane reactors [106], or hypothetically in a semi-batch reactor with an inert quenching. Moreover, dilution of hydrogen can be achieved to a certain extent in continuous reactors with a constant flow of a carrier gas. Thus, comparison of results in the literature should be done with care considering the reactor type used for generation of experimental data.

There are other parameters influencing selectivity as well. A comprehensive study on the influence of metal loading and the feed type was recently published [107,108]. The metal loading was shown to have a clear impact on hydrogen selectivity, and even on the distribution of carbon between the liquid- and gas-phase products.

Structural sensitivity is also discussed in the literature. Metal particle size could also influence the activity and selectivity of APR, however, contradictory results were obtained. Catalyst activity and hydrogen turnover frequency are increasing along with the metal particle size increase according to [55,109]. In another study [110] it was concluded that the reaction rate of the glycerol APR is not affected by changes in the Pt particle size. Total carbon conversion from the liquid to the gas phase even decreased along with the Pt particle increase in the APR of bio-oil low-boiling fraction over Pt/Al_2O_3 [96]. Product distribution was significantly affected by minor changes in metal particle size in the glycerol APR over Pt/Al_2O_3 [111].

Variations of the feed concentration was studied in the crude glycerol APR over 65% Ni/SiO_2-Al_2O_3 catalyst, showed the influence of glycerol concentration on the liquid-phase products distribution and selectivity to methane [99]. The overall reaction rate was accelerated by feed concentration increase in the glycerol APR over Pt/Al_2O_3 [112].

The effects of temperature, pressure, feed concentration and the ratio of the catalyst mass to the glycerol mass flow were studied for the APR of partially purified crude glycerol over Pt/Al_2O_3 catalyst [100]. The results indicated that the product distribution can be significantly affected by the operation variables.

The overall reaction rate is increasing along with temperature increase within a certain range of temperatures. Some insights of temperature influence, such as a minor difference in product composition, were provided in a kinetic model of sorbitol APR [113].

Selectivity to hydrogen and CO_2 exhibited maxima at an optimal pressure at a bubble point region in the *n*-butanol reforming over Ni/CeO_2 and Ni/Al_2O_3 catalysts [114].

Neira d'Angelo et al. [38] showed that APR is an easily tunable process. Application of a physical mixture of Pt/C and Ru/C allowed production of methane and CO_2 from sorbitol with corresponding selectivity of 46 and 47% and traces of the liquid-phase products. Those numbers can be compared to corresponding selectivity to methane, CO_2 and the liquid-phase carbon of 28, 50 and 20% obtained over Ru/C, and 5, 40 and 52% over Pt/C. This clearly indicates that APR can be directly utilized in combination with fuel cells for electricity production without any demanding steps.

APR has a strong industrial potential, allowing hydrogen and alkane production at moderate temperatures and pressure from technical grade feedstock. However, additional research is required for further implementation of APR. The insights, provided in this work, could probably promote further development of this technology.

2. Experimental

2. Experimental

2.1. Chemicals

Xylitol, sorbitol, glycerol, propanol-1 and propane-1,2-diol were obtained from Sigma-Aldrich.

A technical mixture of sorbitol and mannitol was produced by hydrogenating an aqueous solution (50 wt%) of beet sucrose (a food grade sugar purchased from a local food market in the Netherlands) in a trickle bed reactor over 5 wt% Ru/C (KaiDa, Shaanxi, China) catalyst at 453 K. The details of hydrogenation can be found in [**IV**].

2.2. Catalysts

Various mono- and bimetallic catalysts were investigated in the current study. A summary of the experiments is shown in Table 1.

In particular, a commercial Pt/Al_2O_3 provided by Sigma–Aldrich was applied for sorbitol [**I**, **VI**] and galactitol [**I**] APR.

Pt/PBSAC catalyst supported on a polymer-based spherical activated carbon was studied in the APR of 1,2-propanediol [**II**, **VII**], propanol-1, glycerol [**II**], and sorbitol. The catalyst was prepared via an ion exchange according to the method described in [67]. More details about catalyst preparation are given in [**II**].

Performance of Pt/AC-JM2 and Pt/AC-JM3 catalysts supported on activated carbon was studied in the APR of xylitol [**III**, **V**], sorbitol [**IV**] and technical polyols [**IV**]. Both catalysts were provided by Johnson Matthey.

Pt/AC-1 and Pt/AC-4 catalysts were prepared via incipient-wetness impregnation of activated carbon support from Merck and were utilized for the APR of technical polyols [**IV**]. The details of preparation are given in [**IV**].

A set of Pt/Sib, Ni/Sib, Pt-Ni/Sib, Re/Sib, Pt-Re/Sib, Ru/Sib, Pt-Ru/Sib, and Pt-Co/Sib catalysts was prepared by wetness incipient impregnation of a mesoporous carbon Sibunit (Sib) with aqueous solutions of corresponding metal precursors. Catalysts were investigated in the xylitol APR [**III**]. A detailed description of the support pretreatment and catalyst preparation can be found in [**III**].

Table 1. An overview of experiments performed in this work.

Catalyst	*Nominal metal loading [%]*	*Support*	*Feed, concentration**	*T red/**re-red**** [K]*	*Publication*
Pt/Al_2O_3	1	γ-Al_2O_3	sorbitol, 36 g in 1 L	n.a./**523**	[**I**], [**VI**]
Pt/Al_2O_3	1	γ-Al_2O_3	galactitol, 36 g in 1 L	n.a./**523**	[**I**]
Pt/Al_2O_3	1	γ-Al_2O_3	mixture of sorbitol and galactitol, 1:1, 36 g in 1 L	n.a./**523**	[**I**]
Pt/PBSAC	0.5	PBSAC	1,2-propanediol, 50 g in 1 L	-/**523**	[**II**], [**VII**]
Pt/PBSAC	0.5	PBSAC	propanol-1, 50 g in 1 L	-/**523**	[**II**]
Pt/PBSAC	0.5	PBSAC	glycerol, 50 g in 1 L	-/**523**	[**II**]
Pt/PBSAC	0.5	PBSAC	sorbitol, 50 g in 1 L	-/**573**	-
Pt/AC-JM2	2.5	AC	xylitol, 100 g in 1 L	n.a./**523**	[**III**], [**V**]
Pt/AC-JM3	2.5	AC	sorbitol, 50 g in 1 L	n.a./**573**	[**IV**]
Pt/AC-JM3	2.5	AC	technical polyols, 4.6 wt%	n.a./**573**	[**IV**]
Pt/AC-JM3	2.5	AC	technical polyols, 29 wt%	n.a./**573**	[**IV**]
Pt/AC-1	2.5	AC	technical polyols, 15.3 wt%	523/-	[**IV**]
Pt/AC-4	2.5	AC	technical polyols, 5.6 wt%	523/-	[**IV**]
Pt/Sib	3	Sibunit	xylitol, 100 g in 1 L	579/**523**	[**III**]
Ni/Sib	3	Sibunit	xylitol, 100 g in 1 L	613/**523**	[**III**]
Re/Sib	3	Sibunit	xylitol, 100 g in 1 L	586/**623**	[**III**]
Ru/Sib	3	Sibunit	xylitol, 100 g in 1 L	627/**523**	[**III**]
Pt-Ni/Sib	6/(3Pt:3Ni)	Sibunit	xylitol, 100 g in 1 L	613/**503**	[**III**]
Pt-Re/Sib	6/(3Pt:3Re)	Sibunit	xylitol, 100 g in 1 L	603/**523**	[**III**]
Pt-Ru/Sib	6/(3Pt:3Ru)	Sibunit	xylitol, 100 g in 1 L	623/**523**	[**III**]
Pt-Co/Sib	6/(3Pt:3Co)	Sibunit	xylitol, 100 g in 1 L	627/**523**	[**III**]

* - feed concentration is indicated in grams of feed dissolved in 1 L of deionized water, or in weight percent;

** - *T red* indicates reduction temperature, ***T re-red*** in **bold** – indicates temperature of the re-reduction *in-situ,* performed in the continuous reactor prior to the beginning of the experiment.

2.3. Catalysts characterisation

Physicochemical properties of catalysts were identified by various techniques summarized in Table 2. The abbreviations in Table 2 are explained below in the text.

Table 2. Summary of catalysts characterization.

Catalyst/ Method	*Nominal metal loading [wt%]*	*BET*	*CO-chem*	*NH_3-des*	*TPR*	*TG-DTA-MS*	*TPD*	*TPO*	*TEM*	*EDX*	*XPS*	*XRD*	*XRF*	*ICP*
Pt/Al_2O_3	1	-	[**I**]	-	[**I**]	-	-	-	-	-	-	-	-	-
Pt/ PBSAC	0.5	[**II**], [**VII**]	[**II**]	-	[**II**]	-	[**II**]	[**II**]	[**II**]	-	-	-	[**II**]	[**II**]
Pt/AC-JM2	2.5	[**V**]	[**V**]	[**III**], [**V**]	[**V**]	-	-	-	[**III**], [**V**]	-	-	-	[**V**]	-
Pt/AC-JM3	2.5	[**IV**]	[**IV**]	[**IV**]	[**IV**]	-	-	[**IV**]	[**IV**]	-	-	-	[**IV**]	[**IV**]
Pt/AC-1	2.5	-	[**IV**]	-	-	-	-	[**IV**]	-	-	-	-	-	[**IV**]
Pt/AC-4	2.5	-	[**IV**]	-	-	-	-	[**IV**]	-	-	-	-	-	[**IV**]
Pt/Sib	3	-	-	[**III**]	-	[**III**]	-	-	[**III**]	-	[**III**]	-	[**III**]	-
Ni/Sib	3	-	-	[**III**]	-	[**III**]	-	-	[**III**]	-	-	-	-	-
Re/Sib	3	-	-	[**III**]	-	[**III**]	-	-	[**III**]	-	[**III**]	[**III**]	[**III**]	-
Ru/Sib	3	-	-	[**III**]	-	[**III**]	-	-	[**III**]	-	[**III**]	-	[**III**]	-
Pt-Ni/Sib	3+3	-	-	[**III**]	-	[**III**]	-	-	[**III**]	[**III**]	[**III**]	-	[**III**]	-
Pt-Re/Sib	3+3	-	-	[**III**]	-	[**III**]	-	-	[**III**]	-	-	[**III**]	[**III**]	-
Pt-Ru/Sib	3+3	-	-	[**III**]	-	[**III**]	-	-	[**III**]	-	[**III**]	-	-	-
Pt-Co/Sib	3+3	-	-	[**III**]	-	[**III**]	-	-	[**III**]	-	[**III**]	-	-	-
Sibunit		[**III**]		[**III**]										
AC (Merck)		[**IV**]		-										

- ***Nitrogen physisoption (BET)***

The textural properties of the supports [**III**, **IV**], fresh and spent Pt/PBSAC and Pt/AC (JM2 and JM3) catalysts [**II**, **IV**, **V**] were determined using the Brunauer-Emmett-Teller equation by physisorption of nitrogen at 77 K on ASAP-2400 (Micromeritics), Quadrasorb SI and Autosorb iQ/ASiQwin (Quantachrome) instruments.

- ***CO chemisorption (CO-chem)***

The platinum dispersion on the fresh Pt/Al_2O_3, Pt/PBSAC, Pt/AC-1, Pt/AC-4, and Pt/AC (JM2 and JM3) catalysts was evaluated by CO pulse chemisorption (Micromeritics, AutoChem 2900 and AutoChem II) [**I**, **II, IV**].

- ***Ammonia desorption (NH_3-des)***

Acidity of Sibunit-supported catalysts, the support, and the commercial Pt/AC (JM2 and JM3) catalysts was studied by NH_3 temperature-programmed desorption (TPD) on a pulse chemisorption apparatus (Micromeritics, AutoChem 2900) [**III, IV**]. The detailed experimental procedure is described in [55].

- ***Temperature-programmed reduction (TPR)***

Reduction of Pt/Al_2O_3, Pt/PBSAC, Pt/AC-JM2, and Pt/AC-JM3 catalysts was studied in 5% H_2 (Ar) using AutoChem 2900 instrument [**I**, **II, IV, V**].

- ***Thermo-gravimetric differential thermal analysis combined with mass-spectrometry (TG-DTA-MS)***

Sibunit-supported catalysts were studied by TG-DTA-MS analysis performed in argon or hydrogen atmosphere on a Netzsch STA 409 PC equipped with a mass spectrometer SRS UGA 200 [**III**].

- ***Temperature-programmed desorption and oxidation (TPD and TPO)***

TPD and TPO analysis of fresh and spent Pt/PBSAC catalysts was performed with a NETZSCH STA 409 PC instrument [**II**]. The catalysts were heated up to 1273 K (heating rate 5 K/min) in nitrogen or air flow. Fresh and spent Pt/AC-1 and Pt/AC-4 catalysts were studied in air by thermo-gravimetric analysis combined with differential scanning calorimetry (TGA-DSC) performed with SDT Q600 V8.3 thermal analyzing instrument at a heating rate of 5 K/min up to 1173 K [**IV**].

- Transmission electron microscopy (TEM)

The size and the structure of metal particles were studied by transmission electron microscopy (TEM). Both fresh and spent catalysts were characterised on a JEM-2010 microscope (JEOL, Japan). Sibunit-supported Pt, Ni, Pt-Ni, Re, Pt-Re, Ru, Pt-Ru, and Pt-Co catalysts are described in [**III**]. Fresh and spent Pt/C catalysts supported on PBSAC and activated carbon are described in [**II**-**V**].

- Energy-dispersive X-ray spectroscopy (EDX)

EDX analysis was used for determination of metal particle composition of Pt-Ni/Sib catalyst [**III**]. Local elemental analysis was performed using an energy-dispersive X-ray (EDX) spectroscopy with a Phoenix spectrometer (EDAX, USA) equipped with a Si(Li) detector.

- X-ray photoelectron spectroscopy (XPS)

XPS studies were performed for Sibunit-supported Pt, Re, Ru, Pt-Ni, Pt-Ru, and Pt-Co catalyst [**III**]. XPS spectra were recorded using SPECS spectrometer with PHOIBOS-150-MCD-9 hemispherical energy analyzer and X-ray monochromator FOCUS-500. The influence of the reduction conditions, such as the heating rate and the final reduction temperature, was studied.

- X-ray powder diffraction (XRD)

XRD was employed in order to verify a complete reduction of metal supported on Sibunit [**III**]. XRD patterns were recorded with the X-ray diffractometer D8 (Bruker, Germany) and LynxEye detector.

- X-ray fluorescence (XRF)

XRF was used to determine the metal content for Sibunit-supported Pt, Re, Ru, Pt-Ni and Pt-Re catalysts [**III**], and Pt/AC-JM2 [**V**]. A semiquantitative analysis was performed using wavelength dispersive X-ray fluorescence (WDXRF) spectrometry with the powder pellet method.

- Inductively coupled plasma optical emission spectrometry (ICP)

Metal concentration in the fresh Pt/PBSAC and fresh/spent Pt/AC-JM3, Pt/AC-1 and Pt/AC-4 catalysts was determined with ICP optical emission spectrometry (Ciros CCD, Spectro Analytical Instruments) [**II, IV**].

2.4. Catalytic experiments

Aqueous-phase reforming was performed in continuous [**I-VII**] and batch-wise [**IV**] modes.

- Continuous reactor

The catalytic tests were performed in a downflow continuous lab-scale fixed-bed reactor. The experimental setup is shown in Figure 3. The catalyst was placed in the middle of a stainless-steel reactor tube between two layers of sand. The pristine catalyst was applied in [**I**, **II**, **VI**, **VII**], or it was diluted with quartz sand in [**III-V**]. The reactor was located in a furnace and connected to nitrogen (1% He) and hydrogen gas lines, the feed solution inlet and the gas/liquid outlet line. An aqueous solution of the feed was fed via an HPLC pump. Gas-liquid separation took place in a T-shape connector after cooling in a metal spring tube. There was no need in special cooling or any gas-liquid separating equipment, due to constant nitrogen co-feeding during the reaction (flow varied from 20 to 30 ml/min, STP). The liquid samples were periodically taken via a sampling loop for an offline HPLC analysis, while the gas samples were analyzed online by means of Micro-GC. Total organic carbon analysis of the liquid phase was carried out to control the carbon balance in almost all experiments.

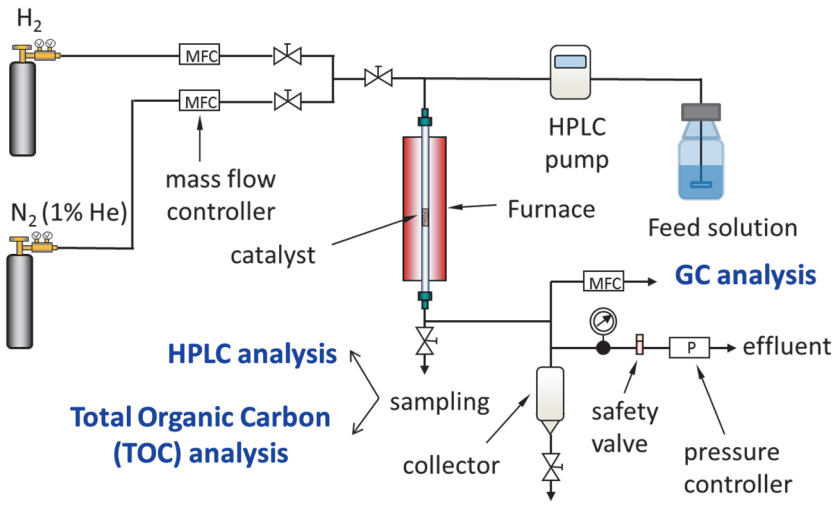

Figure 3. Experimental set-up for aqueous phase reforming.

The catalysts were additionally reduced *in situ* prior to the experiments in hydrogen flow (40 ml/min, STP). The following program was used: flushing with nitrogen, heating in a hydrogen flow from room temperature to 250-350°C with the rate 5°C/min, dwelling for 2 hours, cooling to the operating temperature. Residual hydrogen was removed by flushing with N_2 (25 ml/min, STP) for 20 min.

Evaluation of catalytic activity was performed at 498 K and 29.7 bar. The flow rate ranged from 0.1 to 2 ml/min. The same flow rate was kept for at least 4 hours in order to reach the steady state. Catalysts deactivation was tested by repeating the same flow rate (usually 0.2 ml/min) in between the others.

- Methanation and WGS

Additional studies of methanation and water-gas shift (WGS) were performed over the Pt-Re/Sib catalyst (0.5 g, diluted with quartz sand 1:1) at 498 K and 25 bar [**III**]. Water (0.2 ml/min) was fed together with CO (8 ml/min, STP), hydrogen (8 ml/min, STP), and nitrogen (8 ml/min, STP) in the methanation experiment, which lasted for 15 hours. Thereafter the hydrogen flow was stopped, and CO flow was increased to 16 ml/min (STP) for the next 6 hours during the WGS experiment.

- Batch reactor

APR of the technical feed was performed in an autoclave (300 ml), made from Hasteloy [**IV**]. The autoclave is equipped with a heating/cooling jacket, gas inlet and outlet, an internal thermocouple. A conventional propeller stirrer was applied for an experiment with the powder catalyst Pt/AC-1 and a blank test, while a cage reactor was used for the experiment with the Pt/AC-4 catalyst. The cage reactor is made from two perforated cylinders assembled together with two round holders, in a way that the space in between these cylinders is filled with the catalyst. Water was continuously circulated through this construction, being sucked by built-in impellers from the top and bottom holes, coming out from the holes of the external cylinder. An average hole diameter is 0.9 mm.

Catalytic tests were performed at 498 K and at 30 bar initial N_2 pressure, and the stirring rate of 1000 rpm was applied. The feed and the catalyst were loaded, then the reactor was closed and flushed 10 times with nitrogen. An external cylinder for gas collection was attached to the system. After pressurizing to 30 bars and sealing, the reactor heating was started with a heating rate 5 K/min. The stirring (200 rpm) started

at the same moment. The zero-time of the reaction was taken at the moment, when the temperature reached 498 K, and the stirring rate was increased to 1000 rpm. The reaction was stopped after 2 hours by reducing the stirring rate to 200 rpm, and cooling down the reactor with cold water from the tap. Gas and liquid samples were taken at the moment, when the reactor temperature reached 293-303 K.

2.4.1. Analysis of products

GC, HPLC and TOC analysis was performed to quantify product composition and yields.

Gas products were quantitatively analysed online in the continuous experiments [**I-VII**] by a micro-GC (Agilent Micro-GC 3000A) equipped with four columns: Plot U, OV-1, Alumina and Molsieve. Offline analysis was performed for gas samples collected in the batch experiments [**IV**] by an Agilent Technologies 7890A instrument equipped with JW CP8713 column and TCD detector.

The analysis of the liquid-phase products was performed offline in all experiments by HPLC (Agilent 1100) equipped with an Aminex HPX-87H column, which was quantitatively calibrated for the anticipated reaction products (external standard method). The analysis was performed at 45°C under isocratic conditions and flow rate 0.6 ml/min. The mobile phase consisted of 5 mM H_2SO_4 water solution. The products were analyzed by using a refractive index detector (RI). Peak identification was based on retention times.

Total organic carbon was measured in the liquid samples to determine the total carbon balance in [**I-III**, **V-VII**], CHN analyzer was applied in [**IV**].

Additional analytical methods, such as spiking and GC-MS, were also applied in publications [**I**, **II**, **VII**].

Eighty-nine substances were used in a spiking technique for additional improvement of the confidence of identification in [**I**]. Peak fitting was applied to increase the accuracy of quantification, because of the poor resolution of most the peaks, corresponding to polyols and sugars. A fitting procedure was performed by the data-analysing software OriginPro 9.0 [115]**.**

GC-MS analysis of the organic extracts from the liquid samples was performed in [**II, VII**]. The samples were frozen just after sampling. Prior to analysis they were

defrosted, and organic compounds were extracted with hexanol. Extracts were dried with $CaSO_4$ and analysed using a Hewlett Packard 6890/5973 gas chromatograph coupled to mass selective spectrometer detector. The GC was equipped with an Agilent 19091J-002 capillary column 25 m in length, 0.20 mm internal diameter and 0.11 μm film thickness. Helium was used as a carrier gas. The temperature program consisted of initial holding at 310 K for 5 min, followed by heating to 383 K with 3 K/min and then to 503 K with 20 K/min with the final holding for 2 min.

2.4.2. Calculations

The following equations were used to quantify the results of experiments.

Conversion of the substrates was calculated as:

$$Conversion\ (\%) = \frac{C_{feed\ in} - C_{feed\ out}}{C_{feed\ in}} \cdot 100\%\ , \qquad (1)$$

where $C_{feed\ in}$ – input feed concentration [mol/L], $C_{feed\ out}$ – output feed concentration [mol /L].

Carbon conversion to the gas phase is defined in the following way:

$$Carbon\ conversion\ (\%) = \frac{\nu(CC_{gas})}{\nu(CC_{feed\ in})} \cdot 100\%\ , \qquad (2)$$

where $\upsilon(CC_{gas})$ – the total amount of carbon in all gas-phase products (CO_2, CO and alkanes) or the corresponding molar carbon flow [mol C or mol C/min], $\upsilon(CC_{feed\ in})$ – the total amount of carbon in the input feed or the corresponding molar carbon flow [mol C or mol C/min].

For alkanes, CO_2, CO and products in the liquid phase selectivity was calculated in the following way:

$$Selectivity\ to\ product\ X(\%) = \frac{\upsilon(CC_X)}{\upsilon(CC_{gas})} \cdot 100\%\ , \qquad (3)$$

where $\upsilon(CC_x)$ – carbon, contained in a product X, or the corresponding carbon flow [mol C or mol C/min].

An additional parameter, namely so-called reforming ratio *RR* (H_2/CO_2) was introduced to calculate the selectivity to hydrogen, since hydrogen is produced both from the polyol and via the water-gas shift (WGS) reaction. RR calculation for

1,2-propanediol and propanol-1 can be found in [**II**], RR for glycerol ($C_3H_8O_3$), xylitol ($C_5H_{12}O_5$) and sorbitol/mannitol/galactitol ($C_6H_{14}O_6$) is shown below:

$C_3H_8O_3 \longrightarrow 3CO + 4H_2 \xrightarrow{+3H_2O} 3CO_2 + 7H_2$ RR=7/3

$C_5H_{12}O_5 \longrightarrow 5CO + 6H_2 \xrightarrow{+6H_2O} 5CO_2 + 11H_2$ RR=11/5

$C_6H_{14}O_6 \longrightarrow 6CO + 7H_2 \xrightarrow{+6H_2O} 6CO_2 + 13H_2$ RR=13/6

Selectivity to hydrogen is defined in the following way:

$$Selectivity\ to\ H_2(\%) = \frac{v(H_2)}{v(CC_{gas})} \cdot \frac{1}{RR} \cdot 100\%\ , \tag{4}$$

where $v(H_2)$ – amount of H_2 formed, or the corresponding flow rate [mol or mol/min], and *RR* is the reforming ratio.

The yield to the liquid products is determined by

$$yield\ (\%) = \frac{C_X}{C_{feed\ in}} \cdot 100\%\ ; \tag{5}$$

where C_X is concentration of the product X in the sample [mol/L].

The molar flow of carbon $v(CC_X)$ is determined as:

$$v(CC_X) = C_X \cdot v \cdot n, \tag{6}$$

where v – volumetric flow [L/min]; n – number of carbon atoms in the substance X.

Turnover frequency for xylitol transformation TOF(xyl) and for H_2 production TOF(H_2) was defined per mol of the surface metal atom. In the case of bimetallic catalysts only Pt loading was taken into account. TOF_{xyl} is calculated as:

$$TOF(xyl) = \frac{\nu_{xyl\ in} - \nu_{xyl\ out}}{D \cdot m_{cat} \cdot c_M \cdot M_M}\ , \tag{7}$$

where $\upsilon_{xyl\,in}$ is the input molar flow of xylitol [mol/min], $\upsilon_{xyl\,out}$ is the output molar flow of xylitol [mol/min], D is the metal dispersion, m_{cat} is the catalyst loading [g], c_M is the metal loading, M_M is the molar mass of metal.

Turnover frequency for H_2 is determined as:

$$TOF(H_2) = \frac{\nu_{H_2}}{D \cdot m_{cat} \cdot c_M \cdot M_M}, \tag{8}$$

where υ_{H2} is hydrogen molar flow [mol/min].

3. Results and Discussion

3. Results and Discussion

3.1. Catalysts characterisation

Various analytical techniques were applied for catalysts characterization, including adsorption methods, thermal analysis, electron microscopy, spectroscopies. The structural and textural properties of the catalysts, Sibunit, and activated carbon from Merck are described in Tables 3 and 4. Some properties are shown for both fresh and spent catalysts.

- CO chemisorption and TEM

TEM pictures are presented in [**II**-**V**], and the metal particle distribution is shown in Table 3.

According to TEM analysis, Pt/PBSAC contained two main types of unevenly distributed platinum particles: smaller from 1 to 3 nm, and larger ones from 10 to 15 nm [**II**]. The size of some platinum clusters does not even exceed 0.3 nm, which is comparable with the fine microtexture of carbon support formed by the walls (or probably channels) having a width of ca. 0.3–0.5 nm. This complicates analysis of TEM data because such clusters could be then masked by carbon.

Metal dispersion of Pt decreased by half in PBSAC-supported catalyst after APR of C3-alkohols [**II**] according to CO-chemisorption (Table 3). However, TEM analysis of spent catalysts and high activity in terms of TOF [55] excludes sintering. Contradiction between CO-chemisorption and TEM measurements is typically explained by coking, when the substrate catalytic activity deteriorates, while selectivity is constant [116].

TEM analysis of the fresh Pt/AC-JM2 catalyst confirmed the mean particle size of Pt (d_m = 2.1 nm) to be rather close to the number obtained by CO chemisorption [**V**]. The Pt nanoparticles found by TEM in the spent sample are characterized with a semispherical shape practically without any clearly detectable crystallographic planes. The spent sample is characterized with the mean size of Pt nanoparticles d_m = 1.7 nm (Table 3), close to the mean surface size d_s = 1.8 nm, demonstrating high resistance of Pt NPs to sintering.

The metal particle size of the fresh Pt/AC-JM3 catalyst determined by CO-chemisorption (22.6 nm) is in clear disagreement with the TEM analysis of a fresh

sample (average size of 1.7 nm). Comparison of CO chemisorption and TEM is far from being straightforward in the cases when metal clusters of different sizes are present on the catalyst surface, as the former method gives an average value, while some large clusters could be easily overlooked in the latter technique.

Table 3. Structural properties of catalysts.

Catalyst/ Method	*CO-chem*		*TEM*			
*Fresh/**spent****	*D, [nm]*	*Dispersion, [%]*	*D_n**, [nm]*	*D_s***, [nm]*	*SD, [nm]*	*Dispersion, **** [%]*
Pt/Al_2O_3	2.2	52	-	-	-	-
Pt/PBSAC	5.5/ **10.6**	20.5/**10.7**	n.a./**1.3**	n.a./**1.4**	-	-
Pt/AC-JM2	2.6	43	2.05/**1.7**	2.1/**1.8**	0.6/**0.3**	20.1
Pt/AC-JM3	22.6	5	1.7	-	-	-
Pt/AC-1	8.0	14	-	-	-	-
Pt/AC-4	8.1	14	-	-	-	-
Pt/Sib	-	-	0.9/**1.2**	1/**1.2**	0.2/**0.2**	45.8
Ni/Sib	-	-	7.7/**n.a.**	8.6/**n.a.**	1.9/**n.a.**	13.1
Re/Sib	-	-	< 0.5/**0.7**	< 0.5/**0.7**	0.1/**0.1**	82.5
Ru/Sib	-	-	1/**1.2**	1.1/**1.3**	0.1/**0.2**	41.2
Pt-Ni/Sib	-	-	Pt 1.2/**1.2** Ni 8.5/**n.a.**	-	Pt 0.2/**0.2** Ni 1.4/**n.a.**	Pt 34.4 Ni 11.9
Pt-Re/Sib	-	-	1.1/**n.a.**	1.1/**n.a.**	0.2/**n.a.**	37.5
Pt-Ru/Sib	-	-	1.3/**1.4**	1.6/**1.5**	0.4/**0.3**	31.7
Pt-Co/Sib	-	-	1.3/**1.3**	1.5/**1.4**	0.3/**0.2**	31.7

* - values for fresh samples are given in regular font, for **spent** – in **bold**;

** - D_s is surface average diameter. $D_s = \frac{\Sigma n_i \cdot d_i^3}{\Sigma n_i \cdot d_i^2}$, where *n* is number of particles, and *d* is particle diameter;

*** - D_n is number average diameter, $D_n = \frac{\Sigma n_i \cdot d_i}{\Sigma n_i}$;

**** - dispersion of metals was calculated based on metal particle diameters obtained from TEM measurements for fresh catalysts. The details are provided in [**III**].

All Sibunit-supported catalysts have well-dispersed metal particles with some areas of agglomerations [**III**]. The medium particle size is close to 1 nm, except for Ni/Sib (d_m = 7.7 nm). Pt-Ni/Sib catalyst showed a distinct bimodal distribution with noticeably smaller Pt and bigger Ni species. According to TEM measurements, the size of the metal particles slightly increased after xylitol APR in the case of Pt/Sib, Ru/Sib, Pt-Re/Sib, and Pt-Ru/Sib catalysts.

Calculation of the metal dispersion for the fresh Sibunit-supported catalysts was based on TEM measurements [**III**].

- Nitrogen physisoption (BET)

The surface area of catalysts and carbon supports varied significantly (Table 4). Mesoporous carbon Sibunit support has a surface area of 247 m^2/g, the external surface area is 60 m^2/g, and the total pore volume is 0.24 cm^3/g. Sibunit has a mesopourous structure with a small volume of micropores. The surface area of activated carbon from Merck is 927 m^2/g. PBSAC has a surface area of 2104 m^2/g.

No major changes of the surface area and the metal loading were observed after APR of xylitol and 1,2-propanediol over Pt/PBSAC and Pt/AC-JM2 catalysts.

- Ammonia desorption

Ammonia desorption curves are presented in the paper [**III**]. An insignificant amount of ammonia was detected during desorption from the bare support Sibunit. For the catalysts the amount of acid sites varied from 5 to 12 μmol NH_3/g catalyst depending on the active metal (Table 4). Pt-Ni/Sib and Pt/AC-JM2 catalyst had a noticeably higher number of acid sites being able to adsorb respectively 29.3 and 21.3 μmol NH_3/g catalyst. The desorption energy of ammonia is close to 40-50 kJ/mol*K for all catalysts except for Ru/Sib, Pt-Ru/Sib, and Pt/AC-JM2. This value is consistent with the earlier reported values for Pt/C and Pt/Sib in the range of 45-54 kJ/mol*K [55].

- XRF and ICP

No significant Pt leaching was detected by XRF and ICP for Pt/PBSAC, Pt/AC-JM2, Pt/AC-1, and Pt/AC-4 catalysts (Table 4).

Table 4. Textural and structural properties of catalysts and Sibunit.

Catalyst/ Method	*BET*		*NH_3-des*		*XRF*	*ICP*
*Fresh/**spent****	*Surface area, BET [m^2/g]*	*total pore volume [cm^3/g]*	*E des [kJ/mol* K]*	*Acidity [μmol NH_3/g catalyst]*	*Metal content, [wt%]*	*Metal content, [wt%]*
Pt/Al_2O_3	-	-	-	-	-	-
Pt/PBSAC	2104/ **2107**	1.52/**1.54**			0.47/**0.46**	0.46
Pt/AC-JM2	951/ **1150**	0.8/**0.82**	32.0 [III] 37.0 [V]	21.9	2.5/**2.5**	-
Pt/AC-JM3	963	0.83	40.1	41.7	2.5	-
Pt/AC-1	-	-	-	-	-	2.4/**2.4**
Pt/AC-4	-	-	-	-	-	2.7/**2.5**
Pt/Sib	-	-	40.8	5.2	2.9	-
Ni/Sib	-	-	38.0	7.5		-
Re/Sib	-	-	30.0	5.9	2.9	-
Ru/Sib	-	-	50.7	11.7	3.73	-
Pt-Ni/Sib	-	-	39.0	29.3	3.0 Pt 3.1 Ni	-
Pt-Re/Sib	-	-	42.8	6.7	3.0 Pt 3.0 Re	-
Pt-Ru/Sib	-	-	28.0	7.9	-	-
Pt-Co/Sib	-	-	46.3	12.5	-	-

* - values for fresh samples are given in regular font, for spent – in **bold**;

- EDX

EDX spectroscopy was used to analyze Pt/Sib and Ni/Sib catalysts. The images can be found in the publication [**III**]. No major impurities were found.

- TPR and TG-DTA-MS

All catalysts except Pt/PBSAC, Pt/AC-1, and Pt/AC-4 were reduced twice: during the preparation procedure and directly in the reactor prior to the experiment. The reduction temperature was based on the TPR and TG-DTA-MS analyses performed correspondingly in 5% and 15% H_2/Ar atmosphere. TPR curves are presented in [**I**, **II**, **IV**, **V**], and TG-DTA-MS curves can be found in [**III**].

- Thermogravimetric studies

The TPD and TPO curves obtained for Pt/PBSAC can be found in [**II**]. Both fresh and spent in 1,2-propanediol APR samples are displaying just minor changes during TPD in nitrogen: the total weight loss is less than 4%. In both cases weak surface groups are desorbed at temperatures higher than 890 K. The spent sample is showing an additional peak at 630 K, which can be explained by formation of condensation products during the reaction. Carbon support was completely oxidized during TPO analysis in the air. However, additional peaks at 700 and 790K appeared in the spent sample confirming formation of condensation products.

The TGA/DTG/DSC plots obtained for Pt/AC-1 and Pt/AC-4 samples are presented in [**IV**]. Both fresh and spent in technical polyol APR samples were analysed in air flow (TPO). Both fresh catalysts underwent a substantial mass loss (12-15%) at temperatures from 573 up to 653 K, attributed to the losses of the weakest surface groups through decarboxylation [117]. The Pt/AC-1 exhibited another sharp mass loss (28%) at 733 K, while Pt/AC-4 was slowly oxidized in a temperature range from 627 to 813 K with 20% mass loss. The final period of carbon support burning appeared at 733-893 K, when the support was burnt completely.

The studies of spent Pt/AC-1 and Pt/AC-4 catalysts revealed a presence of highly exothermic mass losses (3-15%) occurred at 393-453 K, attributed to catalytic oxidation of some unknown products, since sorbitol and mannitol oxidation occurs at 623 and 638 K correspondingly [118–120]. Another additional exothermic mass loss occurring in the spent catalysts at 663-673 K is currently challenging to explain due to complexity of the processes taking place in the system.

Activated carbon are in general not very stable at temperatures higher than 673 K. Autoignition of activated carbon occurred during treatment with hot air at 725 K [121]. The losses of surface groups (573-673 K) and subsequent carbon skeleton decomposition (above 673 K) were detected during TPO of activated carbon prepared from Babassu palm petiole [117]. In addition, it was shown that the neat support (Vulcan carbon black) is significantly more thermally stable than the corresponding Pt/C impregnated catalyst with high metal loadings (20-46 wt%) [122–125]. Similar results were obtained for Pt/C catalyst (1-2 wt%), supported on activated carbon [126]. At the same time, the expected temperature of coke burning is above 873 K [113]. TPO/DSC cannot be considered as an effective method for investigation of coke formation over Pt supported on activated carbon due to low stability of the support. However, it could be applied for an approximate estimation of adsorbed initial feed and products from the liquid phase.

- XPS and XRD

Fresh and spent Pt/Sib, Ni/Sib, Pt-Ni/Sib, and Re/Sib catalysts were analysed by XPS in order to identify the electronic state of metals presented mainly on the surface of tested materials. XPS deconvolved spectra can be found in the publication [**III**]. Catalysts were reduced prior to the analysis at temperatures mentioned in Table 1. According to the XPS data all reduced catalysts contained metal in mixed oxidation states. No significant shifts were observed for binding energies of Pt^0 or Pt^{x+} after addition of a second metal, such as Ni or Co, indicating an absence of interactions between metals. However, a 0.2 eV shift to higher binding energy value was found in Pt-Ru for Pt^{4+}, which can be attributed to strong interactions between Pt and Ru.

The bimetallic catalyst Pt-Co/Sib has lost almost all cobalt during the APR experiment, while the signal of Ni_{2p} is similar for the fresh and used Pt-Ni/Sib samples, indicating almost no leaching of Ni.

Re/Sib catalyst contains Re in a high oxidation state along with metallic rhenium according to XPS data. However, high dispersion of Re particles led to overlapping with carbon reflections, therefore additional XRD measurements were carried out to identify the crystal phase [**III**]. XRD patterns of this sample showed presence of Re only in the reduced stated as neither Re oxides, nor $HReO_4$ phase were visible. Similar Re reflections were observed for Re/Sib reduced at 591 and 645 K. XPS results can be

rationalized by existence of well-dispersed Re in higher oxidation states which cannot be detected by XRD.

3.2. Catalytic performance: mass-transfer limitations [III, IV]

Diffusion between liquid and solid phases and within the solid phase could have a major impact on reaction rates estimation. External mass transfer (diffusion through the film surrounding catalyst particles) is usually negligible at high temperatures [127]. Internal mass-transfer limitations reflect diffusion inside the pores. Comparison of intrinsic activity for catalysts prepared with different supports is accurate, when diffusion is faster compared to the kinetics. The absence of internal mass-transfer limitations was evaluated by calculating the Weisz-Prater criterion Φ_{WP} [128]. Such analysis requires estimation of this criterion, defined as:

$$\Phi_{WP} = \frac{r_{w,p}^{obs} \cdot \rho_{cat} \cdot r_p^2}{D_e \cdot C_s}, \quad (9)$$

where $r_{w,p}^{obs}$ is the observed reaction rate per kg of catalyst [mol/s*kg cat], ρ_{cat} is the catalyst density [kg/m^3], r_p is the catalyst particle radius [m], D_e is the effective diffusion coefficient [m^2/s], and C_s is the surface feed concentration [mol/m^3].

For a zero-order reaction Φ_{WP} should be lower than 6, for a first-order lower than 0.6, and for a second-order lower than 0.3. The decomposition of the initial feed in the APR follows the first-order reaction kinetics.

The density of activated carbons varies in general from 200 to 650 kg/m^3, while the Sibunit support density can be ranged from 300 to 800 kg/m^3 depending on the particle size and other parameters. The bulk density of alumina is estimated as 800-1000 kg/m^3.

All catalysts are supported on mesoporous materials, such as alumina, AC, Sibunit and PBSAC. Sibunit and PBSAC have a regular spherical shape due to the special way of preparation. Other supports (activated carbons and alumina) were crushed and sieved to the required grain size, thus the final catalyst particles have more irregular shape. The catalyst particle sizes d_p, as well as the catalyst density considered in the calculations, observed initial reaction rates $r_{w,p}^{obs}$ and corresponding Weisz-Prater criteria, can be found in Table 5.

Table 5. Catalysts particle size.

Catalyst	*Grain size, diameter, d_p [μm]*	*Approximate catalyst density, ρ_{cat}, [kg/m^3]*	*Experiment*	*Initial reaction rate, [mol/s*kg cat]*	Weisz-Prater criterion, Φ_{WP}
Pt/Al_2O_3	125-250	1000	Continuous reactor: sorbitol, 50 g to 1 L	5.64×10^{-4}	0.06
Pt/PBSAC	110-360	650	Continuous reactor: sorbitol, 50 g to 1 L	1.62×10^{-4}	0.02
Pt/AC-JM2	powder, < 125	400	Continuous reactor: xylitol, 50 g to 1 L	4.12×10^{-3}	0.01
Pt/AC-JM3	powder, < 100	400			
Pt/AC-1	powder, < 100	400	Autoclave, propeller stirrer: technical polyols, 15.3 wt%	5.64×10^{-4}	6.24×10^{-4}
Pt/AC-4	1000-2000	400	Autoclave, cage reactor: technical polyols, 5.6 wt%	6.00×10^{-4}	0.8
Pt/Sib	100-180	650	Continuous reactor: xylitol, 50 g to 1 L	1.56×10^{-3}	0.01
Ni/Sib	100-180	650	-	-	-
Re/Sib	100-180	650	-	-	-
Ru/Sib	100-180	650	-	-	-
Pt-Ni/Sib	100-180	650	-	-	-
Pt-Re/Sib	100-180	650	Continuous reactor: xylitol, 50 g to 1 L	1.38×10^{-2}	0.13
Pt-Ru/Sib	100-180	650	-	-	-
Pt-Co/Sib	100-180	650	-	-	-

Concentration of the feed at the catalyst surface C_s is assumed to be equal to the bulk concentration. The effective diffusion coefficient D_e is defined as:

$$D_e = D \cdot \frac{\xi}{\chi}, \tag{10}$$

where the ratio between porosity ξ and tortuosity χ is assumed to be 0.1.

According to Perry's Chemical Engineer's Handbook [129], the Siddiqi-Lucas equation gives a lower average absolute deviation compared to the Wilke-Chang equation for calculation of the diffusion coefficient D of miscellaneous nonelectrolytes in water. The diffusion coefficient of xylitol, sorbitol and mannitol in water according to Siddiqi and Lucas is defined as:

$$D_{AW} = 2.98 \cdot 10^{-7} \cdot V_A^{-0.5473} \cdot \eta_W^{-1.026} \cdot T, \tag{11}$$

Water dynamic viscosity η_W at the reaction conditions is estimated to be 0.1188 cP according to Reid et al. [130]. Molar volume V_A of xylitol and sorbitol/mannitol at boiling point are equal to 155.4 cm^3/mol and 185 cm^3/mol correspondingly, being calculated via the additive method proposed by Le Bas [131].

The calculated diffusion coefficient D_{AW} is equal to 8.34×10^{-5} cm^2/s for xylitol and 7.58×10^{-5} cm^2/s for sorbitol/mannitol. The effective diffusion coefficient D_e is one order of magnitude lower.

Internal mass-transfer limitations are discussed in [**III**, **IV**], where the dimensionless Weisz-Prater criterion Φ_{WP} was calculated for catalysts supported on Sibunit and activated carbon (Merck).

The fastest reaction rate of xylitol decomposition observed over Pt-Re/Sib catalyst (1.38×10^{-2} mol/s·kg cat) and the largest catalyst particles (180 μm) were taken into consideration for xylitol APR in the continuous reactor [**III**]. The Weisz-Prater criterion confirms the negligible influence of pore diffusion limitations being equal to 0.13 for the experiment with the most active Sibunit-supported catalyst. The observed reaction rates were about one order of magnitude lower in the case of other catalysts, e.g. the second most active Sibunit-supported catalyst Pt/Sib (see part 3.4 below) exhibited 1.56×10^{-3} mol/s·kg cat. The overall reaction rate of sorbitol decomposition over the Pt/Al_2O_3 catalyst is equal to 5.64×10^{-4}, and the corresponding Weisz-Prater criterion is equal to 0.06.

Thus, it could be assumed that the experiments in the continuous reactor were performed in the kinetic regime with either negligible or absent internal mass-transfer limitations.

Calculations for the APR of a technical sorbitol/mannitol mixture in the autoclave [**IV**] were based on the observed reaction rate at 2 h reaction, which was equal to 6.00×10^{-4} mol/s·kg cat over Pt/AC-4, and to 5.64×10^{-4} mol/s·kg over Pt/AC-1. Internal diffusion is not limiting the reaction in the case of a powder Pt/AC-1 catalyst (Φ_{WP} is equal to 6.24×10^{-4}). However, the Weisz-Prater criterion confirmed the presence of internal mass-transfer limitations being equal to 0.8 for the experiments with Pt/AC-4 catalyst (grain size 1-2 mm).

3.3. Catalytic performance: flow regime [III]

The flow regime in the continuous reactor is discussed in [**III**]. Based on the values of gas and liquid flows it can be classified as a trickle flow [132]. These values are located within the trickle flow regime in the co-current downflow diagram obtained for an air-water system. The transition regions between trickle and pulse flows are shifted to higher flow velocities with an increased pressure [133].

3.4. Active metal variation [III]

Mono- and bimetallic catalysts were compared in the xylitol APR in terms of activity, selectivity to hydrogen and selectivity to alkanes [**III**]. The following catalysts were compared: Pt/AC-JM2 and the Sibunit-supported set of catalysts (Pt/Sib, Ni/Sib, Re/Sib, Ru/Sib, Pt-Ni/Sib, Pt-Re/Sib, Pt-Ru/Sib, Pt-Co/Sib). Stability issues and carbon conversion to the gas phase were also discussed.

- Activity

Catalyst activity is determined as conversion of the initial feed (xylitol) and presented in Figure 4 A. Pt/AC-JM2 catalyst (2.5 wt%) is more active compared to Pt/Sib (3 wt%). Absence of external mass-transfer limitations was confirmed for both catalysts. The difference in activity can be explained by the difference in the metal particle sizes (0.9 nm in Pt/Sib versus 2.1 nm in Pt/AC-JM2), and by a twofold large amount of the acid sites in the Pt/AC-JM2 catalyst.

The deactivation profile of Pt/AC-JM2 has been presented in [**V**]. The catalyst showed a minor decrease of conversion with TOS and even less pronounced increase of selectivity to H_2 and CO_2.

All other monometallic catalysts displayed significantly lower activity (Ni/Sib) or deactivated very fast (Ru/Sib, Re/Sib). Performance of those catalysts is discussed in [**III**].

Activity of bimetallic Pt-Ni/Sib and Pt-Co/Sib catalysts was practically en par with Pt/Sib, while Pt-Ru/Sib was slightly more active. Pt-Re/Sib displayed an outstanding high activity and the highest amount of converted xylitol per surface Pt. This data is consistent with the results published previously for glycerol APR over bimetallic catalysts supported on carbon black [16,40,41,134,135] and gas-phase glycerol conversion [136].

- Selectivity to H_2, CO_2 and alkanes

Selectivity to hydrogen is decreasing along with conversion increase for all catalysts (Figure 4 B), as it can be expected for consecutive reactions. The highest selectivity was obtained over Pt/AC-JM2, while Pt, Pt-Co, Pt-Ni and Pt-Re supported on Sibunit exhibited slightly lower values. Similar selectivity to hydrogen was described in the literature for xylitol APR over Pt/C [55]. The overall trends for selectivity to CO_2 are

similar to those for hydrogen (Figure 5 A) except the pronounced decrease along with conversion increase. Total selectivity to alkanes (Figure 5 B) was calculated as a sum of selectivity to all determined hydrocarbons: methane, ethane, propane, *n*-butane, *n*-pentane, *iso*-pentane, *neo*-pentane, *n*-hexane, *iso*-hexane, and *n*-heptane. Alkane selectivity is reversed towards CO_2. Selectivity to individual alkanes was found to be metal-specific, the details can be found in [**III**].

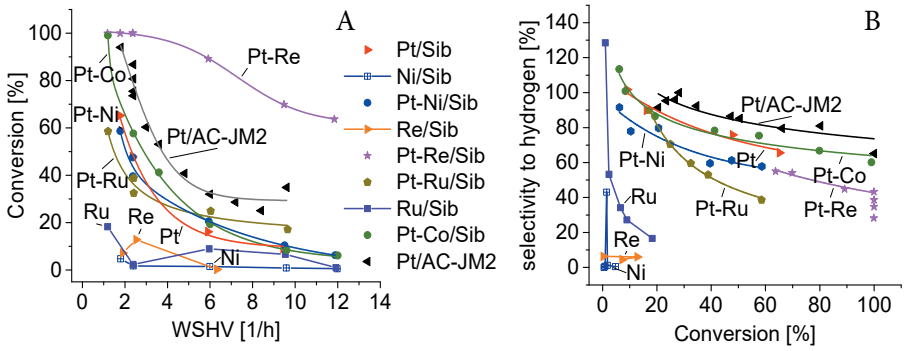

Figure 4. Conversion of xylitol (A) and hydrogen selectivity (B). The following conditions were used: xylitol concentration 100 g/L, T = 498K, P = 29.7 bar, mass of catalyst 0.5 g.

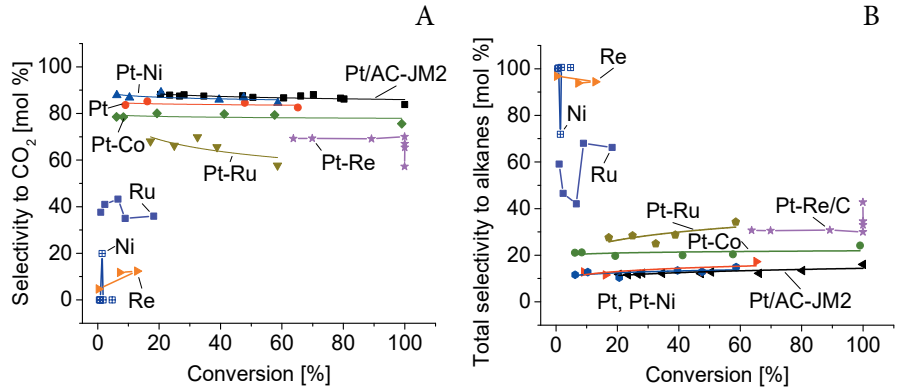

Figure 5. Selectivity to CO_2 (A) and alkanes (B) vs conversion in xylitol APR. The following conditions were used: xylitol concentration 100 g/L, T = 498K, P = 29.7 bar, mass of catalyst 0.5 g.

A more illustrative comparison of selectivity to alkanes and to hydrogen is given in Figure 6 for catalysts with the best performance at 60 % conversion. Pt/AC-JM2 catalyst exhibited the highest selectivity to hydrogen and lowest selectivity to alkanes. Among Sibunit-supported catalysts, Pt/Sib and Pt-Co/Sib are more selective to hydrogen compared to others. Pt-Ni/Sib and Pt-Re/Sib exhibited similar selectivity to hydrogen (57%), at the same time Pt-Re/Sib and Pt-Ru/Sib appeared to be the most selective to alkanes.

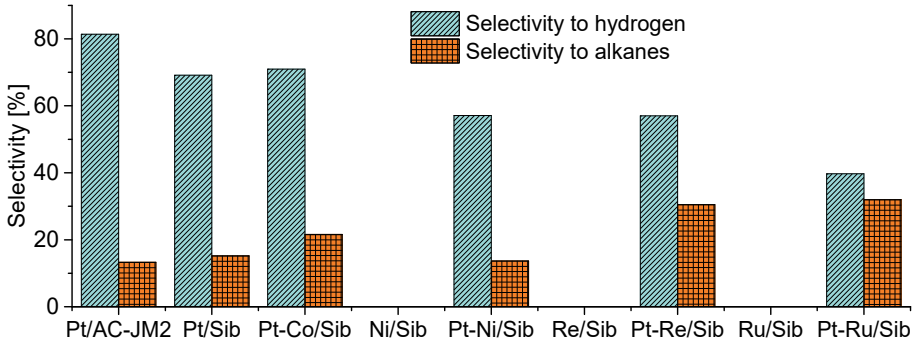

Figure 6. Selectivity to hydrogen and alkanes for APR of xylitol over selected carbon-supported catalysts for a comparable conversion range of 58-66%. The following conditions were used: xylitol concentration 100 g/L, T = 498K, P = 29.7 bar, mass of catalyst 0.5 g.

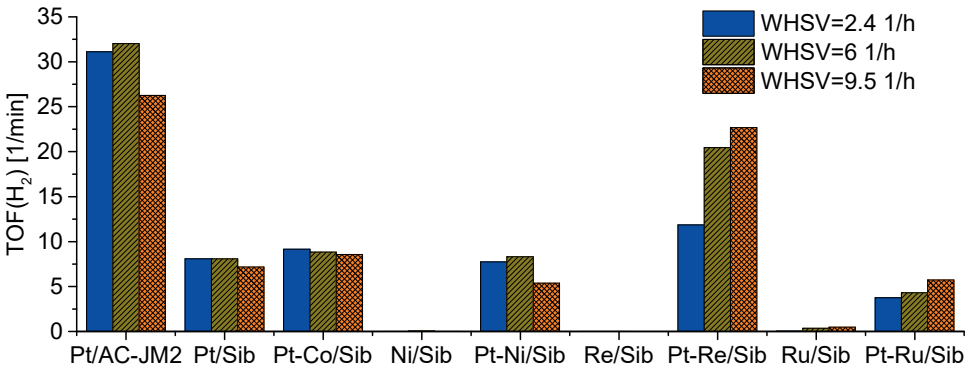

Figure 7. Hydrogen TOF [min^{-1}] of carbon-supported catalysts in xylitol APR at different WHSV. The following conditions were used: xylitol concentration 100 g/L, T = 498K, P = 29.7 bar, mass of catalyst 0.5 g.

TOF(H_2) is presented in Figure 7. Pt/AC-JM2 catalyst generated the largest amount of hydrogen per mole of surface Pt. Despite poor selectivity to hydrogen, the values of TOF(H_2) obtained over Pt-Re/Sib are higher than TOF(H_2) obtained over other Sibunit-supported catalysts. TOF to hydrogen obtained in the current study over both Pt catalysts exceeds substantially the values reported by Kirilin et al. [55].

- Carbon conversion to gas-phase

The distribution of carbon among gas- and liquid-phase products can be utilized for estimation process efficiency. It is beneficial if carbon in the feed is fully utilized, and if the output aqueous stream does not require sophisticated purification. Full conversion to the gas phase is preferable. It could be achieved by selection of a proper catalyst and recycling of waste aqueous stream. The last option is discussed for the sorbitol APR in [**VI**].

The amount of carbon stored in intermediates is compared for platinum and bimetallic catalysts in Figure 8 and discussed in detail in [**III**]. The amount of carbon in the liquid phase is higher for Pt-Re, Pt-Ru, and Pt-Co/Sib catalyst compared to Pt/AC-JM2. This carbon represents the intermediates formed from xylitol during subsequent reactions and not transformed yet to the final products, such as alkanes or CO_2/CO. Comparison of individual liquid-phase products obtained in the xylitol APR is given in detail in [**III**].

Pt/Sib appeared to be the best candidate for hydrogen production. However, taking into consideration the techno-economical analysis of hydrogen production from sorbitol [**VI**], Pt-Re/Sib could be more beneficial due to a higher activity, since alkanes can be successfully utilized for production of all needed heat.

Selectivity to individual alkanes was found to be metal-specific, the details can be found in [**III**].

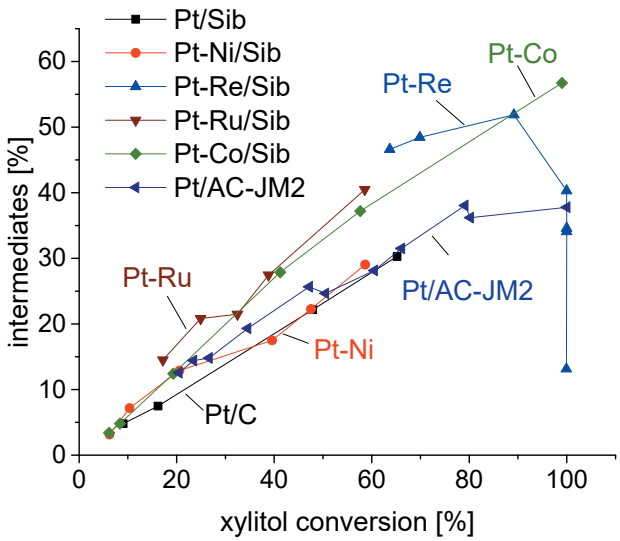

Figure 8. Carbon stored in the liquid-phase intermediates [molar percent] versus conversion of xylitol over Pt/AC-JM2, Pt/Sib, Pt-Re/Sib, Pt-Ru/Sib, Pt-Ni/Sib, and Pt-Co/Sib. Carbon in intermediates was calculated as $100 \cdot (\upsilon(CC_{xyl}) - \upsilon(CC_{gas}))/ \upsilon(CC_{xyl}))$, where $\upsilon(CC_{xyl})$ is the carbon molar flow in the unreacted feed, and $\upsilon(CC_{gas})$ is the total carbon molar flow in all gas-phase products, such as CO, CO_2 and alkanes. The following conditions were used: xylitol concentration 100 g/L, T = 498K, P = 29.7 bar, mass of catalyst 0.5 g.

3.5. Reaction network [I, II, VII]

Possible reaction pathways were proposed and discussed from the thermodynamic point of view based on studies of sorbitol and galactitol APR in [**I**]. The same principles were applied for xylitol APR [**III**, **V**], and APR of propanol-1, 1,2-propandiol and glycerol [**II**, **VII**]. Some details about methane formation are clarified in [**II**, **III**].

Importance of the reaction mechanism investigation can be supported by the fact that almost 42% carbon (fed to the reactor in the form of polyol) is still present in the liquid phase in the form of oxygenated products, whereas conversion of the initial substrate already reached 100% (Figure 9). Similar results were obtained in the xylitol APR over Pt/AC-JM2 [**III**].

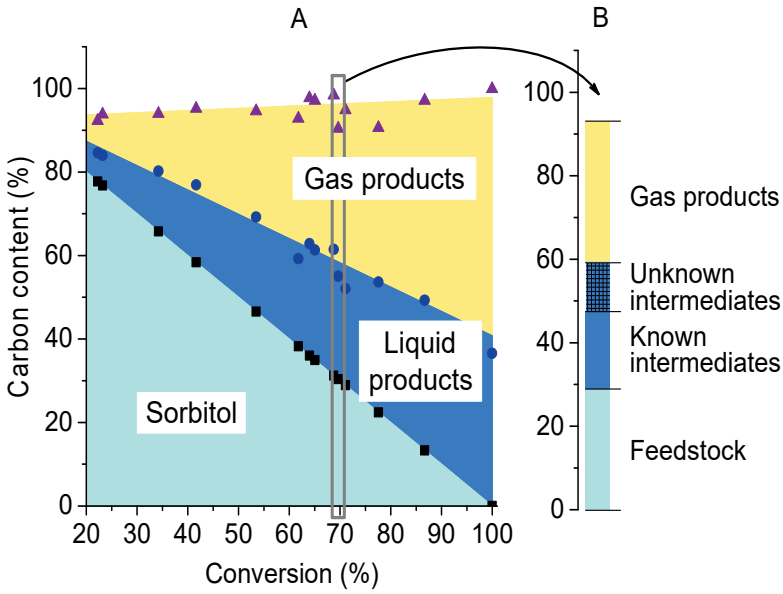

Figure 9. Carbon distribution between the liquid and gas phases and total carbon balance versus conversion in APR of sorbitol at 498 K and 29.7 bar. a: the whole conversion region. b: carbon distribution at 62 % conversion.

3.5.1. Reaction pathways [I]

The scheme of the main reaction pathways (Figure 10) proposed in [**I**] was based on the product analysis of sorbitol and galactitol APR over Pt/Al_2O_3. The substrate, C_6-polyol, can be transformed into C_5-polyol via consecutive dehydrogenation/decarbonylaton steps **1**, **2** occurring on the metal sites [137–139]. Subsequent repetitions of these steps result in a complete conversion of the substrate to CO and hydrogen. Almost all CO reacts with water forming CO_2 and additional H_2 via the WGS reaction.

Intermediate aldols can desorb from the surface. Aldehydes C_4-C_6 can be transformed into stable cyclic products (substituted tetrahydrofurans and tetrahydropyrans) via cyclization through dehydration **3** proceeding on acidic sites. Hydrogenolysis of primary hydroxyl-groups **4** gives molecules with a non-reactive methyl-group at the end, and less reactive secondary hydroxyl-groups. These secondary alcohols are either transformed into ketones via dehydrogenation **1** or dehydration **3,** or undergo complete reduction to form alkanes **5**. Desorbed aldehydes are converted into gemi-diols, which can be dehydrogenated on Pt with formation of acids (Figure 11) [19,112,140–142]. Cannizzaro disproportionation is usually given to explain acid formation. However, usually it requires presence of strong bases [143]. Also, only aldehydes with no α-hydrogen atom give the Cannizzaro reaction, otherwise aldol condensation is preferable. α-keto aldehydes could give internal Cannizzaro reaction.

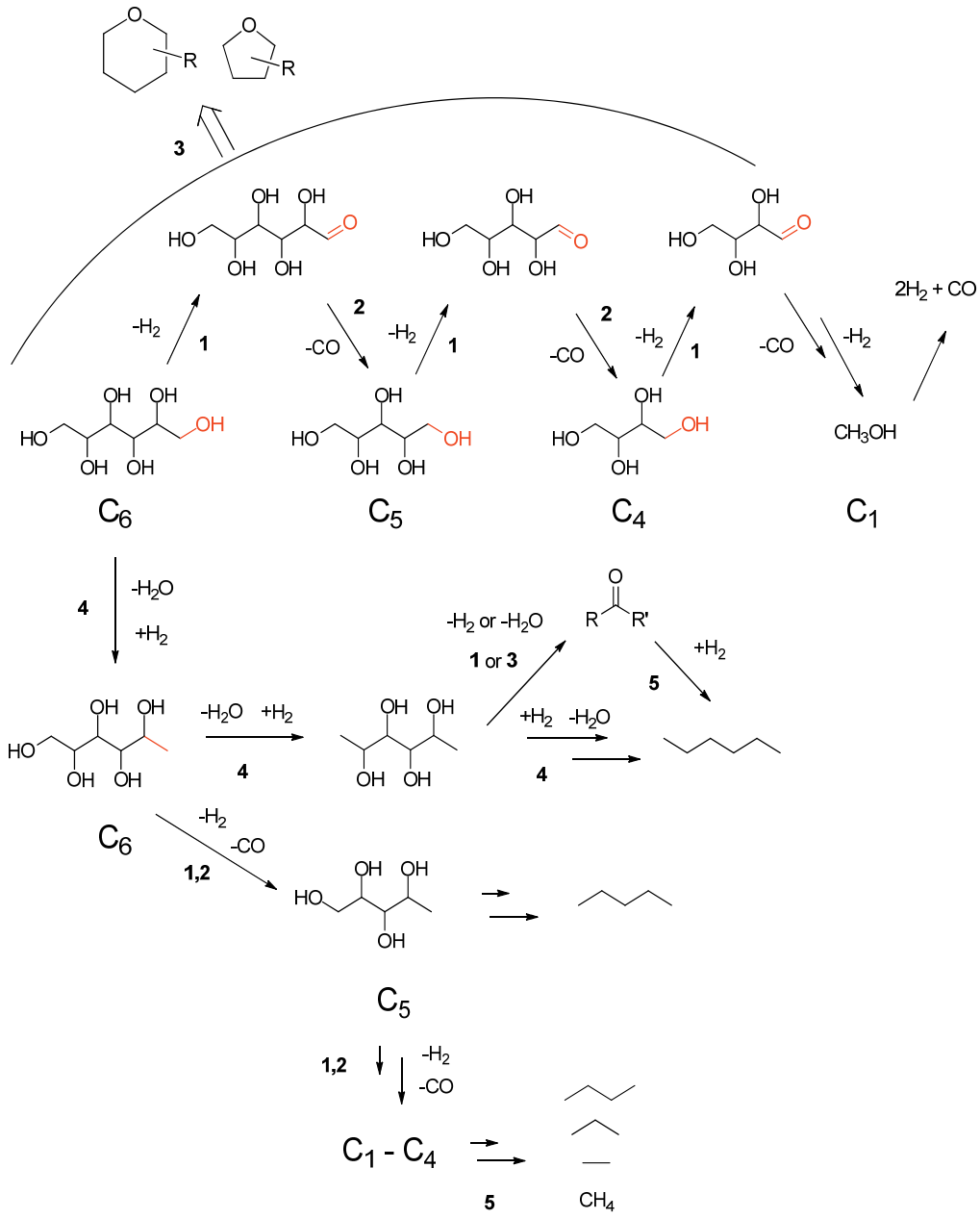

Figure 10. The main reaction pathways in APR of sorbitol and galactitol.

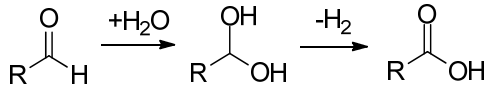

Figure 11. Formation of acids from aldehydes via gemi-diol dehydrogenation.

All possible optically active hexoses and pentaols formed starting from D-galactitol and D-sorbitol are shown in Figure 12, assuming that only steps **1** and **2** take place. Neither glucose, nor xylitol can be produced from galactitol via this path, however, they were found in small amounts among the liquid-phase products. Transition metals like Au, Pd or Ru are known to catalyze the racemization of alcohols being used as a heterogeneous catalyst in dynamic kinetic resolution in combination with enzymes [144–146]. However, Pt itself was not so widely applied probably due to interactions with enzymes [147,148]. Thus, one can tentatively assume that diastereomerization also takes place during APR (see Figure 13).

Despite the fact that the retro-aldol reaction was assumed in many papers to be one of the possible reaction paths, no clear evidences were presented in the literature and in the current study for presence of this reaction during APR on Al_2O_3- or carbon-based catalysts. This reaction requires some specific conditions, such as a special type of support or addition of a basic promoter. Base-catalyzed retro-aldol reaction allowed production of significant amounts of glycerol from sorbitol and both glycerol and ethylene glycol from xylitol during hydrogenolysis on Pt/NaY zeolite [149] or in presence of $Ca(OH)_2$ [150–152]. It should be noted that two molecules of glycerol can be formed from sorbitol only through transformations to ketohexose, but not aldohexose. However, transformation of an aldehyde form to a keto form should occur rather easy. Therefore, the exact mechanism of dehydrogenation is still unclear. The distribution of gas and liquid products in our experiments does not confirm the retro-aldol reaction to play a significant role for APR transformations. However, this reaction is thermodynamically possible as described in [**I**].

Secondary alcohols with non-substituted neighboring atoms do not undergo C-C bond cleavage, which is supported by the experimental data [153].

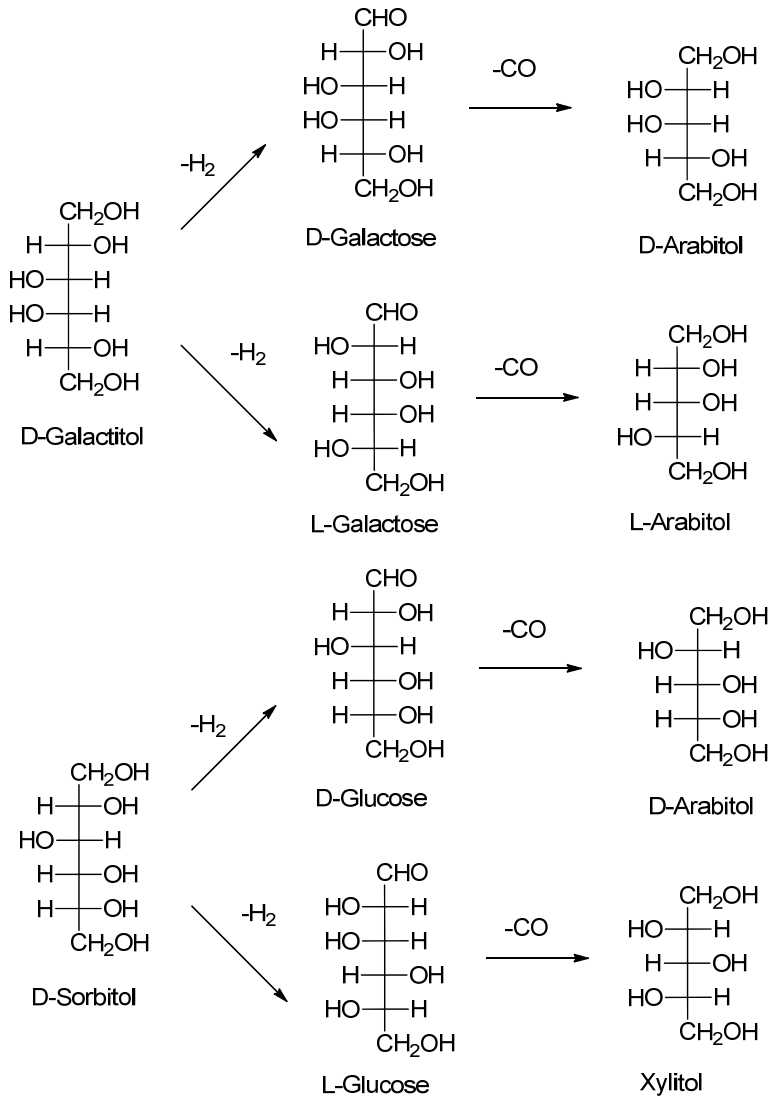

Figure 12. Galactitol and sorbitol dehydration/decarbonylation in APR.

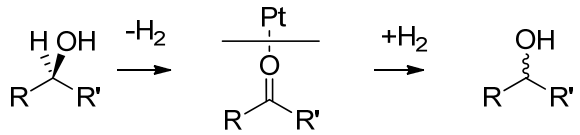

Figure 13. Diastereomerization of carbohydrates on Pt surface via dehydrogenation/hydrogenation steps.

One of the unexpected products was *n*-heptane, which contains an extra carbon atom compared to the substrate. Formation of hexane was detected [31] during APR of xylitol over Pt/HZSM-5 and Ni/HZSM-5 catalysts. This was explained by ketones formation from xylitol with subsequent aldol-condensation and hydrodeoxygenation. Another explanation was based on the Fischer-Tropsch synthesis. It should be noted that only branched alkanes could be produced after croton-condensation, however, the authors did not mention if linear or branched hexane was observed in [31]. No Fischer-Tropsch synthesis occurs during APR, which was proven by additional tests of the complementary water-gas shift reaction, where the relationship between the APR and the WGS was thoroughly studied [37,50,154], [**III**]. Thus, formation of compounds with a longer carbon chain could be a result of a sequence of condensation reactions. A possible pathway is illustrated in Figure 14, showing aldol and subsequent croton condensations. This process is reversible and under these experimental conditions a retro-aldol reaction can also occur too.

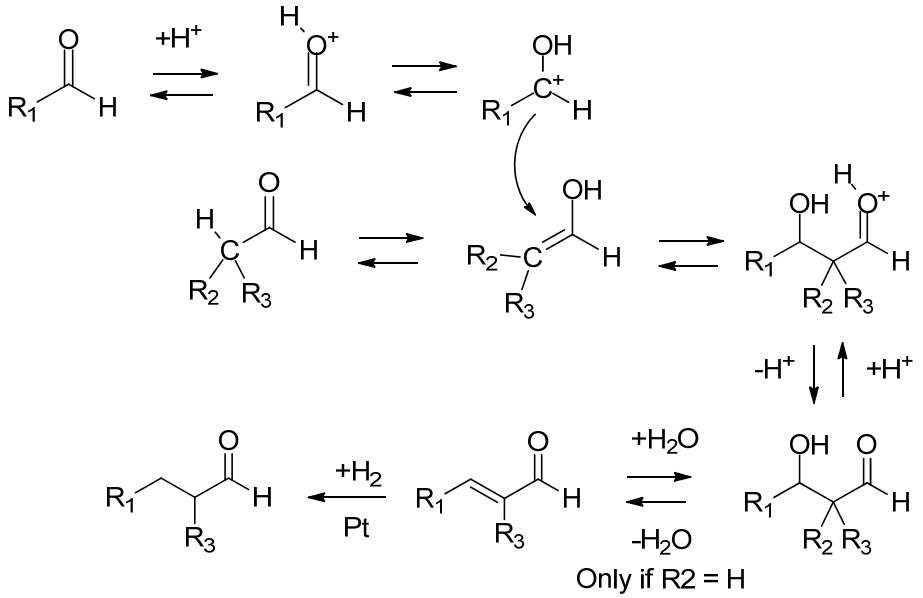

Figure 14. Extension of a carbon chain and formation of branched alkanes via aldol and croton condensation and the retro-aldol reaction.

Some amounts of branched pentane and *iso*-hexane were detected in the gas phase, indicating the presence of skeletal isomerization during APR. However, *iso*-butane or unsaturated compounds were not observed. Branched alkanes were not previously detected for the APR over Pt/Al_2O_3, however, an addition of a solid acid such as SiO_2-Al_2O_3 promoted formation of ca. 5% of branched alkanes [155]. Substantial quantities of isoparafins were observed for APR of sorbitol over Ni/HZSM-5 catalyst [156,157].

At 498 K and 30 bar the ionization constant of water [158] is $K_w = 5.597\times10^{-12}$ corresponding to the pH of c.a. 5.6, which can promote reactions requiring protonation steps. Typically heterogeneous catalytic isomerization of alkanes requires strong acidity, thus demanding another explanation of branched alkane formation. Pinacol-pinacolone rearrangement of desorpted aldehydes (Figure 15) can also be a plausible explanation for branching.

The reaction pathways proposed above are discussed from the thermodynamical point of view in the publication [**I**]. Free Gibbs energies of formation $\Delta G°_f(498K)$ of some reactants and products were calculated using HSC Chemistry 6.0 [159] or estimated via molecular modeling software HyperChem 8.0 [160], using a semi-empirical quantum-mechanical method PM3. Gibbs energies for the most meaningful reactions can be found in [**I**].

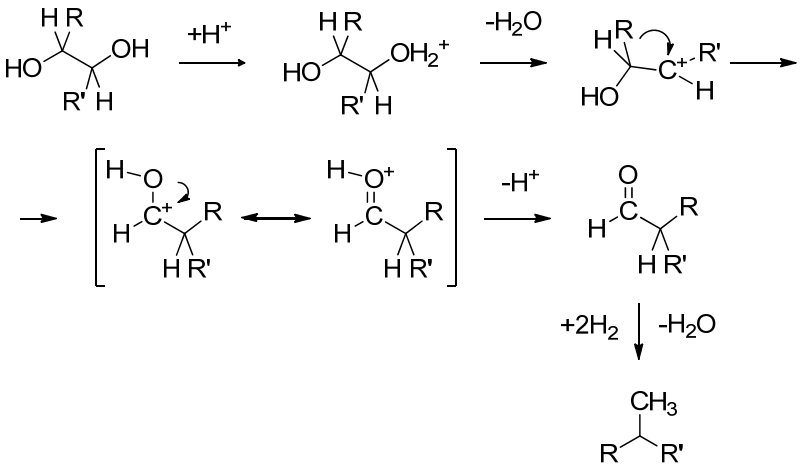

Figure 15. Pinacol-pinacolone rearrangement with a subsequent reduction to branched alkane.

3.5.2. Quantum-chemical calculations [VII]

Publication [**VII**] describes a detailed study of 1,2-propanediol decomposition pathways on a Pt catalyst model, obtained by DFT calculations. Different reaction paths on a Pt(111) model surface were computationally screened. A mechanistic approach was used to trace the preferred paths according to the calculated activation barriers of the elementary steps. The gas- and liquid-phase products distribution was obtained for 1,2-propanediol APR over Pt/C catalyst in the continuous reactor at 498 K. The experimental data was combined with the DFT calculations to advance a reaction mechanism. Hydroxyacetone (HA) was demonstrated to be among the most favored decomposition products. Most of the species identified experimentally were connected to specific molecular pathways in the model.

A tentative reaction mechanism was proposed for the initial 1,2-propanediol transformations through APR (Figure 16). The lowest activation barriers were taken into account. The reaction can proceed with the following order of molecular events: 1,2-PDO → INT2 → INT5 → INTa → INTb → INTf → INTj. The two last reaction intermediates are the only ones, in which the C-C bond breaking, via decarbonylation, becomes competitive with dehydrogenation. It is worth mentioning that hydroxyethylidene (HTE) and an acetyl (ACT) fragment are formed through the bond cleavage from INTf and INTj. These latter species may be the precursors of experimentally found ethanol or acetic acid. The competition between C–H, O–H, and C–C bond cleavages revealed that shortening of the carbon chain occurs most likely via decarbonylation steps.

3.5.3. Methanation [I, II, III]

Methane formation was discussed in the publications [**I**, **II**, **III**], since methanation of CO could be competitive to hydrogen formation through WGS. Methane formation could proceed by three different reaction routes: hydrogenation of a terminal C-CH_3 with a C-C bond scission, hydrogenation of CO, or hydrogenation of methanol. Methanation of CO is thermodynamically favorable (-96.66 kJ/mol) [**I**]. However, it was demonstrated, that methanation does not occur under experimental conditions of APR on Pt, Re, Rh, Pt-Re and Rh-Re catalysts supported on Al_2O_3 or carbon

[37,73,76], [**III**]. It was shown that no methane is formed from propanol-1 converted over Pt/C at 498 K and 29.7 bar [**II**].

This implies that neither the -CH_2-CH_3 bond is exposed to C-C scission, nor methanation is happening over Pt/C. Methane can be formed through reforming of the intermediate product, methanol, or by a bond scission between a terminal methyl group and –CHOH– or –CO– fragments via hydrogenation.

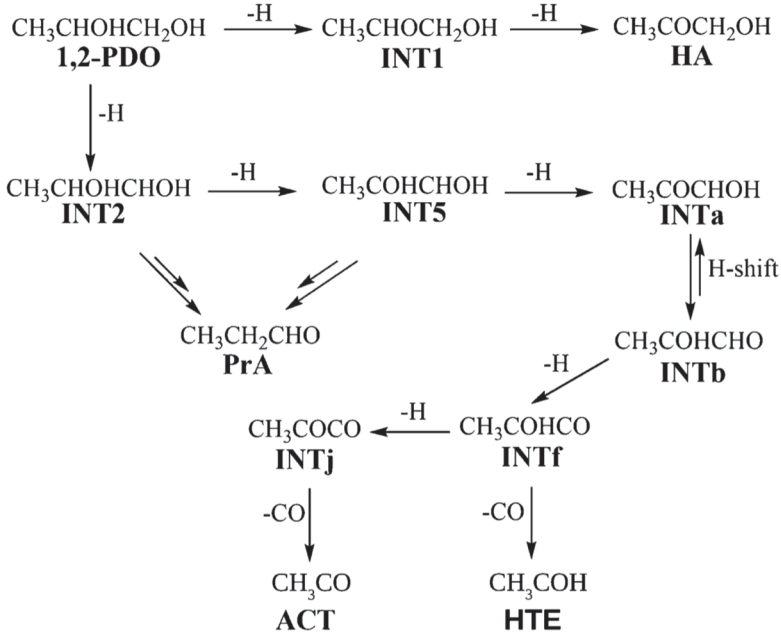

Figure 16. Proposed reaction mechanism for 1,2-propanediol APR.

3.6. Feed variation

3.6.1. Influence of chirality [I]

Two sugar alcohols, namely galactitol and sorbitol, were studied over Pt/Al_2O_3 catalyst in the continuous fixed-bed reactor at 498 K [**I**]. Gas and liquid products were thoroughly studied by GC and HPLC analysis with the carbon balance being close to 90-95%. Reliability of the liquid-phase products analysis was considerably improved due to application of a spiking technique for qualitative analysis and subsequent peak fitting for quantification. Selection of substances applied for identification was based on the data reported in the literature [113,139,153,161–165].

Aqueous solutions of sorbitol (3.6 wt%), galactitol (3.6 wt%) and a mixture of both polyols (1.8+1.8 wt%) were applied for a better comparison. The experimental sequence can be found in [**I**]. Influence of chirality can be estimated by comparison of feed conversion and selectivity to the gas- and liquid-phase products.

Conversion levels were similar in the experiments with sorbitol, galactitol and their mixture (Figure 17). A small discrepancy between the conversion level of sorbitol and galactitol was attributed to differences in the catalyst wetting, rather than the properties of the substances, since exactly the same levels of conversion were obtained in the experiment with both polyols and their 1:1 mixture.

Selectivity to H_2, CO and CO_2 were similar for both polyols and their mixture in the whole range of substrate conversion (Figure 18 A and B). Selectivity to CO was close to zero indicating that almost all carbon monoxide was converted to CO_2 via WGS. It is noteworthy, that the total selectivity to alkanes (Figure 18 B) appeared to be slightly different in the sequential experiment with both polyols and their mixture, which probably happened due to minor changes in the equipment with time. The detailed comparison of alkanes revealed that the selectivity to alkanes was identical for both substrates showing no effect of chirality on it.

In the present study a composition of the liquid phase was thoroughly elucidated by HPLC, which allowed identification of approximately 68% of carbon stored in all intermediates. The distribution of identified (80 % from the total input carbon) and unknown carbon is shown at 62% conversion of sorbitol in Figure 9 B. The identified products were compared in [**I**] with the previous studies on APD/H of sorbitol on different catalysts [139,153,162].

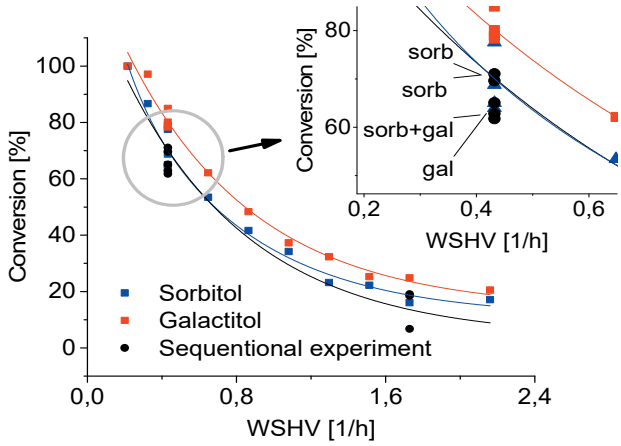

Figure 17. Conversion of the substrate as a function of WHSV for sorbitol and galactitol over Pt/Al_2O_3 at 498 K and 29.7 bar. "Sorb" – the experiment with sorbitol only, "gal" – the experiment with galactitol,"sorb+gal" – sequential experiment with both polyols.

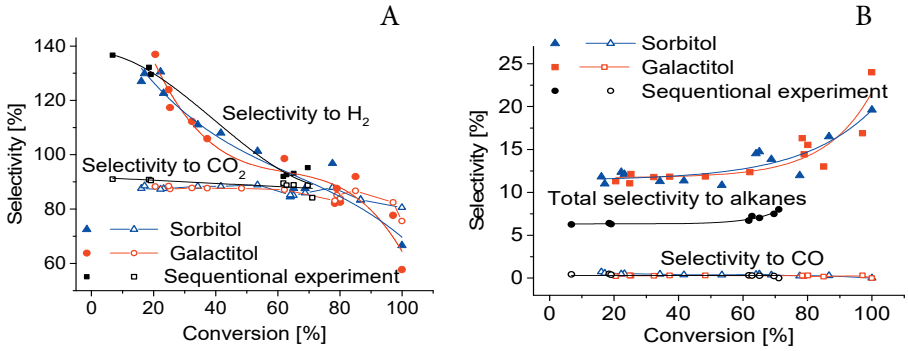

Figure 18. Selectivity to H_2 and CO_2 (A) and to CO and alkanes (B) versus carbon conversion in APR of sorbitol and galactitol over Pt/Al_2O_3 at 498 K and 29.7 bar.

The composition is very similar for the samples obtained during APR of sorbitol and galactitol; in both cases similar sugars, polyols, alcohols, acids, carbonyl compounds and furans were found. One notable exception is the presence of distinct primary intermediates, such as glucose and galactose. No galactose was found in the sample from sorbitol and only traces of glucose appeared in the sample from galactitol. However, HPLC analysis does not give a good separation of sugars and sugar alcohols, therefore only substances with high concentration can be taken into account. The

selectivity to arabitol was also significantly higher in the case of galactitol, indicating that diastereomerisation reaction can take place. It is worth noting that such substances as tartaric and fumaric acids (2,3-dihydroxybutendioic and 2-butenedioic acids correspondingly) were found as the products of sorbitol conversion, but not in the case of galactitol.

Chirality of the substrate does not have a considerable influence on selectivity to the final products or to the intermediates, which is an advantage for industrial processing, where the feedstock can be a mixture of isomers.

3.6.2. Technical feed [IV]

Sugars obtained from the biomass, e.g. sucrose from sugarcane, are easily accessible and comparably cheap. According to the literature, sugar APR is leading to fast catalyst deactivation due to high coke formation rates and formation on multiple condensation products. Addition of a preliminary hydrogenation step can substantially increase the overall hydrogen production and catalysts stability. APR of a polyol appears to be more beneficial compared to sugar APR. Hydrogenation of sugars is a well-known process, which leads to formation of a polyols mixture due to isomerization. In the previous part (3.6.1.) it was shown that chirality of the initial feed has no influence on catalyst activity and selectivity to hydrogen, CO_2 and alkanes.

Hydrogen production from polyol via APR is becoming competitive to methane steam reforming if the polyol price is less than 0.3$/kg per kg according to the calculations provided in part 3.10. The current sucrose price is 0.28 $/kg according to indexmundi (indexmundi.com). The target polyol price of 0.3$/kg is clearly not achievable via sucrose hydrogenation, however, the overall process has all the benefits of APR, e.g. zero net green-house gas emission.

In the current study commercial sorbitol and the technical mixture of sorbitol and mannitol were compared in terms of gas production, conversion of polyols and selectivity to hydrogen, CO_2 and alkanes. Hydrogenated glucose solution was studied previously [85], however, the catalyst deactivation issue was not discussed. This topic was considered in the current study for the first time.

A technical mixture of sorbitol and mannitol was produced by hydrogenating an aqueous sucrose solution (50 wt%) in a trickle bed reactor over 5 wt% Ru/C catalyst at 453 K. HPLC analysis confirmed absence of major impurities. Traces of glucose and sucrose were found, along with 1,2-propanediol, ethanol and glycerol. The initial mixture of technical polyols was diluted to 29 wt% to avoid crystallization in the feeding source and lines.

Aqueous-phase reforming of the technical polyol solution was performed in continuous and batch-wise modes. Pt/AC-JM3 catalyst was utilized in the continuous set-up for APR of the technical feed and commercial sorbitol. A batch reactor was applied for the technical feed APR over Pt/AC-1 and Pt/AC-4 catalysts. The details of the experimental procedure can be found in [**IV**].

The technical and the commercial feed were showing similar conversion (Figure 19 A). It should be noted that although the same catalyst sample was utilized for both experiments, the activity was restored during the regeneration procedure, previously implemented successfully [161]. Both feeds displayed similar selectivity to the main final products, such as alkanes, CO_2 and hydrogen (Figure 19 B). Similar results obtained for the individual alkanes ranging from C_1 to C_6 are described in [**IV**].

The catalyst activity is decreasing along with time-on-stream with the same rate for both feeds (Figure 20). The conversion decrease is more pronounced after the periods, when a higher feeding flow rates were applied, being practically restored to the original values after long periods with a low flow rate. Catalytic activity obtained in this study correlates well with the data of sorbitol APR obtained over 1% Pt/Al_2O_3 in [**I**]. The overall gas production is lower in the case of technical polyols mixture, however, similar patterns are obtained for both feeds (Figure 21). A similar enhancement effect is observed for the gas production from sorbitol after long periods of low flow rates. This phenomena was not reported previously, thus requiring additional experimental efforts.

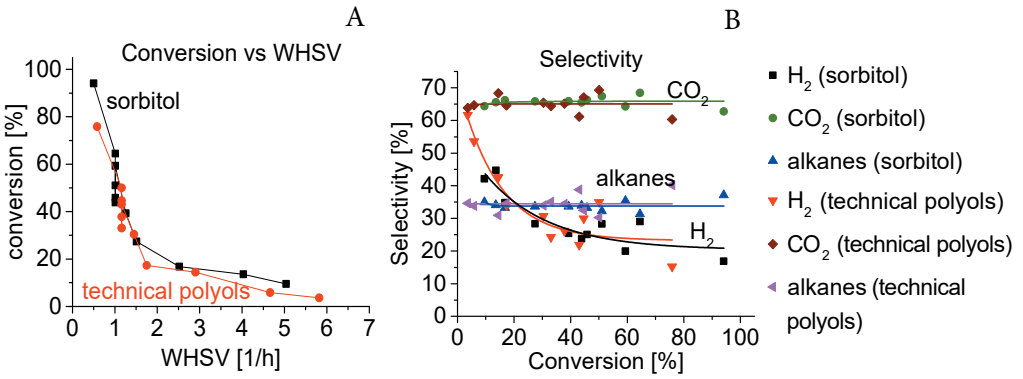

Figure 19. APR of sorbitol or technical polyols over Pt/AC-JM3. A: conversion of sorbitol or technical polyols vs. WHSV. B: selectivity to hydrogen, CO_2 and total selectivity to alkanes vs conversion of sorbitol or technical polyols. The following conditions were applied: T = 498K, P = 29.7 bar, mass of catalyst 0.5 g.

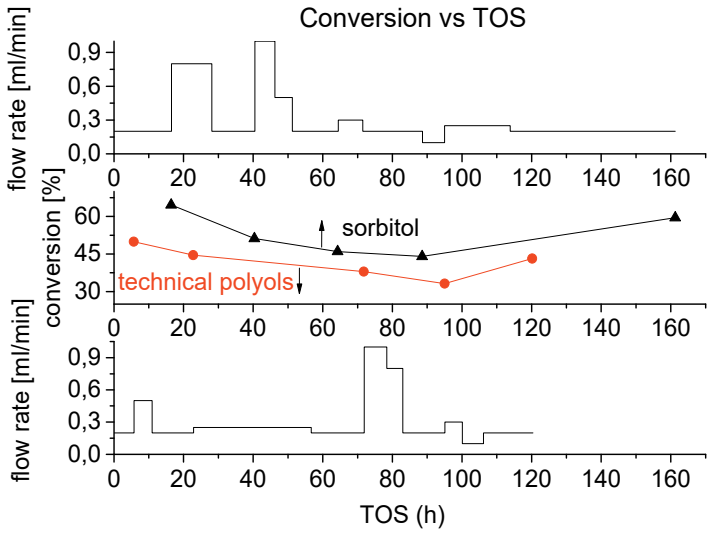

Figure 20. Conversion of sorbitol or technical polyols in APR over Pt/AC-JM3 versus TOS. The flow rates applied during the experiment are shown above and below conversion dependences for sorbitol and the technical mixture respectively. The following conditions were applied: T = 498K, P = 29.7 bar, mass of catalyst was 0.5 g.

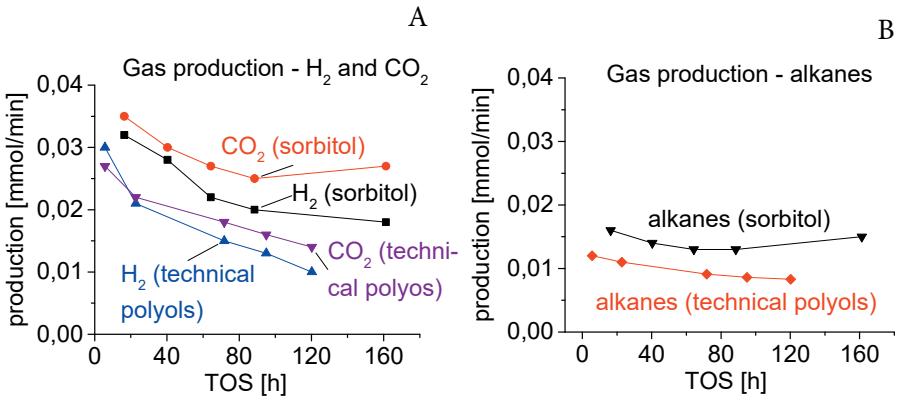

Figure 21. Gas production of hydrogen and CO_2 (A), and total alkanes (B) from sorbitol or technical polyols in APR over Pt/AC-JM3 versus TOS. The following conditions were applied: T = 498K, P = 29.7 bar, mass of catalyst was 0.5 g.

A detailed comparison of the liquid-phase intermediates did not show any major differences between commercial sorbitol and technical polyols. The details of this comparison along with some insights of the difference between carbon and alumina supports can be found in [**IV**].

An additional study of a concentrated technical polyols mixture (29 wt%) APR over the Pt/AC-JM3 catalyst is discussed in [**IV**].

The results of the technical feed conversion in the batch mode are discussed in [**IV**]. A higher alcohol content assigned to hydrogenation reactions was more pronounced in the batch mode compared to the continuous one. The overall rate of gas formation was approximately twofold lower in the batch mode. Batch-wise processing appeared to be considerably less effective for hydrogen production compared to the continuous mode. The main reason for this is the fast consumption of produced hydrogen in various hydrogenation reactions and mass-transfer limitations.

3.8. Kinetic modelling [V]

Xylitol APR over Pt/AC-JM2 is discussed in [**III**] in terms of catalyst screening. Additional details are provided in [**V**], where the experimental data were utilized for kinetic modeling. A simplified reaction network was focused predominantly on the xylitol consumption and formation of gas-phase products (Figure 22). Several intermediates with different carbon numbers have been considered, leading to CO_2 and hydrogen as well as different alkanes.

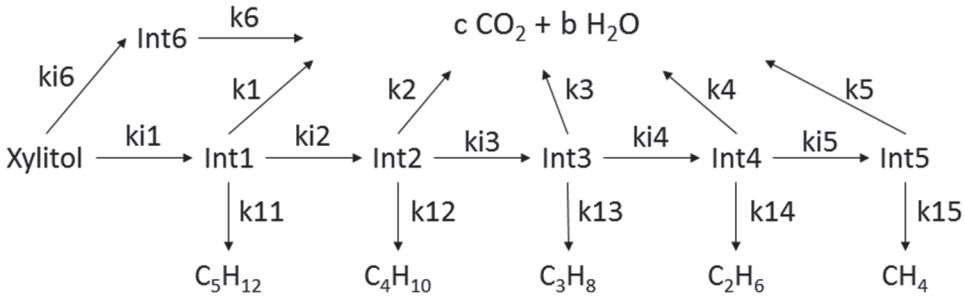

Figure 22. Reaction network used in kinetic modelling of xylitol APR. Int. denotes various intermediates.

Kinetic equations for the generation rates are given in [**V**]. Several consideration were taken into account. First, only xylitol adsorption was taken into account in the kinetic model. Initial parameter estimation showed a rather low coverage of other reactants. Nevertheless, the corresponding constants in the equations for formation rates of intermediates, CO_2 and H_2 are in fact lumped ones comprising also respective adsorption constants.

Second, the reaction rates for alkane formation displayed the first order in hydrogen. Such order is very often observed in various hydrogenation reactions, especially at low partial pressures of hydrogen. Preliminary calculations with a model assuming competitive adsorption of hydrogen on the same sites resulted in negligible influence of the hydrogen adsorption term; therefore, it was omitted in subsequent calculations.

Third, it was suggested that CO formed in APR is converted very fast via the WGS reaction giving CO_2 and additional hydrogen, since measured CO concentration was

very low. Gas phase compounds C_6H_{14} were not included in the model due to their low concentrations. For data fitting purposes, all intermediates were lumped into one pseudo-component named “intermediates”.

Kinetic modeling was done for all reaction rates using a steady state model of a packed bed reactor. The changes in the concentration profiles of the reagents and products along the reactor length (proportional to residence time) were described as a set of differential equations. Those equations were solved by means of ModEst software for the parameters estimation. The volume changes were taken into account. The proposed kinetic model fits the experimental data rather well (Figure 23). Some deviations were observed for minor components such as pentane, present in almost trace amounts. Due to a large number of parameters on one hand and lumping intermediates to a single pseudo-component, the errors of some parameters are rather high; thus their absolute values should be treated with caution. The same holds for calculated concentrations of intermediates. The calculations suggest that intermediates responsible for ethane and pentane formation are mostly present in the liquid phase, while others are transformed in a fast way to respective alkanes.

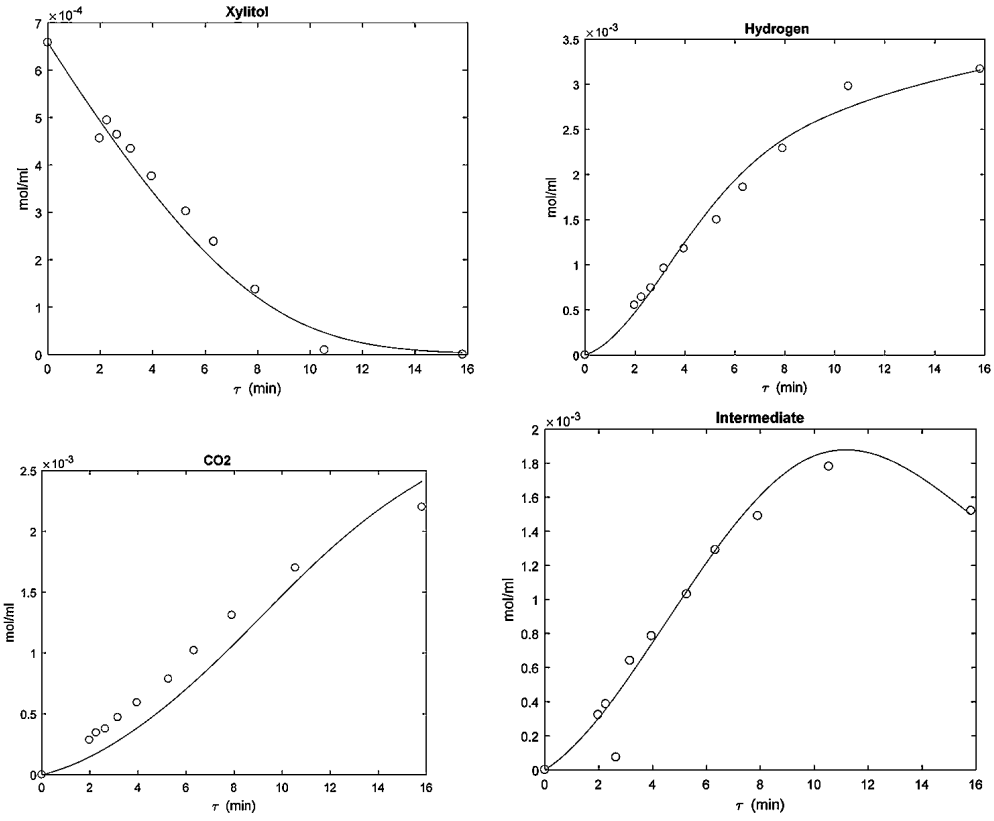

Figure 23. Comparison between experimental and calculated data as a function of residence time τ.

3.9. Flow-sheeting [V]

Dynamic model simulations of the reactor performance were performed to explore the influence of various parameters on xylitol APR. The effect of the fluid–solid mass transfer coefficient on the concentration of reactants vs time was studied. As a next step, it was tempting to make the simulations for a larger scale unit. Flow-sheeting was based on the reactor simulation data.

Unit capacity was specifically selected for the production of 500 kg/h of H_2 from xylitol feedstock. The Aspen HYSYS with Peng–Robinson thermodynamic package was used to simulate such processes as heating, cooling, recycling, and separation. The process flow diagram is displayed in Figure 24, which also contains simulation data.

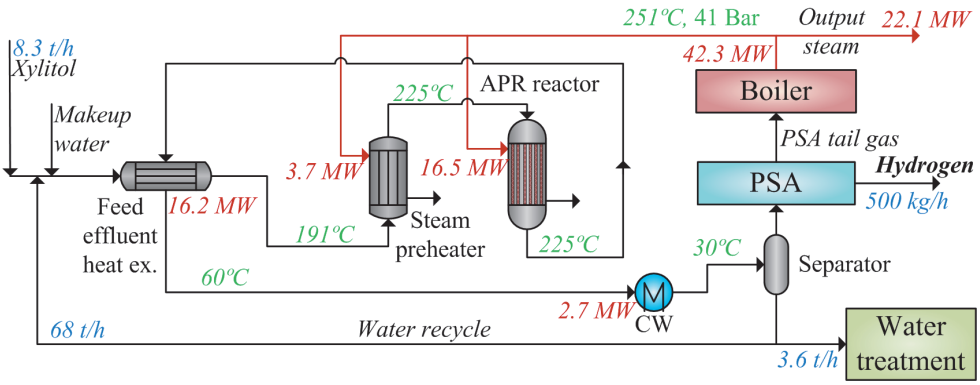

Figure 24. Xylitol APR process flow diagram.

A mixture of the feedstock, makeup, and recycling water is heated to a near-reaction temperature in a feed-effluent heat exchanger, then heated up to a reaction temperature of 498 K by high pressure steam (41 bar, 524 K) and directed to the APR tubular reactor. The reactor characteristics are as follows: tube bundle diameter = 1.9 m; tube length = 3.0 m; tube internal diameter = 25.4 mm; number of tubes is 2650; heat transfer surface = 714 m^2; catalyst loading =3.5 t (4.0 m^3). The size of the catalyst particles was supposed to be 750 μm (egg-shell type of catalyst, ensuring negligible impact of mass transfer limitations). The reactor is also supplied by high pressure steam (HPS) to sustain the isothermal conditions. The reactor product stream consisting of aqueous and gas phases is cooled down in the feed-effluent heat exchanger and water cooler to 303 K to separate the gaseous product and to direct it

to the pressure swing adsorption unit (PSA) for hydrogen separation. A PSA unit was modeled with a hydrogen recovery rate of 85%. Such a recovery level is rather typical for 4–6 bed adsorption. Higher values, corresponding to 90–95% hydrogen retrieval are achieved with 10 bed units. This can be, however, recommended to be used only for units with a capacity exceeding 5000 kg/h. The PSA tail gas comprising of H_2, CO_2, and alkanes is combusted in the boiler to generate high-pressure steam, which is supplied to the reactor and preheater. Boiler fuel efficiency was selected as 90%. The generated heat of 42.3 MW supplies the reactor (16.5 MW) and preheater (3.7 MW). The rest of the energy, 22.1 MW, can provide extra income from the process, decreasing thereby hydrogen production costs. A fraction of the recycled water can be drawn to wastewater treatment to prevent accumulation of relatively stable liquid components in the recycle such as acids and furans.

Overall, it can be summarized that the process design does not require any external heat source due to utilization of process byproducts - alkanes C1–C5. These calculations demonstrate that the catalyst for hydrogen production should not be too selective toward hydrogen and CO_2 but from the process optimization viewpoint should also generate alkanes as byproducts. In fact, 159 MJ (44 kW·h) per kilogram of hydrogen of heat can be produced for the designed hydrogen capacity of 500 kg/h. Such scale can be required for stand-alone green diesel production plants located close to pulp mills, where hydrogen is not readily available and installment of a small-scale methane steam reformer can be economically unattractive.

3.10. Reactor modelling and techno-economical analysis [VI]

A hydrogen production process via sorbitol APR was designed, optimized and evaluated from the economics point of view in [**VI**]. The economic parameters, influencing hydrogen costs, were determined. The emphasis was placed on process simulation and cost estimations of the major equipment (reactors, heat-exchangers, hydrogen purification unit and utilities).

3.10.1. Reactor simulation

The reactor model was based on the following assumptions:

- stoichiometric conversion of sorbitol using a simplified network of reforming reactions;
- water–gas shift reaction being at chemical equilibrium;
- in-situ phase equilibrium of the vapour and liquid phases;
- conversion of recycled alcohols reaching 100% per pass giving alkanes, CO_2 and hydrogen;
- independence of selectivity on the reaction temperature, pressure, feed dilution and WHSV.

The mass balance for the reactor design was based on the experimental data obtained in sorbitol APR over Pt/Al_2O_3. The details of the experiment are discussed in [**I**] and completed with the product distribution for the full conversion of sorbitol in [**VI**].

A new feature in the simulations was consideration of in-situ phase equilibrium for the reactor heat demand calculations not previously described in connection with APR. Optimal reaction conditions were determined according to those calculations. The extent of water evaporation was carefully considered since it is influencing the reactor thermal behavior giving a substantial contribution to the reactor duty. For example, it was found that the pressure elevation from 30 to 50 bar allows to reduce the extent of water evaporation from 62 to 12 % for 10 wt% sorbitol solution at 498 K. Therefore, application of higher pressure may reduce the reactor heat duty in isothermal conditions.

Another important parameter is sorbitol concentration. A higher sorbitol content at the reactor inlet results in a higher gas formation, which facilitates water evaporation

to sustain its partial pressure. In case if sorbitol concentration is higher than 15 wt%, water is entirely evaporated at 30 bar and 498 K according to calculations.

Feed dilution also affects temperature changes at adiabatic conditions. According to the simulations it is possible to operate an APR reactor adiabatically only below 5 wt% sorbitol concentration. In this case the adiabatic temperature change is 22–29 K. A higher sorbitol content in the feed requires the interstage heating or hot water injection due to high sensitivity of APR to temperature changes.

3.10.2 Flow-sheeting and techno-economical analysis

The aim of the techno-economical analysis was to estimate total costs of hydrogen production including both operational costs and required capital investments to the APR reaction section, hydrogen purification and utilities. Aspen HYSYS software was used to design a 500 kg/h hydrogen production plant operation with sorbitol syrup as a feedstock. The process described in [**VI**] uses sorbitol syrup with 70 wt% of polyol content as the feedstock, which is currently produced in significant amounts by hydrogenation of glucose. The capacity was selected based on an estimated amount needed for 100 000 t of green diesel annual production from tall oil. Such facility has been recently installed in Finland [166]. All the calculated values of heat consumption or costs are referred to this specific hydrogen capacity. The optimized (compared to publication [**V**]) process design is shown in Figure 25. The detailed process streams data and the material balance can be found in [**VI**].

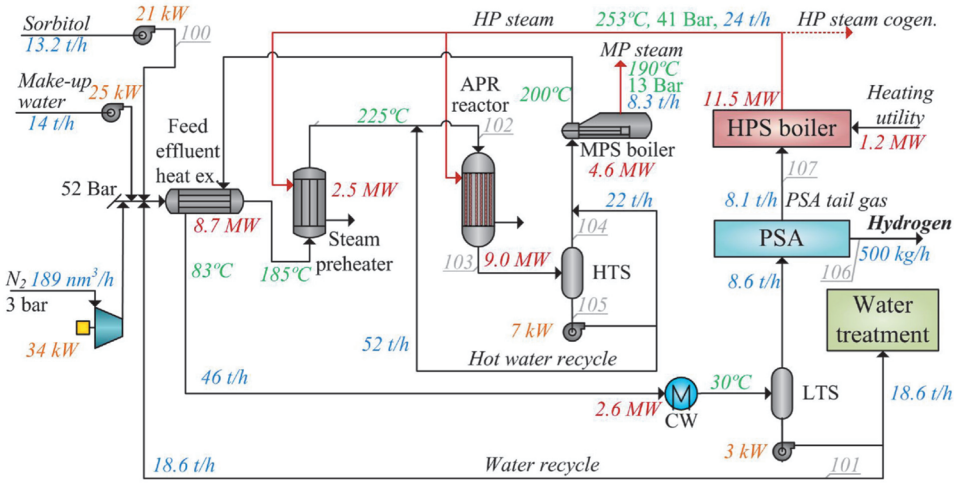

Figure 25. APR process design.

A mixture of the sorbitol syrup, make-up and recycling water, and the sweep gas (nitrogen) is preheated to a 483 K in a feed-effluent heat exchanger. The inlet sorbitol concentration is 10 wt%. Nitrogen co-feeding ratio was selected as 2 $nm^3 N_2 / m^3$ liquid at the reactor inlet [39]. High pressure steam (HPS) boiler is applied to subsequent input stream heating to the reaction temperature (498 K) due to a required precise temperature control. The reaction takes place at 50 bar in a downflow plug flow multitubular reactor, which is supplied with HPS to sustain the isothermal conditions.

The product stream contains both aqueous and gas phases. A hot temperature separator (HTS) or a special reactor design with a separation zone can be applied. For optimization purposes unreacted hot water could be separated before cooling and recycled back to the reactor inlet. As a result, a flowrate and corresponding duties of the preheater and the effluent heat exchanger can be decreased. Another way of optimization is to use the hot reactor effluent as a heat source for medium pressure (MP) steam generation.

Afterwards, the product stream is cooled down to 303 K in the feed-effluent heat exchanger and water cooler for separation of the gaseous products, which are directed to the pressure swing adsorption (PSA) unit. The PSA unit with 85% H_2 recovery was selected for separation of gas phase products from carbon dioxide. The PSA tail gas with pressure below 3 bar is combusted in the boiler to generate HPS, which is then supplied to the reactor and preheater. The excess of HPS can provide extra income. In cases of a highly diluted feed, the amount of tail gas is not enough to cover the reactor heat duty, therefore an external heating utility is required.

A fraction of the recycled water can be drawn to waste water treatment in order to prevent accumulation of relatively stable liquid components in the recycle such as acids and furans.

The process design discussed above was further utilized for an approximate equipment sizing and cost calculations. The methods used in the current work are conventionally applied in costs calculations giving typically errors within c.a. ±20–30% [167].

The major contribution to the operating costs and the corresponding specific hydrogen cost is the feedstock cost (92%). Other operating costs (electricity and water treatment) are partially covered by the revenue of steam cogeneration. Optimal reaction conditions were determined on the basis of water evaporation and the reactor

heat duty. Utilization of pressures above 40 bar is reducing the heat duty of the reactor and can provide a cost-efficient operation with the diluted feed. The process optimization illustrates that the medium pressure steam co-generation and hot water recycle can significantly decrease the operation costs.

Considering concentrations of sorbitol between 5 and 30 wt%, the costs of hydrogen do not change significantly in the range of 13-14 $/kg, while the operating costs vary to a larger extent. The optimized design has lower capital costs due to a decrease of heating/cooling equipment duty and also a lower hydrogen price because of revenues from stream cogeneration.

As mainly the feedstock costs contribute to the hydrogen price, the influence of sorbitol price on hydrogen costs at different hydrogen yields and WHSV equal to 0.2 h^{-1} was analyzed (Figure 26). The feedstock costs were considered on the dry basis. The hydrogen yield was determined as the amount of hydrogen obtained per mol of input sorbitol. Yields from 5.8 to 13 were considered, varying the main reaction selectivity from moderate to the "best-case" scenario based on complete conversion of sorbitol to hydrogen without formation of liquid products and alkanes ($C_6H_{14}O_6$ + 6 $H_2O \rightarrow 6\ CO_2 + 13\ H_2$).

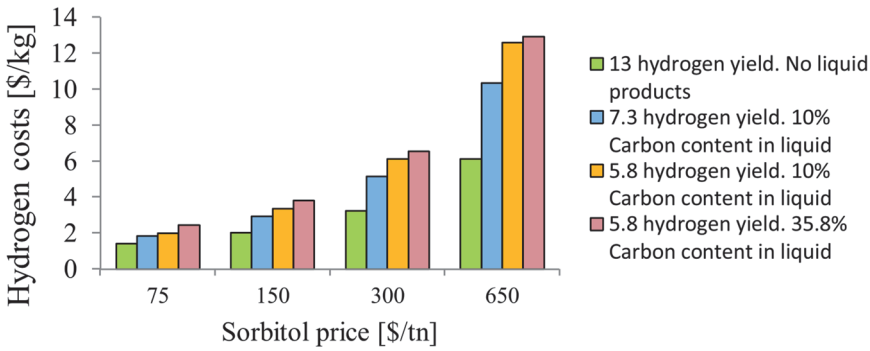

Figure 26. Influence of sorbitol price and H_2 yield on hydrogen costs.

Simulation results clearly show that the hydrogen cost below 4 $/kg can be achieved at the sorbitol price lower than 300 $/t and hydrogen yield above 7.3 mol H_2 /mol sorbitol. To compare the process with steam methane reforming (SMR), the data taken from [168] were used for calculation of hydrogen costs and specific capital cost

of SMR. The cost of hydrogen produced by the latter process [168] is approximately 1.8$/kg (not including the catalyst costs and capital charge). To reach similar product costs the sorbitol price for APR process should be lower than 150$/t. Such low feedstock price of 150–300 $/t is achievable only if sorbitol would be efficiently produced from cellulosic biomass.

4. Conclusions

4. Conclusions

1) Pt, Ni, Re, Ru, Pt–Ni, Pt–Re, Pt–Ru, and Pt–Co catalysts supported on a mesoporous carbon Sibunit were compared in xylitol APR to the Pt catalyst supported on activated carbon [**III**]. Pt–Re/Sibunit displayed an outstanding activity compared to all other catalysts, which was accompanied by a significantly higher selectivity to C_4–C_5 alkanes at the expense of selectivity to hydrogen and a higher amount of the liquid-phase intermediates. Other bimetallic catalysts showed activity levels similar to monometallic Pt. While the main focus of this study was devoted to hydrogen production, an important observation was made concerning hydrocarbon production. In particular, alkane distribution was shown for the first time to be metal-specific, forming characteristic patterns not depending on the polyol conversion.

2) The reliability of liquid-phase product identification was significantly improved due to the introduction of a spiking technique and peak fitting. A high precision of product identification allowed improvement of the reaction mechanism [**I**].

Different reaction pathways of the initial APR stages were computationally evaluated by DFT calculations and combined with the experimental data to further improve the reaction mechanism [**VII**]. Hydroxyacetone was demonstrated to be one of the most favored decomposition products, formed in the 1,2-propanediol APR. Competition between C–H, O–H, and C–C bond cleavages revealed that shortening of the carbon chain occurs most likely via decarbonylation.

Methanation does not occur under experimental conditions [**III**]. Methane could be formed through reforming of the intermediate methanol, or by a C-C bond scission in –CHOH–CH_3 or –CO–CH_3 fragments [**II**, **III**].

3) Chirality of the feed, as well as minor impurities (sugars, alcohols), are insignificant for catalyst activity and selectivity to the final products, such as hydrogen, CO_2, and alkanes [**I**, **IV**]. APR of sorbitol, galactitol, and their equimolar mixture resulted in a similar gas-phase composition, and minor, but noticeable, differences for some liquid-phase intermediates [**I**]. Equal selectivity to the gas-phase products, yields of the liquid-phase products and very close conversion were obtained in APR of commercial sorbitol and a hydrogenated sucrose solution over Pt/C [**IV**]. The technical feed containing mainly sorbitol and mannitol was not showing any significant differences

from the model polyol, indicating a large potential of its APR for hydrogen production.

4) A kinetic model was proposed in [**V**] based on the simplified reaction mechanism proposed in [**I**] and experimental data obtained during xylitol APR over Pt/C [**III**]. The reaction network was focused predominantly on the consumption of xylitol and formation of hydrogen, CO_2, and alkanes. A very good correspondence of the calculated results to the experimental data was obtained.

5) Experimental data obtained in xylitol APR over Pt/C [**III**] and in sorbitol APR over Pt/Al_2O_3 (partially published in [**I**]) was utilized for flow-sheeting of a unit capable of production of 500 kg/h of H_2 in [**V**] and [**VI**] correspondingly.

Dynamic model simulations were performed in [**V**] and utilized further for process design, which does not require any external heat source due to utilization of alkanes C_1–C_5 for heat production. Therefore, the catalyst for hydrogen production should preferentially not be too selective towards hydrogen and CO_2, being able to generate also alkanes as byproducts.

A reactor model in [**VI**] was based on phase equilibrium simulations, not discussed previously for APR. Process design was developed and optimized for the reduction of the operation costs [**VI**]. Techno-economical analysis of hydrogen production plant (500 kg H_2/h) operating with a sorbitol syrup as a feedstock was applied for the estimation of the hydrogen production price. The major cost contributor (92 % of total costs) is the feedstock. Based on the current sorbitol market price (650 $/t), hydrogen price is estimated as 13 $/kg, being c.a. seven fold higher than hydrogen costs from methane steam reforming. The most feasible way of making APR industrially attractive is production of polyols from the lignocellulosic biomass in an economic way.

5. Appendix

5. Appendix

Table A1. Carbon-supported catalysts studied in APR.

Catalyst	*Fixed bed*	*Autoclave*
graphene	ethylene glycol [8]	glucose [7]; glycerol [7]
Co/C	ethanol [169]	ethylene glycol [15]; cellulose [17]
Co-ZnO/C	ethanol [169]	
Cu/C	glycerol [170]	ethylene glycol [171]; glycerol+NaOH [171]
Cu-Ni/C	glycerol [170]	
Cu-Pd/C		glycerol+NaOH [171] xylitol+NaOH [171]; sorbitol+NaOH [171]
Ir/C		cellulose [17]
Ni/C	ethylene glycol [20]; ethylene glycol+KOH [20]; glycerol [170]	ethylene glycol [15,20]; ethylene glycol+KOH [20]; ethylene glycol+NaOH [20]; ethylene glycol+Ca(OH)2 [20]; ethylene glycol+Mg(OH)2 [20], sorbitol+ $Ba(OH)_2$ [19]; guaiacol [52]; syringol [52]; cellulose [17]
Ni-Ir/C		sorbitol+$Ba(OH)_2$ [19]
Ni-Re/C		sorbitol+$Ba(OH)_2$ [19]
Ni-Ru/C		sorbitol+ $Ba(OH)_2$ [19]
Pd/C	ethanol [58]	glycerol+NaOH [171]; cellulose [17]; wheat straw hydrolysate [172]
Pd-Zn/C	ethanol [58]	
Pt/C	ethylene glycol [18,20,35,36,44,45,48,54,56]; propanol-1 [173]; propane-1,2-diol [173]; glycerol [29,34,37,56,134,173–175]; xylitol [55,174]; sorbitol [38,54] *ATR-IR cell:* glycerol [176] *ceramic membrane reactor:* sorbitol [106] *microreactor:* glycerol [40,41]	ethylene glycol [15]; 1,2-propanediol [175]; glycerol [13,37,43,135,175–177]; glucose [78]; guaiacol [52]; syringol [52]; cellulose [17,88,90]; kenaf hydrolysate [86]; wheat straw hydrolysate [14,57,172] *Semibatch:* glycerol [51]; crude glycerol [51]
Pt-Ag/C	ethylene glycol [18]	

Catalyst	*Fixed bed*	*Autoclave*
Pt-Ba/C	ethylene glycol [18]	
Pt-Co/C	ethylene glycol [32,53]; glycerol [16,33,34]	glycerol [13]
Pt-Cs/C	ethylene glycol [18]	
Pt-Cu/C	glycerol [16]	glycerol [13]
Pt-Fe/C	ethylene glycol [18,178]; glycerol [16,178]; xylitol [178]; sorbitol [178]	
Pt-Ga/C	ethylene glycol [18]	
Pt-Ir/C	glycerol [16]	
Pt-Mn/C	ethylene glycol [18]	glycerol [177]
Pt-Mo/C	ethylene glycol [18]; glycerol [34,179]	
Pt-Ni/C	glycerol [16]	glycerol [13]; glycerol+CaO [13]; sorbitol+ $Ba(OH)_2$ [19]; wheat straw hydrolysate [14]
Pt-Ni-Sn/C		wheat straw hydrolysate [14]
Pt-Os/C	glycerol [16]	
Pt-Pd/C	glycerol [13]	
Pt-Re/C	ethylene glycol [18,36]; propylene glycol [36]; glycerol [16,36,37,134]; sorbitol [36] *ATR-IR cell:* glycerol [176] *microreactor:* glycerol [40,41]	formic acid [180]; ethanol [180]; acetaldehyde [180]; acetic acid [180]; glycerol [37,43,135,176]; soybean-based waste vegetable oil [101]
Pt-Rh/C	glycerol [16]	
Pt-Ru/C	sorbitol [38]	glycerol [13]; wheat straw hydrolysate [14]; cellulose [88]
Pt-Sn/C	glycerol [16]	wheat straw hydrolysate [14]
Re/C	ethylene glycol [36]; glycerol [37,134] *microreactor:* glycerol [40]	glycerol [37,135]; sorbitol+ $Ba(OH)_2$ [19]
Rh-Re/C	glycerol [37]	glycerol [37]
Rh/C	glycerol [37]	glycerol [37]
Ru/C	sorbitol [38]; acetic acid [181]	wheat straw hydrolysate [181]

Table A2. Carbon supports studied in APR.

Carbon support	*Active metal*
3D-BMC	Pt [54,174]
AC	Co [17]; Cu [171]; Ir [17]; Ni [17,19,52]; Ni-Ir [19] ; Ni-Re [19]; Ni-Ru [19]; Pd [17,172]; Pd-Cu [171]; Pt [14,17,29,37,38,40,41,43–45,48,51,52,54,55,57,78,86,90,135,172,176,177]; Pt-Fe [178]; Pt-Mn [177]; Pt-Ni [14,19]; Pt-Ni-Sn [14]; Pt-Re [36,37,40,41,43,101,135,176]; Pt-Ru [14,38]; Pt-Sn [14]; Re [19,37,40,135]; Rh [37]; Rh-Re [37]; Ru [38,172]
Carbon textile	Pt [88]; Pt-Ru [88]
Carbon black	Co-ZnO [169]; Co [169]; Pd [58]; Pd-Zn [58]; Pt [134]; Pt-Re [16,134,180]; Pt-Co [16]; Pt-Cu [16]; Pt-Fe [16]; Pt-Ir [16]; Pt-Ni [16]; Pt-Mo [179]; Pt-Os [16]; Pt-Rh [16]; Pt-Sn [16]; Re [134]
CMK-3	Pt [18,36,48,54,56,175]; Pt-Ag [18]; Pt-Ba [18]; Pt-Cs [18]; Pt-Fe [18]; Pt-Ga [18]; Pt-Mn [18]; Pt-Mo [18]; Pt-Re [18,36]; Re [36]
CMK-5	Pt [56]
CMK-8	Pt [54]
CMK-9	Pt-Fe [178]
CNF	Co [15]; Cu [15]; Ni [15,20]; Pt [15,20]
CNT	Pd [58]; Pd-Zn [58]; Ru [181]
Graphene	None [7,8]
Graphene oxide	Cu [171]; Cu-Pd [171]; Pd [171]; Pt [57]
Kenaf AC	Pt [86]
Mesoporous carbon	Cu [171]; Pt [106]
MWCNT	Cu [170]; Cu-Ni [170]; Ni [170]; Pt [13,14,33,34,45,57]; Pt-Co [13,33,34]; Pt-Cu [13]; Pt-Mo [34]; Pt-Ni-Sn [14]; Pt-Ni [13,14]; Pt-Pd [13]; Pt-Ru [13,14]; Pt-Sn [14]
Polymer-derived carbon	Pt [173]
Sibunit	Pt [55]

Carbon support	*Active metal*
Superdarco carbon	Pt [57]
SWCNT	Cu [171]; Pt [53,57]; Pt-Co [32,53]
TiC-CDC	Pt [55]

Table A3. Feed studied in APR.

Acidic	*Neutral*	*Basic*
	C1	
	methanol	formic acid
	C2	
acetic acid	ethanol	ethanol + buffer (10)*
acetaldehyde		ethanol + NaOH (10)
	ethylene glycol	ethylene glycol + $Ca(OH)_2$
	ethylene glycol + K_2SO_4	ethylene glycol + KOH
	ethylene glycol + KCl	ethylene glycol + $Mg(OH)_2$
	ethylene glycol + KNO_3	ethylene glycol + NaOH
	C3	
	propanol-1	
	1,2-propanediol	
	1,3-propanediol	
	hydroxyacetone	
glycerol + CH_3COOH (2.46)	glycerol (5.76)	glycerol + KOH (13.29)
glycerol + CH_3COOH + CH_3OH (2.53)	glycerol + CH_3OH (6.46)	glycerol + KOH + CH_3OH (13.4)
	glycerol + CH_3COOH + KOH (6.8)	glycerol + CH_3COOH + KOH (11.84)
	glycerol + KOH + CH_3COOH + CH_3OH (6.5)	glycerol + KOH + CH_3COOH + CH_3OH (11.93)
	glycerol + CH_3COOH + NaOH (7.09)	glycerol + NaOH

Acidic	*Neutral*	*Basic*
	glycerol + H_2SO_4 + KOH (7.25)	glycerol + CaO
	glycerol + H_3PO_4 + KOH (6.75)	
	glycerol + H_2SO_4 + NaOH (7.08)	
	glycerol + H_3PO_4 + NaOH (6.83)	
	glycerol + CH_3OH + NaCl	glycerol + CH_3OH + Na oleate
		glycerol + CH_3OH + NaCl + Na oleate
C4		
	n-butanol	
C5		
	xylitol	xylitol + NaOH
C6		
	galactitol	
	hydrogenated glucose	
	sorbitol	sorbitol + NaOH
		sorbitol + $Ba(OH)_2$
phenolic feed		
	catechol	
	guaiacol	
	syringol	
	phenol	
sugars		
	fructose	
	glucose	
	lactose	
	sucrose	
	glucose + fructose	

Acidic	*Neutral*	*Basic*
complex feed		
office wastepaper + H_2SO_4	cellulose	
pine sawdust + H_2SO_4	lignin	
	cheese whey	
	alginate	
	wheat straw hydrolysate	
	sorghum hydrolyzate	
	kenaf hydrolysate	
aqueous phase of oak-wood pyrolysis oil	low-boiling fraction of rice husk pyrolyzed bio-oil	
	purified crude glycerol	crude glycerol
	waste soy-bean oil	
	sunflower oil	
filtered fermentation broth (5)	filtered fermentation broth + NaOH (6)	

* - pH is given in parenthesis

6. Notation

6. Notation

6.1. Nomenclature

K_w - ionization constant of water

6.2. Abbreviations

3D-BMC - 3D bimodal mesoporous carbon

AC - activated carbon

ACT - acetyl fragment

APD/H - aqueous-phase dehydration/hydrogenation

APR – aqueous-phase reforming

BAC - birch activated carbon

BET - Brunauer–Emmett–Teller equation

CDC – carbide-derived carbon

CMK - ordered mesoporous carbon “Carbon Mesoporous Korea”

CNF – carbon nanofibers

CNT – carbon nanotubes

EDX - energy-dispersive X-ray spectroscopy

GC – gas chromatography

HPS – high pressure steam

HPLC - high-performance liquid chromatography

HTE – hydroxyethylidene

HTS – hot temperature separator

ICP - inductively coupled plasma optical emission spectrometry

MWCNT - multi-wall carbon nanotubes

PBSAC - polymer based spherical activated carbons

PrA – proionaldehyde

PSA - pressure swing adsorption

RR - reforming ratio (H_2/CO_2)

SMR – steam methane reforming

STP – standard temperature and pressure

SWCNT - single-wall carbon nanotubes

TG-DTA-MS - thermo-gravimetric differential thermal analysis combined with mass-spectrometry

TOC - total organic carbon analysis

TOF - turnover frequency

TPD - temperature-programmed desorption

TPO - temperature-programmed oxidation

TPR - temperature-programmed reduction

WDXRF - wavelength dispersive X-ray fluorescence spectrometry

WGS – water-gas shift reaction

WHSV - weightly-hour space velocity

XPS - X-ray photoelectron spectroscopy

XRD - X-ray powder diffraction

7. References

7. References

[1] L.R. Lynd, C.E. Wyman, T.U. Gerngross, Biocommodity engineering, Biotechnol. Prog. (1999) 777–793.

[2] H. Zabed, J.N. Sahu, A.N. Boyce, G. Faruq, Fuel ethanol production from lignocellulosic biomass: An overview on feedstocks and technological approaches, Renew. Sustain. Energy Rev. 66 (2016) 751–774.

[3] A. Wawrzetz, Aqueous phase reforming of glycerol over supported catalysts, Ph.D thesis, Technischen Universität München, 2008.

[4] R.R. Davda, J.W. Shabaker, G.W. Huber, R.D. Cortright, J.A. Dumesic, A review of catalytic issues and process conditions for renewable hydrogen and alkanes by aqueous-phase reforming of oxygenated hydrocarbons over supported metal catalysts, Appl. Catal. B Environ. 56 (2005) 171–186.

[5] B. Liu, Catalytic generation of hydrogen and chemicals from biomass derived polyols, Ph.D thesis, University of Pittsburgh, 2008.

[6] L. He, D. Chen, Hydrogen production from glucose and sorbitol by sorption-enhanced steam reforming: challenges and promises, ChemSusChem. 5 (2012) 587–595.

[7] I. Esteve-Adell, B. Crapart, A. Primo, P. Serp, H. Garcia, Aqueous phase reforming of glycerol using doped graphenes as metal-free catalysts, Green Chem. 19 (2017) 3061–3068.

[8] I. Esteve-Adell, N. Bakker, A. Primo, E.J.M. Hensen, H. García, Graphene as metal-free catalyst for aqueous phase reforming of ethylene glycol, ChemistrySelect. 2 (2017) 6338–6343.

[9] I. Coronado, M. Stekrova, M. Reinikainen, P. Simell, L. Lefferts, J. Lehtonen, A review of catalytic aqueous-phase reforming of oxygenated hydrocarbons derived from biorefinery water fractions, Int. J. Hydrogen Energy. 41 (2016) 11003–11032.

[10] G.W. Huber, J.W. Shabaker, S.T. Evans, J.A. Dumesic, Aqueous-phase reforming of ethylene glycol over supported Pt and Pd bimetallic catalysts, Appl. Catal. B Environ. 62 (2006) 226–235.

[11] T. Nozawa, A. Yoshida, S. Hikichi, S. Naito, Effects of Re addition upon aqueous phase reforming of ethanol over TiO_2 supported Rh and Ir catalysts, Int. J. Hydrogen Energy. 40 (2015) 4129–4140.

[12] R.R. Davda, J.W. Shabaker, G.W. Huber, R.D. Cortright, J.A. Dumesic, Aqueous-phase reforming of ethylene glycol on silica-supported metal catalysts, Appl. Catal. B Environ. 43 (2003) 13–26.

[13] C. He, J. Zheng, K. Wang, H. Lin, J.-Y. Wang, Y. Yang, Sorption enhanced aqueous phase reforming of glycerol for hydrogen production over Pt-Ni supported on multi-walled carbon nanotubes, Appl. Catal. B Environ. 162 (2015) 401–411.

[14] B. Kaya, S. Irmak, A. Hasanoğlu, O. Erbatur, Developing Pt based bimetallic and trimetallic carbon supported catalysts for aqueous-phase reforming of biomass-derived compounds, Int. J. Hydrogen Energy. 40 (2015) 3849–3858.

[15] T. van Haasterecht, C.C.I. Ludding, K.P. de Jong, J.H. Bitter, Stability and activity of carbon nanofiber-supported catalysts in the aqueous phase reforming of ethylene glycol, J. Energy Chem. 22 (2013) 257–269.

[16] E.L. Kunkes, R.R. Soares, D.A. Simonetti, J.A. Dumesic, An integrated catalytic approach for the production of hydrogen by glycerol reforming coupled with water-gas shift, Appl. Catal. B Environ. 90 (2009) 693–698.

[17] G. Wen, Y. Xu, Z. Xu, Z. Tian, Direct conversion of cellulose into hydrogen by aqueous-phase reforming process, Catal. Commun. 11 (2010) 522–526.

[18] H.-D. Kim, H.J. Park, T.-W. Kim, K.-E. Jeong, H.-J. Chae, S.-Y. Jeong, C.-H. Lee, C.-U. Kim, Hydrogen production through the aqueous phase reforming of ethylene glycol over supported Pt-based bimetallic catalysts, Int. J. Hydrogen Energy. 37 (2012) 8310–8317.

[19] J. Zhang, F. Lu, W. Yu, J. Chen, S. Chen, J. Gao, J. Xu, Selective hydrogenative cleavage of C–C bonds in sorbitol using Ni–Re/C catalyst under nitrogen atmosphere, Catal. Today. 234 (2014) 107–112.

[20] T. van Haasterecht, C.C.I. Ludding, K.P. de Jong, J.H. Bitter, Toward stable nickel catalysts for aqueous phase reforming of biomass-derived feedstock under reducing and alkaline conditions, J. Catal. 319 (2014) 27–35.

[21] H.-J. Lee, G.S. Shin, Y.-C. Kim, Characterization of supported Ni catalysts for aqueous-phase reforming of glycerol, Korean J. Chem. Eng. 32 (2015) 1–6.

[22] F. Bastan, M. Kazemeini, A.S. Larimi, Aqueous-phase reforming of glycerol for production of alkanes over Ni/Ce_xZr_1-xO_2 nano-catalyst: Effects of the support's composition, Renew. Energy. 108 (2017) 417–424.

[23] I. Coronado, M. Stekrova, L. García Moreno, M. Reinikainen, P. Simell, R. Karinen, J. Lehtonen, Aqueous-phase reforming of methanol over nickel-based catalysts for hydrogen production, Biomass and Bioenergy. 106 (2017) 29–37.

[24] G. Pan, Z. Ni, F. Cao, X. Li, Hydrogen production from aqueous-phase reforming of ethylene glycol over Ni/Sn/Al hydrotalcite derived catalysts, Appl. Clay Sci. 58 (2012) 108–113.

[25] J.W. Shabaker, G.W. Huber, J.A. Dumesic, Aqueous-phase reforming of oxygenated hydrocarbons over Sn-modified Ni catalysts, J. Catal. 222 (2004) 180–191.

[26] J.W. Shabaker, D.A. Simonetti, R.D. Cortright, J.A. Dumesic, Sn-modified Ni catalysts for aqueous-phase reforming: Characterization and deactivation studies, J. Catal. 231 (2005) 67–76.

[27] A.D. Pienaar, A. de Klerk, Nickel catalyst stability toward carboxylic acids, Ind. Eng. Chem. Res. 47 (2008) 4962–4965.

[28] M. El Doukkali, A. Iriondo, P.L. Arias, J. Requies, I. Gandarías, L. Jalowiecki-Duhamel, F. Dumeignil, A comparison of sol–gel and impregnated Pt or/and Ni based γ-alumina catalysts for bioglycerol aqueous phase reforming, Appl. Catal. B Environ. 125 (2012) 516–529.

[29] G. Wen, Y. Xu, H. Ma, Z. Xu, Z. Tian, Production of hydrogen by aqueous-phase reforming of glycerol, Int. J. Hydrogen Energy. 33 (2008) 6657–6666.

[30] T. Jiang, Q. Zhang, T.-J. Wang, Q. Zhang, L.-L. Ma, High yield of pentane production by aqueous-phase reforming of xylitol over Ni/HZSM-5 and Ni/MCM22 catalysts, Energy Convers. Manag. 59 (2012) 58–65.

[31] T. Jiang, T. Wang, L. Ma, Y. Li, Q. Zhang, X. Zhang, Investigation on the xylitol aqueous-phase reforming performance for pentane production over Pt/HZSM-5 and Ni/HZSM-5 catalysts, Appl. Energy. 90 (2012) 51–57.

[32] X. Wang, N. Li, Z. Zhang, C. Wang, L.D. Pfe, G.L. Haller, High-yield hydrogen production from aqueous phase reforming over single-walled carbon nanotube supported catalysts, ACS Catal. 2 (2012) 1480–1486.

[33] P.J. Dietrich, M.C. Akatay, F.G. Sollberger, E.A. Stach, T. Miller, W.N. Delgass, F.H. Ribeiro, Effect of Co loading on the activity and selectivity of PtCo aqueous phase reforming catalysts, ACS Catal. 4 (2014) 480–491.

[34] P.J. Dietrich, F.G. Sollberger, M.C. Akatay, E.A. Stach, W.N. Delgass, J.T. Miller, F.H. Ribeiro, Structural and catalytic differences in the effect of Co and Mo as promoters for Pt-based aqueous phase reforming catalysts, Appl. Catal. B Environ. 156–157 (2014) 236–248.

[35] X. Wang, N. Li, L.D. Pfefferle, G.L. Haller, Pt–Co bimetallic catalyst supported on single walled carbon nanotube: XAS and aqueous phase reforming activity studies, Catal. Today. 146 (2009) 160–165.

[36] H.-D. Kim, H.J. Park, T.-W. Kim, K.-E. Jeong, H.-J. Chae, S.-Y. Jeong, C.-H. Lee, C.-U. Kim, The effect of support and reaction conditions on aqueous phase reforming of polyol over supported Pt–Re bimetallic catalysts, Catal. Today. 185 (2012) 73–80.

[37] A. Ciftci, D.A.J.M. Ligthart, E.J.M. Hensen, Aqueous phase reforming of glycerol over Re-promoted Pt and Rh catalysts, Green Chem. 16 (2014) 853.

[38] M.F. Neira D'Angelo, V. Ordomsky, J. van der Schaaf, J.C. Schouten, T.A. Nijhuis, Selective production of methane from aqueous biocarbohydrate streams over a mixture of platinum and ruthenium catalysts., ChemSusChem. 7 (2014) 627–30.

[39] M.F. Neira D'Angelo, V. Ordomsky, J. van der Schaaf, J.C. Schouten, T.A. Nijhuis, Continuous hydrogen stripping during aqueous phase reforming of sorbitol in a washcoated microchannel reactor with a Pt–Ru bimetallic catalyst, Int. J. Hydrogen Energy. 39 (2014) 18069–18076.

[40] D.L. King, L. Zhang, G. Xia, A.M. Karim, D.J. Heldebrant, X. Wang, T. Peterson, Y. Wang, Aqueous phase reforming of glycerol for hydrogen production over Pt–Re supported on carbon, Appl. Catal. B Environ. 99 (2010) 206–213.

[41] L. Zhang, A.M. Karim, M.H. Engelhard, Z. Wei, D.L. King, Y. Wang, Correlation of Pt–Re surface properties with reaction pathways for the aqueous-phase reforming of glycerol, J. Catal. 287 (2012) 37–43.

[42] Z. Wei, A.M. Karim, Y. Li, D.L. King, Y. Wang, Elucidation of the roles of Re in steam reforming of glycerol over Pt–Re/C catalysts, J. Catal. 322 (2015) 49–59.

[43] A. Ciftci, D.A.J.M. Ligthart, E.J.M. Hensen, Influence of Pt particle size and Re addition by catalytic reduction on aqueous phase reforming of glycerol for carbon-supported Pt(Re) catalysts, Appl. Catal. B Environ. 174–175 (2015) 126–135.

[44] J.W. Shabaker, G.W. Huber, R.R. Davda, R.D. Cortright, J.A. Dumesic, Aqueous-phase reforming of ethylene glycol over supported platinum catalysts, Catal. Letters. 88 (2003) 1–8.

[45] X. Wang, N. Li, J.A. Webb, L.D. Pfefferle, G.L. Haller, Effect of surface oxygen containing groups on the catalytic activity of multi-walled carbon nanotube supported Pt catalyst, Appl. Catal. B Environ. 101 (2010) 21–30.

[46] J. Liu, B. Sun, J. Hu, Y. Pei, H. Li, M. Qiao, Aqueous-phase reforming of ethylene glycol to hydrogen on Pd/Fe_3O_4 catalyst prepared by co-precipitation: Metal–support interaction and excellent intrinsic activity, J. Catal. 274 (2010) 287–295.

[47] A.O. Menezes, M.T. Rodrigues, A. Zimmaro, L.E.P. Borges, M.A. Fraga, Production of renewable hydrogen from aqueous-phase reforming of glycerol over Pt catalysts supported on different oxides, Renew. Energy. 36 (2011) 595-599.

[48] T.-W. Kim, H.-D. Kim, K.-E. Jeong, H.-J. Chae, S.-Y. Jeong, C.-H. Lee, C.-U. Kim, Catalytic production of hydrogen through aqueous-phase reforming over platinum/ordered mesoporous carbon catalysts, Green Chem. 13 (2011) 1718.

[49] J.Q. Ma, Y. Xu, Y.F. Xu, H. Li, H.X. Li, P. Li, X.G. Zhou, Aqueous-phase reforming of ethylene glycol to hydrogen on supported Pt catalysts, Adv. Mater. Res. 347–353 (2011) 2511–2514.

[50] Y. Guo, M.U. Azmat, X. Liu, Y. Wang, G. Lu, Effect of support's basic properties on hydrogen production in aqueous-phase reforming of glycerol and correlation between WGS and APR, Appl. Energy. 92 (2012) 218–223.

[51] D.A. Boga, F. Liu, P.C.A. Bruijnincx, B.M. Weckhuysen, Aqueous-phase reforming of crude glycerol: effect of impurities on hydrogen production, Catal. Sci. Technol. 6 (2015) 134–143.

[52] M. Otromke, L. Theiss, A. Wunsch, A. Susdorf, T. Aicher, Selective and controllable purification of monomeric lignin model compounds via aqueous phase reforming, Green Chem. 17 (2015) 3621–3631.

[53] X. Wang, N. Li, L.D. Pfefferle, G.L. Haller, Pt–Co bimetallic catalyst supported on single-walled carbon nanotubes: effect of alloy formation and oxygen containing groups, J. Phys. Chem. C. 114 (2010) 16996–17002.

[54] H.J. Park, H.-D. Kim, T.-W. Kim, K.-E. Jeong, H.-J. Chae, S.-Y. Jeong, Y.-M. Chung, Y.-K. Park, C.-U. Kim, Production of biohydrogen by aqueous phase reforming of

polyols over platinum catalysts supported on three-dimensionally bimodal mesoporous carbon., ChemSusChem. 5 (2012) 629–33.

[55] A. V. Kirilin, B. Hasse, A. V. Tokarev, L.M. Kustov, G.N. Baeva, G.O. Bragina, A.Y. Stakheev, A.-R. Rautio, T. Salmi, B.J.M. Etzold, J.-P. Mikkola, D.Y. Murzin, Aqueous-phase reforming of xylitol over Pt/C and Pt/TiC-CDC catalysts: catalyst characterization and catalytic performance, Catal. Sci. Technol. 4 (2014) 387–401.

[56] K.E. Jeong, H.D. Kim, T.W. Kim, J.W. Kim, H.J. Chae, S.Y. Jeong, C.U. Kim, Hydrogen production by aqueous phase reforming of polyols over nano- and micro-sized mesoporous carbon supported platinum catalysts, Catal. Today. 232 (2014) 151–157.

[57] B. Kaya, S. Irmak, A. Hasanoglu, O. Erbatur, Evaluation of various carbon materials supported Pt catalyts for aqueous-phase reforming of lignocellulosic biomass hydrolysate, Int. J. Hydrogen Energy. 39 (2014) 10135–10140.

[58] H. Xiong, A. DeLaRiva, Y. Wang, A.K. Datye, Low-temperature aqueous-phase reforming of ethanol on bimetallic PdZn catalysts, Catal. Sci. Technol. 5 (2015) 254–263.

[59] Z. Zhu, A. Li, S. Zhong, F. Liu, Q. Zhang, Preparation and characterization of polymer-based spherical activated carbons with tailored pore structure, J. Appl. Polym. Sci. 109 (2008) 1692–1698.

[60] B. Böhringer, O. Guerra Gonzalez, I. Eckle, M. Müller, J.-M. Giebelhausen, C. Schrage, S. Fichtner, Polymer-based spherical activated carbons-from adsorptive properties to filter performance, Chemie-Ingenieur-Technik. 83 (2011) 53–60.

[61] Q. Wang, X. Liang, W. Qiao, C. Liu, X. Liu, L. Zhan, L. Ling, Preparation of polystyrene-based activated carbon spheres with high surface area and their adsorption to dibenzothiophene, Fuel Process. Technol. 90 (2009) 381–387.

[62] A.J. Romero-Anaya, M. Ouzzine, M.A. Lillo-Ródenas, A. Linares-Solano, Spherical carbons: Synthesis, characterization and activation processes, Carbon N. Y. 68 (2014) 296–307.

[63] S. Yenisoy-Karakaş, A. Aygün, M. Güneş, E. Tahtasakal, Physical and chemical characteristics of polymer-based spherical activated carbon and its ability to adsorb organics, Carbon N. Y. 42 (2004) 477–484.

[64] X. Wang, S. Dai, A simple method to ordered mesoporous carbons containing nickel nanoparticles, Adsorption. 15 (2009) 138–144.

[65] N. Sun, C. Sun, H. Liu, J. Liu, L. Stevens, T. Drage, C.E. Snape, K. Li, W. Wei, Y. Sun, Synthesis, characterization and evaluation of activated spherical carbon materials for CO_2 capture, Fuel. 113 (2013) 854–862.

[66] C. Schrage, A. Modrow, S. Fichtner, J.M. Giebelhausen, B. Böhringer, Funktionalisierte polymerbasierte sphärische aktivkohle für flüssig-und gasphasenanwendungen, Chemie-Ingenieur-Technik. 86 (2014) 27–34.

[67] H. Klefer, M. Munoz, A. Modrow, B. Böhringer, P. Wasserscheid, B.J.M. Etzold, Polymer-based spherical activated carbon as easy-to-handle catalyst support for hydrogenation reactions, Chem. Eng. Technol. (2016) 276–284.

[68] G. V. Plaksin, O.N. Baklanova, A. V. Lavrenov, V.A. Likholobov, Carbon materials from the Sibunit family and methods for controlling their properties, Solid Fuel Chem. 48 (2014) 349–355.

[69] V.B. Fenelonov, V.A. Likholobov, A.Y. Derevyankin, M.S. Mel'gunov, Porous carbon materials prepared from C_1-C_3 hydrocarbons, Catal. Today. 42 (1998) 341–345.

[70] A. Tanksale, J.N. Beltramini, G.M. Lu, A review of catalytic hydrogen production processes from biomass, Renew. Sustain. Energy Rev. 14 (2010) 166–182.

[71] L. Vilcocq, A. Cabiac, C. Especel, E. Guillon, D. Duprez, Transformation of sorbitol to biofuels by heterogeneous catalysis: chemical and industrial considerations, Oil Gas Sci. Technol. 68 (2013) 841–860.

[72] Y. Wei, H. Lei, Y. Liu, L. Wang, L. Zhu, X. Zhang, G. Yadavalli, B. Ahring, S. Chen, Renewable hydrogen produced from different renewable feedstock by aqueous-phase reforming process, J. Sustain. Bioenergy Syst. 4 (2014) 113–127.

[73] J. Liu, X. Chu, L. Zhu, J. Hu, R. Dai, S. Xie, Y. Pei, S. Yan, M. Qiao, K. Fan, Simultaneous aqueous-phase reforming and KOH carbonation to produce CO(x)-free hydrogen in a single reactor., ChemSusChem. 3 (2010) 803–806.

[74] J. Remón, J. Ruiz, M. Oliva, L. García, J. Arauzo, Effect of biodiesel-derived impurities (acetic acid, methanol and potassium hydroxide) on the aqueous phase reforming of glycerol, Chem. Eng. J. 299 (2016) 431–448.

[75] J. Remón, C. Jarauta-Córdoba, L. García, J. Arauzo, Effect of acid (CH_3COOH, H_2SO_4 and H_3PO_4) and basic (KOH and NaOH) impurities on glycerol valorisation by aqueous phase reforming, Appl. Catal. B Environ. 219 (2017) 362–371.

[76] R.D. Cortright, R.R. Davda, J.A. Dumesic, Hydrogen from catalytic reforming of biomass-derived hydrocarbons in liquid water, Nature. 418 (2002) 964–967.

[77] A. Tanksale, Y. Wong, J.N. Beltramini, G.Q. Lu, Hydrogen generation from liquid phase catalytic reforming of sugar solutions using metal-supported catalysts, Int. J. Hydrogen Energy. 32 (2007) 717–724.

[78] B. Meryemoglu, S. Irmak, A. Hasanoglu, O. Erbatur, B. Kaya, Influence of particle size of support on reforming activity and selectivity of activated carbon supported platinum catalyst in APR, Fuel. 134 (2014) 354–357.

[79] R.R. Davda, J.A. Dumesic, E. Drive, Renewable hydrogen by aqueous-phase reforming of glucose, Chem. Commun. (2004) 2003–2004.

[80] M.B. Valenzuela, C.W. Jones, P.K. Agrawal, Batch aqueous-phase reforming of woody biomass, Energy & Fuels. 42 (2006) 1744–1752.

[81] G. Wen, Y. Xu, Z. Xu, Z. Tian, Characterization and catalytic properties of the Ni/Al_2O_3 catalysts for aqueous-phase reforming of glucose, Catal. Letters. 129 (2008) 250–257.

[82] J. Remon, J. Ruiz, M. Oliva, L. Garcia, J. Arauzo, Cheese whey valorisation: Production of valuable gaseous and liquid chemicals from lactose by aqueous phase reforming, Energy Convers. Manag. 124 (2016) 453–469.

[83] J. Remon, L. Garcia, J. Arauzo, Cheese whey management by catalytic steam reforming and aqueous phase reforming, Fuel Process. Technol. 154 (2016) 66–81.

[84] Q. Lai, M.D. Skoglund, C. Zhang, A.R. Morris, J.H. Holles, Use of hydrogen chemisorption and ethylene hydrogenation as predictors for aqueous phase reforming of lactose over Ni@Pt and Co@Pt bimetallic overlayer catalysts, Energy & Fuels. 30 (2016) 8587–8596.

[85] S. Irmak, B. Meryemoglu, A. Hasanoglu, O. Erbatur, Does reduced or non-reduced biomass feed produce more gas in aqueous-phase reforming process?, Fuel. 139 (2015) 160–163.

[86] B. Meryemoglu, S. Irmak, A. Hasanoglu, Production of activated carbon materials from kenaf biomass to be used as catalyst support in aqueous-phase reforming process, Fuel Process. Technol. 151 (2016) 59–63.

[87] B. Meryemoğlu, A. Hasanoğlu, B. Kaya, S. Irmak, O. Erbatur, Hydrogen production from aqueous-phase reforming of sorghum biomass: An application of the response surface methodology, Renew. Energy. 62 (2014) 535–541.

[88] A.C.-C. Chang, R.F. Louh, D. Wong, J. Tseng, Y.S. Lee, Hydrogen production by aqueous-phase biomass reforming over carbon textile supported Pt–Ru bimetallic catalysts, Int. J. Hydrogen Energy. 36 (2011) 8794–8799.

[89] S.J. You, I.G. Baek, Y.T. Kim, K.-E. Jeong, H.-J. Chae, T.-W. Kim, C.-U. Kim, S.-Y. Jeong, T.J. Kim, Y.-M. Chung, S.-H. Oh, E.D. Park, Direct conversion of cellulose into polyols or H_2 over Pt/Na(H)-ZSM-5, Korean J. Chem. Eng. 28 (2011) 744–750.

[90] T. Sotak, M. Hronec, I. Vavra, E. Dobrocka, Sputtering processed tungsten catalysts for aqueous phase reforming of cellulose, Int. J. Hydrogen Energy. 41 (2016) 21936–21944.

[91] J. Zhang, W. Yan, Z. An, H. Song, J. He, Interface-promoted dehydrogenation and water−gas shift toward high-efficient H_2 production from aqueous phase reforming of cellulose, ACS Sustain. Chem. Eng. 6 (2018) 7313–7324.

[92] B. Yan, W. Li, J. Tao, N. Xu, X. Li, G. Chen, Hydrogen production by aqueous phase reforming of phenol over Ni/ZSM-5 catalysts, Int. J. Hydrogen Energy. 42 (2017) 6674–6682.

[93] B. Yan, W. Li, J. Tao, N. Xu, X. Li, G. Chen, Hydrogen production by aqueous phase reforming of phenol derived from lignin pyrolysis over NiCe/ ZSM-5 catalysts, Int. J. Hydrogen Energy. 42 (2016) 6674–6682.

[94] G. Pipitone, D. Tosches, S. Bensaid, A. Galia, R. Pirone, Valorization of alginate for the production of hydrogen via catalytic aqueous phase reforming, Catal. Today. 304 (2017) 153–164.

[95] T.P. Vispute, G.W. Huber, Production of hydrogen, alkanes and polyols by aqueous phase processing of wood-derived pyrolysis oils, Green Chem. 11 (2009) 1433–1445.

[96] A. Chen, P. Chen, D. Cao, H. Lou, Aqueous-phase reforming of the low-boiling fraction of bio-oil for hydrogen production: The size effect of Pt / Al_2O_3, Int. J. Hydrogen Energy. 40 (2015) 14798–14805.

[97] A. Chen, H. Guo, Y. Song, P. Chen, H. Lou, Recyclable CeO_2–ZrO_2 and CeO_2–TiO_2 mixed oxides based Pt catalyst for aqueous-phase reforming of the low-boiling fraction of bio-oil, Int. J. Hydrogen Energy. 42 (2017) 9577–9588.

[98] C. Pan, A. Chen, Z. Liu, P. Chen, H. Lou, X. Zheng, Aqueous-phase reforming of the low-boiling fraction of rice husk pyrolyzed bio-oil in the presence of platinum catalyst for hydrogen production, Bioresour. Technol. 125 (2012) 335–339.

[99] A. Seretis, P. Tsiakaras, Crude bio-glycerol aqueous phase reforming and hydrogenolysis over commercial SiO_2-Al_2O_3 nickel catalyst, Renew. Energy. 97 (2016) 373–379.

[100] J. Remón, J.R.R. Giménez, A. Valiente, L. García, J. Arauzo, Production of gaseous and liquid chemicals by aqueous phase reforming of crude glycerol: Influence of operating conditions on the process, Energy Convers. Manag. 110 (2016) 90–112.

[101] D. Kim, D.R. Vardon, D. Murali, B.K. Sharma, T.J. Strathmann, Valorization of waste lipids through hydrothermal catalytic conversion to liquid hydrocarbon fuels with in situ hydrogen production, ACS Sustain. Chem. Eng. 4 (2016) 1775–1784.

[102] S.M. Swami, V. Chaudhari, D.-S. Kim, S.J. Sim, M. a. Abraham, Production of hydrogen from glucose as a biomass simulant: integrated biological and thermochemical approach, Ind. Eng. Chem. Res. 47 (2008) 3645–3651.

[103] A.S. Oliveira, J.A. Baeza, L. Calvo, N. Alonso-Morales, F. Heras, J. Lemus, J.J. Rodriguez, M.A. Gilarranz, Exploration of the treatment of fish-canning industry effluents by aqueous-phase reforming using Pt/C catalysts, Environ. Sci. Water Res. Technol. (2018) 11–14.

[104] M.F. Neira D'Angelo, V. Ordomsky, J. van der Schaaf, J.C. Schouten, T.A. Nijhuis, Aqueous phase reforming in a microchannel reactor: the effect of mass transfer on hydrogen selectivity, Catal. Sci. Technol. 3 (2013) 2834–2842.

[105] M.F. Neira D'Angelo, J.C. Schouten, J. Van Der Schaaf, T.A. Nijhuis, Three-phase reactor model for the aqueous phase reforming of ethylene glycol, Ind. Eng. Chem. Res. 53 (2014) 13892–13902.

[106] M.F. Neira D'Angelo, V. Ordomsky, J.C. Schouten, J. van der Schaaf, T.A. Nijhuis, Carbon-coated ceramic membrane reactor for the production of hydrogen by aqueous-phase reforming of sorbitol., ChemSusChem. 7 (2014) 2007–2015.

[107] H.A. Duarte, M.E. Sad, C.R. Apesteguía, Production of bio-hydrogen by liquid processing of xylitol on Pt/Al_2O_3 catalysts: Effect of the metal loading, Int. J. Hydrogen Energy. 42 (2017) 4051–4060.

[108] H.A. Duarte, M.E. Sad, C.R. Apesteguía, Bio-hydrogen production by APR of C_2-C_6 polyols on Pt/Al_2O_3: Dependence of H_2 productivity on metal content, Catal. Today. 296 (2017) 59–65.

[109] M.L. Barbelli, F. Pompeo, G.F. Santori, N.N. Nichio, Pt catalyst supported on α-Al_2O_3 modified with CeO_2 and ZrO_2 for aqueous-phase-reforming of glycerol, Catal. Today. 213 (2013) 58–64.

[110] K. Lehnert, P. Claus, Influence of Pt particle size and support type on the aqueous-phase reforming of glycerol, Catal. Commun. 9 (2008) 2543–2546.

[111] J. Callison, N.D. Subramanian, S.M. Rogers, A. Chutia, D. Gianolio, C.R.A. Catlow, P.P. Wells, N. Dimitratos, Directed aqueous-phase reforming of glycerol through tailored platinum nanoparticles, Appl. Catal. B Environ. 238 (2018) 618–628.

[112] A. Wawrzetz, B. Peng, A. Hrabar, A. Jentys, A.A. Lemonidou, J.A. Lercher, Towards understanding the bifunctional hydrodeoxygenation and aqueous phase reforming of glycerol, J. Catal. 269 (2010) 411–420.

[113] F. Aiouache, L. McAleer, Q. Gan, A.H. Al-Muhtaseb, M.N. Ahmad, Path lumping kinetic model for aqueous phase reforming of sorbitol, Appl. Catal. A Gen. 466 (2013) 240–255.

[114] B. Roy, H. Sullivan, C.A. Leclerc, Effect of variable conditions on steam reforming and aqueous phase reforming of n-butanol over Ni/CeO_2 and Ni/Al_2O_3 catalysts, J. Power Sources. 267 (2014) 280–287.

[115] OriginPro 9.0.0, OriginLab Corporation: Northhampton, USA, 2012., (n.d.).

[116] D.Y. Murzin, T. Salmi, Catalytic kinetics: chemistry and engineering, 2nd ed., Elsevier, 2016.

[117] C. Síntese, C.E. Estudo, D.A. Atividade, J. Aparecida, R. Afonso, A. Campano, L. Agostinho, D. Oliveira, P. Rogério, Thermogravimetric and spectroscopic study (TG–DTA/FT–IR) of activated carbon from the renewable biomass source Babassu, Quim. Nova. 40 (2017) 284–292.

[118] E.M. Schwarz, V.V. Grundstein, A.F. Ievins, Thermal investigation of polyols I. Hexitols and pentitols, J. Therm. Anal. 4 (1972) 331–337.

[119] G. Kumaresan, R. Velraj, S. Iniyan, Thermal analysis of D-mannitol for use as phase change material for latent heat storage, J. Appl. Sci. 11 (2011) 3044–3048.

[120] N. Birta, N. Doca, G. Vlase, T. Vlase, Kinetic of sorbitol decomposition under non-isothermal conditions, J. Therm. Anal. Calorim. 92 (2008) 635–638.

[121] J.S. Hardman, P.J. Street, Spontaneous ignition behaviour of TEDA*-carbon, Fuel. 59 (1980) 213–214.

[122] Y. Holade, C. Morais, K. Servat, T.W. Napporn, K.B. Kokoh, Enhancing the available specific surface area of carbon supports to boost the electroactivity of nanostructured Pt catalysts, Phys. Chem. Chem. Phys. 16 (2014) 25609–25620.

[123] V.E. Guterman, S. V Belenov, V. V Krikov, L.L. Vysochina, W. Yohannes, N.Y. Tabachkova, E.N. Balakshina, Reasons for the differences in the kinetics of thermal oxidation of the support in Pt/C electrocatalysts, J. Phys. Chem. C. (2014) 23835–23844.

[124] R. Sellin, J.M. Clacens, C. Coutanceau, A thermogravimetric analysis/mass spectroscopy study of the thermal and chemical stability of carbon in the Pt/C catalytic system, Carbon N. Y. 48 (2010) 2244–2254.

[125] O.A. Baturina, S.R. Aubuchon, K.J. Wynne, Thermal stability in air of Pt/C catalysts and PEM fuel cell catalyst layers, Carbon N. Y. 5 (2006) 1498–1504.

[126] J.E. Mudd, T.J. Gardner, A.G. Sault, Platinum catalyzed decomposition of activated carbon: 1. Initial studies, Report, 2001.

[127] J.M. Thomas, W.J. Thomas, Principles and Practice of Heterogeneous Catalysis, Weinheim, New York, VCH, 1997.

[128] P.B. Weisz, Diffusivity of Porous Particles I. Measurements and Significance for Internal Reaction Velocities, Zeitschrift Für Phys. Chemie, Neue Folge. 15 (1957) 1–15.

[129] R. Perry, D. Green, J. Maloney, Perry's chemical engineers' handbook, The McGraw-Hill Companies, 1997.

[130] R.C. Reid, J.M. Prausnitz, T.K. Sherwood, The properties of gases and liquids, 3rd ed., McGraw-Hill: New York, 1977.

[131] G. Le Bas, The molecular volumes of liquid chemical compounds, Longmans, Green, New York, 1915.

[132] S.T. Sie, R. Krishna, Process development and scale up: III. scale-up and scale-down of trickle bed processes, Rev. Chem. Eng. 14 (1998) 203–252.

[133] A.K. Saroha, K.D.P. Nigam, Trickle bed reactors, Rev. Chem. Eng. 12 (1996) 207–346.

[134] E.L. Kunkes, D.A. Simonetti, J.A. Dumesic, W.D. Pyrz, L.E. Murillo, J.G. Chen, D.J. Buttrey, The role of rhenium in the conversion of glycerol to synthesis gas over carbon supported platinum–rhenium catalysts, J. Catal. 260 (2008) 164–177.

[135] A. Ciftci, D.A.J.M. Ligthart, A.O. Sen, A.J.F. van Hoof, H. Friedrich, E.J.M. Hensen, Pt-Re synergy in aqueous-phase reforming of glycerol and the water-gas shift reaction, J. Catal. 311 (2014) 88–101.

[136] D.A. Simonetti, E.L. Kunkes, J.A. Dumesic, Gas-phase conversion of glycerol to synthesis gas over carbon-supported platinum and platinum–rhenium catalysts, J. Catal. 247 (2007) 298–306.

[137] B. Peng, C. Zhao, I. Mejía-Centeno, G.A. Fuentes, A. Jentys, J.A. Lercher, Comparison of kinetics and reaction pathways for hydrodeoxygenation of C_3 alcohols on Pt/Al_2O_3, Catal. Today. 183 (2012) 3–9.

[138] N. Li, G.A. Tompsett, T. Zhang, J. Shi, C.E. Wyman, G.W. Huber, Renewable gasoline from aqueous phase hydrodeoxygenation of aqueous sugar solutions prepared by hydrolysis of maple wood, Green Chem. 13 (2011) 91–101.

[139] N. Li, G.W. Huber, Aqueous-phase hydrodeoxygenation of sorbitol with $Pt/SiO_2–Al_2O_3$: Identification of reaction intermediates, J. Catal. 270 (2010) 48–59.

[140] F. Auneau, S. Noël, G. Aubert, M. Besson, L. Djakovitch, C. Pinel, On the role of the atmosphere in the catalytic glycerol transformation over iridium-based catalysts, Catal. Commun. 16 (2011) 144–149.

[141] D. Roy, B. Subramaniam, R. V. Chaudhari, Aqueous phase hydrogenolysis of glycerol to 1,2-propanediol without external hydrogen addition, Catal. Today. 156 (2010) 31–37.

[142] I. Gandarias, P.L. Arias, J. Requies, M.B. Güemez, J.L.G. Fierro, Hydrogenolysis of glycerol to propanediols over a Pt/ASA catalyst: The role of acid and metal sites on product selectivity and the reaction mechanism, Appl. Catal. B Environ. 97 (2010) 248–256.

[143] M.B. Smith, March's advanced organic chemistry reactions, mechanisms and structure, 7th ed., Wiley, 2013.

[144] A. Parvulescu, J. Janssens, J. Vanderleyden, D. de Vos, Heterogeneous catalysts for racemization and dynamic kinetic resolution of amines and secondary alcohols, Top. Catal. 53 (2010) 931–941.

[145] S. Nishimura, Y. Yakita, M. Katayama, K. Higashimine, K. Ebitani, The role of negatively charged Au states in aerobic oxidation of alcohols over hydrotalcite supported AuPd nanoclusters, Catal. Sci. Technol. 3 (2013) 351–359.

[146] W. Kim, R. Karvembu, J. Park, Alumina-supported ruthenium catalysts for the racemization of secondary alcohols, Bull. Korean Chem. Soc. 25 (2004) 931–933.

[147] J. Shi, X. Li, Q. Wang, Y. Zhang, Y. Tang, Platinum-encapsulated zeolitically microcapsular catalyst for one-pot dynamic kinetic resolution of phenylethylamine, J. Catal. 291 (2012) 87–94.

[148] B. Martín-Matute, J.-E. Bäckvall, Dynamic kinetic resolution catalyzed by enzymes and metals., Curr. Opin. Chem. Biol. 11 (2007) 226–32.

[149] M. Banu, S. Sivasanker, T.M. Sankaranarayanan, P. Venuvanalingam, Hydrogenolysis of sorbitol over Ni and Pt loaded on NaY, Catal. Commun. 12 (2011) 673–677.

[150] I. Clark, Hydrogenolysis of sorbitol, Ind. Eng. Chem. 50 (1958) 1125–1126.

[151] L. Zhao, J.H. Zhou, Z.J. Sui, X.G. Zhou, Hydrogenolysis of sorbitol to glycols over carbon nanofiber supported ruthenium catalyst, Chem. Eng. Sci. 65 (2010) 30–35.

[152] J. Sun, H. Liu, Selective hydrogenolysis of biomass-derived xylitol to ethylene glycol and propylene glycol on supported Ru catalysts, Green Chem. 13 (2011) 135–142.

[153] L. Vilcocq, A. Cabiac, C. Especel, S. Lacombe, D. Duprez, New insights into the mechanism of sorbitol transformation over an original bifunctional catalytic system, J. Catal. 320 (2014) 16–25.

[154] A. Ciftci, D.A.J.M. Ligthart, A.O. Sen, A.J.F. van Hoof, H. Friedrich, E.J.M. Hensen, Pt-Re synergy in aqueous-phase reforming of glycerol and the water – gas shift reaction, J. Catal. 311 (2014) 88–101.

[155] G.W. Huber, R.D. Cortright, J.A. Dumesic, Renewable alkanes by aqueous-phase reforming of biomass-derived oxygenates., Angew. Chem. Int. Ed. Engl. 43 (2004) 1549–1551.

[156] Q. Zhang, K. Qiu, B. Li, T. Jiang, X. Zhang, L. Ma, T. Wang, Isoparaffin production by aqueous phase processing of sorbitol over the Ni/HZSM-5 catalysts: Effect of the calcination temperature of the catalyst, Fuel. 90 (2011) 3468–3472.

[157] Q. Zhang, T. Wang, B. Li, T. Jiang, L. Ma, X. Zhang, Q. Liu, Aqueous phase reforming of sorbitol to bio-gasoline over Ni/HZSM-5 catalysts, Appl. Energy. 97 (2012) 509–513.

[158] A. V. Bandura, S.N. Lvov, The ionization constant of water over wide ranges of temperature and density, J. Phys. Chem. Ref. Data. 35 (2006) 15–30.

[159] HSC Chemistry 6.0, Outotec Oy: Espoo, Finland, 2006., (n.d.).

[160] HyperChem Pro 8.0.8; Hybercube, Inc.: Gainesville, FL, U.S.A., 2009., (n.d.).

[161] A. V. Kirilin, A. V. Tokarev, L.M. Kustov, T. Salmi, J. Mikkola, D.Y. Murzin, Aqueous phase reforming of xylitol and sorbitol: Comparison and influence of substrate structure, Appl. Catal. A Gen. 435–436 (2012) 172–180.

[162] B.M. Moreno, N. Li, J. Lee, G.W. Huber, M.T. Klein, Modeling aqueous-phase hydrodeoxygenation of sorbitol over $Pt/SiO_2–Al_2O_3$, RSC Adv. 3 (2013) 23769–23784.

[163] L. Vilcocq, A. Cabiac, C. Especel, S. Lacombe, D. Duprez, Hydrocarbon fuel synthesis from sorbitol over bifunctional catalysts: association of tungstated titania with platinum , palladium or iridium, Catal. Today. 242 (2015) 91–100.

[164] X. Jin, B. Subramaniam, R. V Chaudhari, Activity and selectivity of base promoted mono and bimetallic catalysts for hydrogenolysis of xylitol and sorbitol, in: Nov. Mater. Catal. Fuels Process. ACS Symp. Ser., American Chemical Society, 2013: pp. 273–285.

[165] A. V. Kirilin, A. V. Tokarev, E. V. Murzina, L.M. Kustov, J.-P. Mikkola, D.Y. Murzin, Reaction products and transformations of intermediates in the aqueous-phase reforming of sorbitol., ChemSusChem. 3 (2010) 708–718.

[166] J.K. Laurikko, N.-O. Nylund, P. Aakko-Saksa, S. Mannonen, V. Vauhkonen, P. Roslund, Crude tall oil-based renewable diesel in passenger car field test, SAE Tech. Pap. 2014-01-2774. (2014).

[167] G. Towler, R.K. Sinnott, Chemical engineering design. Principles, practice and economics of plant and process design, 1st ed., 2008.

[168] R.A. Meyers, Handbook of petroleum refining processes, McGraw-Hill Professional, NY, USA, 2003.

[169] S.D. Davidson, J. Sun, Y. Hong, A.M. Karim, A.K. Datye, Y. Wang, The effect of ZnO addition on Co/C catalyst for vapor and aqueous phase reforming of ethanol, Catal. Today. 233 (2014) 38–45.

[170] M.M. Rahman, H2 production from aqueous-phase reforming of glycerol over Cu-Ni bimetallic catalysts supported on carbon nanotubes, Int. J. Hydrogen Energy. 40 (2015) 14833–14844.

[171] X. Jin, L. Dang, J. Lohrman, B. Subramaniam, S. Ren, R. V Chaudhari, Lattice-matched bimetallic CuPd-graphene nanocatalysts for facile conversion of biomass-derived polyols to chemicals., ACS Nano. 7 (2013) 1309–1316.

[172] B. Meryemoglu, A. Hesenov, S. Irmak, O.M. Atanur, O. Erbatur, Aqueous-phase reforming of biomass using various types of supported precious metal and raney-nickel catalysts for hydrogen production, Int. J. Hydrogen Energy. 35 (2010) 12580–12587.

[173] L.I. Godina, A. V. Tokarev, I.L. Simakova, P. Mäki-Arvela, E. Kortesmäki, J. Gläsel, L. Kronberg, B. Etzold, D.Y. Murzin, Aqueous-phase reforming of alcohols with three carbon atoms on carbon-supported Pt, Catal. Today. 301 (2018) 78–89.

[174] T.-W. Kim, H. Ju, Y.-C. Yang, S.-Y. Jeong, C.-U. Kim, Hydrogen production via the aqueous phase reforming of polyols over three dimensionally mesoporous carbon supported catalysts, Int. J. Hydrogen Energy. 39 (2014) 11509–11516.

[175] E. D'Hondt, S. Van de Vyver, B.F. Sels, P.A. Jacobs, Catalytic glycerol conversion into 1,2-propanediol in absence of added hydrogen., Chem. Commun. (Camb). (2008) 6011–6012.

[176] Z. Wei, A. Karim, Y. Li, Y. Wang, Elucidation of the roles of Re in aqueous-phase reforming of glycerol over Pt-Re/C catalysts, ACS Catal. 5 (2015) 7312–7320.

[177] F. Bossola, X.I. Pereira-Hernandez, C. Evangelisti, Y. Wang, V. Dal Santo, Investigation of the promoting effect of Mn on a Pt/C catalyst for the steam and aqueous phase reforming of glycerol, J. Catal. 349 (2017) 75–83.

[178] M.C. Kim, T.W. Kim, H.J. Kim, C.U. Kim, J.W. Bae, Aqueous phase reforming of polyols for hydrogen production using supported Pt-Fe bimetallic catalysts, Renew. Energy. 95 (2016) 396–403.

[179] P.J. Dietrich, R.J. Lobo-Lapidus, T. Wu, A. Sumer, M.C. Akatay, B.R. Fingland, N. Guo, J.A. Dumesic, C.L. Marshall, E. Stach, J. Jellinek, W.N. Delgass, F.H. Ribeiro, J.T. Miller, Aqueous phase glycerol reforming by PtMo bimetallic nano-particle catalyst: product selectivity and structural characterization, Top. Catal. 55 (2012) 53–69.

[180] J. Fu, S.H. Hakim, B.H. Shanks, Aqueous-phase processing of bio-oil model compounds over Pt–Re supported on carbon, Top. Catal. 55 (2012) 140–147.

[181] D.J.M. Vlieger, L. Lefferts, K. Seshan, Ru decorated carbon nanotubes – a promising catalyst for reforming bio-based acetic acid in the aqueous phase, Green Chem. 16 (2014) 864–874.

ISBN 978-952-12-3779-9